THE UNIVERSITY OF CHICAGO

HYPOTHETICAL ICY MOON SEISMIC PROFILES FOR COMPARISON TO FUTURE SEISMIC DATA

A DISSERTATION SUBMITTED TO
THE FACULTY OF THE DIVISION OF THE PHYSICAL SCIENCES
IN CANDIDACY FOR THE DEGREE OF
DOCTOR OF PHILOSOPHY

DEPARTMENT OF PHYSICS

BY
ANDREA SIMONE BRYANT

CHICAGO, ILLINOIS
JUNE 2024

To Jesus and all those who paved the way for me to be here.

"At first glance it may look too hard, but look again, always looks again"

TABLE OF CONTENTS

LIST OF FIGURES

LIST OF TABLES

ACKNOWLEDGMENTS

I would like to acknowledge that it takes a village to raise a child. While I am now an adult, I have most definitely felt like a science child. And now I am gaining my wings. I would like to thank firstly my mother Margea Chenault-Ward without whom I would not be here and my father Allen Bryant Jr., whose love and support over the years has meant the world. Thank you Mom and Dad for always believing in me and instilling in me a desire to always strive for the best, and Daddy for always saying I was the smartest girl in the world– I always would laugh and shrug it off, but you helped instill a confidence in me to never give up. I love you both! Of course my aunties, especially Auntie Spring, Auntie Mary Alice, Auntie Jean; my cousins, especially Tanesha and the fam, Sydnee and William! Thank to my loving siblings, Nazareth, Naahlyee, and Ariel. Thank you to my friend Joy (Jones) Maxwell whose prayers and support over the years has truly been a Godsend. My best friends: Linnea Kremer, Cynthia Celedonio-Feliciano, Lois Yena Chang, Susmitha Edukutharayil, Victoria Sweeney, and Robynne Nashay Davis all of whose friendship, unconditional love and support and has helped me weather some of my darkest days. Thank you for the support: Auntie Jean, Cherisse Mims– love y'all. And I would want to mention my Grandma Ruth Norfleet Bryant I wish she could see this day– I love you.

I would also like to acknowledge my amazing office-mates over the years, your presence has been a breath of fresh air to me, ERC 590 will never be the same: John Hood, Rebecca Diesing, Grace Chesmore, Emily Simon, Alice Burington-Luna, and Kayla Owens. You all have made grad school soo much fun and I will miss our pow-wows, coworking under string lights, the cowboy cat light (Rud Scoots) and all the support and love you all have given. During my time in graduate school I would have never gotten through without my advisors Steve Meyer and especially Mark Panning of JPL–so grateful for your taking me under your wing. Grateful for my Bridge program family, especially Dr. David Reid, Dr. Jelani Hannah, Dr. Joel Fuentes, Aaron Ortega, Bridget Haas, and of course the wonderful

and prolific NYTimes writer Dr. Katrina Miller (the third African-American/Black woman in the history of the University of Chicago's Department of Physics to earn a doctorate in Physics–last year in April 2023). I was so encouraged by meeting Dr. Willetta Green Johnson, the first Black woman to graduate from UChicago's Department of Physics, and I wouldn't even know that I was the fourth without Katrina's support and the work that she did find out the history of those who paved the way for us.

Other dear friends and encouraging mentors/teachers: Chéma Hernandez, Nikita Mehta, Camille Avestruz, Brittany Kamai (in whose footsteps I walk–grateful for your desk lamp!), John Carlstrom, Wendy Freedman, Craig Hogan (Holometer & the encouragement that a PhD is just a thing you do–so I should just finish the thing), Zoheyr Doctor and the LIGO fam (for teaching me how to use a Jupyter notebook and introducing me to Github), Nadejda Marounina (for teaching me how to navigate Fortran), Zhaodi Pan (for all your knowledge of the SPT cryostat), Adam Anderson (SPT mentor), Sasha Rahlin (SPT mentor), Andrew Neil (for teaching me how to use a HPC), Kristian Mackewicz (GR tutor), Sandra Charles of Fermilab (game changer) and so many others.

In the physics office: Zosia Krusberg, Young Kee-Kim, Putri Kusumo, Peter Littlewood, Tiffany Kurns, and Shadla Cycholl; as well as Shirley Prosby and Emily Easton in the Dean of Students office for all your warmth and snacks (lol) over the years! I would be remiss to not acknowledge all the help and support from Ashley Walker, Brian Nord and Lucianne Walkowicz especially during one of the hardest seasons of my doctoral journey during the start of the pandemic in 2020. Members of the Dragonfly team and the entire Dragonfly Guest Investigator Program especially Lynnae Quick, Zibi Turtle, and Morgan Cable.

My graduate coop: Gamma Alpha, where I've made friends who have become like family: Kévin-Orly Irakóze, Nan Zhou, Catrin Dowd, Armun Liaghat, Tomal Hossain, Pablo Lechón Alonso (affectionately known as Pablito), Dr. Zeynep Tezer, Sofia Sheikh, Daniel Braithwaite, Gerry and Antje, Dr. Hanne Graverson, Dr. Abshishek Battacharyya, Tanima, Dr.

Neal Patterson Miller and so many others (only added the "Dr." here to denote those who had already graduated before me!). You all have made coming home and graduate school so much fun, living in a coop was definitely challenging at times but I'm grateful for all of your smiling faces, warm hugs, playful banter, and delicious meals (especially from Chef Kévin). Also my dear friends Katlo Siyanda Mohutsiwa, Caressa Franklin, and all the ladies of the BLTR, love you all dearly. Of course my Carver 47 fam and the amazing singer/artist and chef Lizz Wright and your team (esp. Michael, Brian, and Lee), and Retreat (RIP!, was such an amazing space!).

My Los Angeles family my heart aches with gratefulness and joy for the time I spent you all especially my family at Mosaic South Pasadena and the bustling Young Adults group– thank you all for so much support and love and so much fun. And of course, the amazing friends like family I made there Megan Jones, Nancy Keyes, India Wallace, Sara Carreras, Gavi Yariv, and my neighbor Bryan Orozco for all the rides to and from JPL.

The MoonsGG group especially Marshall Styczinski, Steve Vance, Katherine Psarakis, Ceri Nunn, Baptiste Journaux, Angela Marusiak-Schools (whose friendship and mentorship has meant the world), Ashley Schoenfeld, Jack Diab, Bing Chua, Shaila Saifee, and of course the Posselt's for allowing me to lodge in your beautiful home during an incredibly fun and productive summer of 2022 in LA.

My amazing therapist Asabi Yakini, a fellow Black woman with a PhD who knows all the struggles and has helped me get through.

My Art, Science and Cultural Initiative collaborator, friend, and phenomenal digital artist Nimrod Astarhan.

In the Astronomy and Astrophysics department I would like to thank Carolina Ceballos, Sereda Henry for your wonderful conversations and friendship over the years. Laticia "Letty" Rebeles, Julia Brazas, and Jennifer Smith for all of your kindness and help(!) over the years. Thank You so much, from the bottom of my heart.

I would also like to thank Maryfrances Miley, without your help at the beginning of all of this I wouldn't be here. Thank you so much and also to Sandy Heinz– you all the are the absolute best <3

I would of course be remiss to forget about the late Ms.Criss my second grade teacher who was the first to call me "Dr. Bryant", encouraging me to always strive to do my best. As well as Drs. Erin Bonning and Arri Eisen my undergraduate mentors and advisors, as well as my Angie Stryker and the Bread Coffeehouse family– where my dream to become an astrophysicist began.

ABSTRACT

This dissertation provides a look at the major findings of my work on Titan seismology during my tenure as a graduate student. The introduction lays out the field of extraterrestrial seismology as it is today, and contextualizes my work on Titan in that regard as well as provides background on some of the key physics concepts needed to understand my work. In Chapter 2, I present my work published in the paper ('The Effects of Methane Clathrates on the Thermal and Seismic Profile of Titan's Icy Lithosphere') as well as some additional analysis that I led, supplemental to the paper. In Chapter 3, I present my first-authored publication on long period seismology ('Long Period Seismology on Titan in the Presence of a Methane Clathrate Lid'). In Chapter 4, I present the most recent publication ('Seismology of High Pressure Ice on Titan'). And in the last chapter I provide a brief summary of all of the findings of this body of work, as well as present some future directions.

CHAPTER 1

INTRODUCTION

1.1 Brief Intro to Seismology & Selected Physics Underpinnings

1.1.1 Discovering Earth

The interior of the Earth would be a mystery without measuring the differences in the seismic wave speeds between the layers of the materials that make up the subsurface. The science of seismology, or the study of the seismic waves that propagates through the Earth (or a planetary/lunar body) and what it can tell us about the interior structure and the physics of the seismic events is relatively new (Shearer [2019]). Earthquakes, or at least the most massive and destructive events have been felt and recorded since antiquity. The earliest recorded seismic instrument was invented by Chinese philosopher Chang Hêng (also known as Choko and Tyoko) in 132 A.D., but it wasn't until 1875 that the first seismograph was invented, although with very low sensitivity (Dewey and Byerly [1969]).Earthquakes are continuously happening with smaller earthquakes occurring several hundred times a day. Every day there are about fifty strong earthquakes that can be felt locally, while earthquakes that are capable of structural damage, occur ever few days (Shearer [2019]).

1.1.2 Basics of Seismology: Body Waves

Seismology is the study of waves in a planetary body. This leads to the solutions of the seismic wave equation that exists in whole spaces, also known as body waves. P waves or compressional waves are the fastest traveling waves, with particle motion aligned with propagation direction. Next are S waves or shear waves that travel with particle motion perpendicular to the propagation direction. Generally on Earth, P waves are about twice the speed of S waves, and seismic velocities increase with depth. A key parameter to note

is that S waves do not travel in a liquid (have no shear strength), meaning that wherever there is a liquid, the P waves will keep traveling, but S waves will not travel and will reflect at the boundary. This is a key property for understanding the structure of the interior of the Earth, particularly regarding the location and nature of the Earth's core.

1.1.3 Basics of Seismology: Surface Waves

Besides body waves, other waves are possible, particularly in the case where free surfaces exist in a vertically heterogeneous medium. These are called surface waves. On Earth the main types of surfaces waves are Love and Rayleigh waves. Because my dissertation focuses on producing synthetic seismograms of Titan, motivated by the NASA Dragonfly mission, I focus mainly on waves in the vertical component (as the Dragonfly rotorcraft's seismometer will on by sensitive to vertically oriented seismic waves, which excludes Love waves (Lorenz et al. [2021a]).

(Surface) Rayleigh Waves

Rayleigh waves are polarized in the P/SV system particle motion perpendicular to the propagation direction and exist at any free surface (Shearer [2019]). In the case of icy ocean worlds, shorter period Rayleigh waves don't interact with the bottom of the ice shell and are similar to Rayleigh waves seen on Earth, with a characteristic retrograde elliptical motion. Due to lower gravity, the velocity gradient is very small with depth, so Rayleigh waves have very little dispersion in ice shells (Stähler et al. [2017]).

In the case of a roughly spherically-symmetric floating water ice shell, Rayleigh waves are essentially non-dispersive (due to the nearly constant P and S wave velocities throughout the ice shell). This in the case of the thick ($\approx$ 100 km)Titan ice shells modeled in this dissertation. Velocities at lower frequencies sensitive to the base of the ice shell are more variable and discussed in more detail in Chapter 3.

1.1.4 Dispersion

When waves have frequency-dependent properties within the same medium, the medium is said to be dispersive. This is a phenomenon from wave theory demonstrating the frequency dependence of the phase velocity and group velocity of waves in a medium. Phase velocity is the velocity at which a particular phase of periodic motion (i.e. crest or trough) propagates, and the group velocity is the velocity of the envelope (or energy packets) of groups of these crests and troughs. I define more in depth below.

Take the example of two harmonic waves with differing frequency (ω) and wavenumber (k) from Shearer [2019]:

$$u(x,t) = \cos(\omega_1 t - k_1 t) + \cos(\omega_2 t - k_2 t). \tag{1.1}$$

Now defining the modulated frequencies (ω_1, ω_2) and wavenumbers (k_1, k_2) in regards to an average frequency (ω) and wavenumber (k):

$$\omega_1 = \omega - \delta\omega, \qquad k_1 = k - \delta k \tag{1.2}$$

$$\omega_2 = \omega + \delta\omega, \qquad k_2 = k + \delta k \tag{1.3}$$

Now substituting these definitions into (1.1) and using the identity
$2\cos A\cos B = \cos(A+B) + \cos(A-B)$, we obtain a resulting waveform of a signal with with average frequency (ω) that is modulated by a longer period wave with frequency $\delta\omega$:

$$u(x,t) = 2\cos(\omega t - kx)\cos(\delta k x - \delta\omega t). \tag{1.4}$$

This resulting waveform illustrates the concept of dispersion.

Qualitatively, the actual dispersion itself is caused by boundary conditions of the medium

(in the case of Titan- eg. the ice shell/ocean interface) or the interaction of the waves themselves with the medium (eg. waves propagating within a materially-heterogeneous ice shell).

In the case of two harmonic waves with differing frequency or wavenumber, when summed, result in a single modulated wave. In the new modulated wave the phase velocity is the velocity of the individual peaks and the group velocity is the velocity of the wave packets (larger grouping of the sinusoidal nature of the overall shape of the individual peaks; crests and troughs).

Group Velocity: The velocity at which the overall envelope (smooth curve outlining the extremes of the oscillating signal- a modulated sine curve) propagates through space. The group velocity,

$$v_g \equiv \frac{\partial \omega}{\partial k} \tag{1.5}$$

where ω is the angular frequency, and k is the wavenumber.

Phase Velocity: Phase velocity is the velocity of individual phases of sinusoidal oscillation (e.g. peaks and troughs). The phase velocity, $v_p \equiv \frac{\omega}{k}$, is often denoted as c.

1.1.5 Normal Modes

One dimensional case– wave on a string: A string only vibrates at certain frequencies, when constrained by boundary conditions. These are standing waves and the string only vibrates at certain standing waves. Any motion of the string can be described as a weighted sum of the standing waves of the string.

The eigenvalue problem: the resonant frequencies are the eigenfrequencies and the string displacements are the eigenfunctions. In the string case, the eigenfunctions are the sines and cosines (naturally in the Fourier representation).

In music: the lowest frequency is the "fundamental mode", and the higher modes are

the harmonics or "overtones".

In a spherically symmetric body: Normal mode theory for a spherically symmetric body like the earth is more complicated, and non-trivial to describe. I will briefly summarize in the following paragraphs.

There are two types of modes (*spheroidal modes*—P/SV & Rayleigh wave motion [radial and horizontal motion; compressional and shear velocity sensitivity] and *toroidal modes*—SH and Love wave motion [shear velocity sensitivity only]). Earth and Titan are not perfectly spherically symmetric, but these are a very good first order approximation.

Spheroidal mode observations at long periods provide gravity sensitivity and allow for direct constraints on Earth's density structure, so in the same way could allow for direct constraints on Titan's density structure and could provide sensitivity of Titan's gravity field which we can already constrain using *Cassini-Huygens* data. If spheroidal mode long period data could be resolved from Dragonfly's single seismometer and geophones, it could allow for further refinement of Titan's interior structure.

The spherically symmetric eigenvalue problem: the eigenfunctions are best described as spherical harmonics, and provide an orthogonal set of basis functions on a spherical surface that can be summed to generate a complete seismogram (as has been done in Chapter 3 of this dissertation). Aki and Richards [2002] provides a complete description of how to approach this formulation, and I provide a brief summary below.

Spherical harmonics are defined by:

$$Y_l^m(\theta,\phi) = (-1)^m \left[\frac{2l+1}{4\pi}\frac{(l-m)!}{(l+m)!}\right]^{1/2} P_l^m(\cos\theta)e^{im\phi}, \tag{1.6}$$

where here m is the azimuthal order, defined by $2l + 1$ integer values between $\pm l$, l is the spherical harmonic degree or angular order number, θ is the polar (co-latitudinal) angle, ϕ is the azimuthal (longitudinal) angle, and P_l^m is the associated Legendre polynomial.The total number of zero crossings is determined by l, the total number of zero crossings passing

through the pole are given by m. The following figure from Shearer [2019], illustrates the three lower order spherical harmonics (Figure 1.1).

It is important to note that spherical harmonics are dependent on the placement of the poles as well as the relevant coordinate system (in this case we are using spherical coordinates). If rotated the spherical harmonic function can be expressed as a sum of the same l, but would need a different set of m values, in other words the angular order number would be the same, but the weighting of the azimuthal order numbers would change.

Upon rotation of spherical harmonics (Equations 1.7), toroidal modes are designated as ${}_nT_l^m$ and spheroidal modes are designated as ${}_nS_l^m$, where n is the radial order number, also indicating the number of zero crossings in radius present in the function.

$$R_l^m(\theta,\phi) = Y_l^m \hat{r} \tag{1.7}$$

$$S_l^m(\theta,\phi) = \frac{1}{\sqrt{l(l+1)}}\left[\frac{\partial Y_l^m}{\partial \theta}\hat{\theta} + \frac{1}{\sin\theta}\frac{\partial Y_l^m}{\partial \phi}\hat{\phi}\right] \tag{1.8}$$

$$T_l^m(\theta,\phi) = \frac{1}{\sqrt{l(l+1)}}\left[\frac{1}{\sin\theta}\frac{\partial Y_l^m}{\partial \phi}\hat{\theta} - \frac{\partial Y_l^m}{\partial \theta}\hat{\phi}\right] \tag{1.9}$$

The solutions for n=0 are the fundamental modes, and n>0 are the overtones. In the case of a spherically symmetric Earth or Titan, the eigenfrequencies at constant n and l are identical for all values of m, and it is commonly seen that they are denoted by their radial and angular order numbers are corresponding frequencies; ${}_nT_l$ and ${}_nS_l$ and the corresponding frequencies as ${}_n\omega_l$. The fundamental spheroidal mode is ${}_0S_0$ and is known as the "breathing" mode, it represents the expansion and contraction of the planetary body. ${}_0S_1$ is not used in seismology as it would describe a shift in the center of mass of the Earth, something that could not result from solely internal forces Shearer [2019].

For a spherically symmetric solid, normal mode eigenfrequencies are identical for different

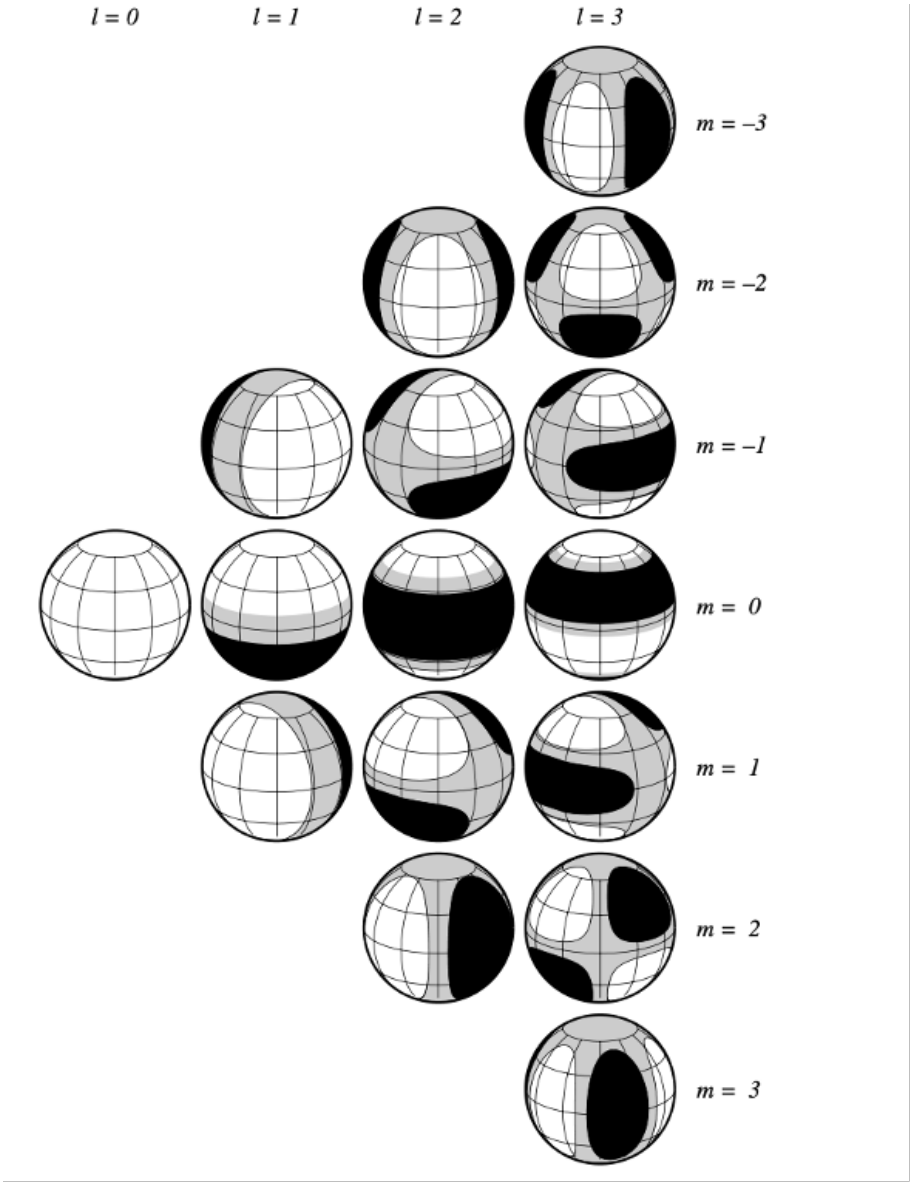

Figure 1.1: Figure (8.12) from Shearer [2019] illustrating how the motion of a (approximately) spherically symmetry body like the Earth or Titan is described using spherical harmonics. Shown here are the spherical harmonics functions up $l = 3$. The colors illustrate negative (black), positive (white), and near zero values (gray).

azimuthal order numbers m, or in other words eigenfrequencies are degenerate for a spherically symmetric solid. But Earth and Titan's small departures from spherical symmetry can cause the eigenfrequencies to separate, described as non-degenerate-"splitting". This is seen as a single spectral peaks being split into a multiplet composed of the separate peak for different values of m. Features on Earth that are known to cause azimuthal order (m) eigenfrequency non-degeneracies include ellipticity, general three-dimensional heterogeneities and rotation, among other things.

In the case of attenuation and normal mode amplitudes, normal modes are useful to help constrain Q, the seismic quality factor, at very long periods as attenuation causes mode amplitudes to decay with time.

In the case of computing synthetic seismograms, this can be done by summing the normal modes for long period seismology. The number of modes required increases proportional to the square of the frequency which can be computationally expensive.

1.2 Computational Seismology: Synthetic Data Creation Pipeline

In the absence of seismometer data, synthetic seismograms for realistic Earth or planetary data are a good first approximation. Solving for the propagation effects in realistic velocity structures is the most difficult component of computing synthetic seismograms.

1.2.1 ***PlanetProfile****: Interior Models*

The open-source code *PlanetProfile* was designed for investigations of icy moon interiors. The code generates self-consistent radial profiles of thermodynamic, mechanical, and electrical properties from measured and observed properties from missions and laboratory equation-of-state data (Vance et al. [2018b], Journaux et al. [2019], Styczinski et al. [2023a]). In particular, the depth profiles of geophysically crucial quantities (e.g.,seismic wave velocites, density, electrical conductivity, etc.) are calculated from bulk properties (e.g., moment

of inertia, radius, mass, temperature, and pressure) Vance et al. [2018b], Styczinski et al. [2023a].

1.2.2 ***AxiSEM****: Parallel Spectral Element Method*

After a velocity profile is generated, three-dimensional wave propagation in a spherically symmetric, anisotropic, visco-elastic structure can be determined for the profile of choice (Nissen-Meyer et al. [2014]).

The basic idea of the computation of the wavefield arises from making the approximation the planetary body of choice as spherically symmetric. Then defining an axis of symmetry through the center of the planet and the seismic source. The response to a single force point or a moment tensor (more complicated source) can be expanded in a series of multipoles– taking advantage of the axisymmetry of the model (Nissen-Meyer et al. [2014]). This three-dimensional solution is computed on a two-dimensional disk, the third dimension (azimuthal) is solved analytically, using the spectral element method (Nissen-Meyer et al. [2014]). An in depth derivation of the spectral element method as a method of computing synthetic seismograms is provided in Igel [2017].

1.2.3 ***Instaseis****: Green's Functions: Sources and Receivers*

Green's functions allow for all the elastic properties of the material, to be accounted for with the necessary boundary conditions (Shearer [2019]). These Green's functions are stored in a database for near-instantaneous extractions for the generation of arbitrary seismograms (based upon the wavefield generated with *AxiSEM*) (van Driel et al. [2015]). In this approach, we use a database of the wavefield for surface sources. Instaseis then makes use of source-receiver reciprocity to generate seismograms at a surface station for sources anywhere within the wavefield database volume.

1.3 Extraterrestrial Seismology

As of today we have extraterrestrial seismic data only from the Moon and Mars. In fact, data from Mars *InSight* mission (2018-2022) was the first time there was data from another planetary body since delivery of lunar data in the 1970s (Nakamura [2020]).

1.3.1 Seismology of Icy Ocean Worlds

Seismology is a powerful tool that can reveal details of interior structures of planets that are otherwise not accessible. For example, it has been argued that seismology is the best tool to determine "vital signs" (fluid flow induced ground motion), on icy ocean worlds (Vance et al. [2018a]). Compared to seismology on Earth where rock is the primary medium on the surface, ice is the dominant medium near the surface on these bodies, and there are specific seismic phases that are distinct to icy moon seismology (eg. Flexural, Toroidal,and Crary waves). On Earth, Love and Rayleigh waves are the dominant surface waves expressed. Table 6 (here Figure 1.2) from Stähler et al. [2017], gives an overview of the various scientific observables that can be used to determine scientific objectives (Stähler et al. [2017]).

One of the most important properties crucial for understanding the internal composition of icy ocean worlds is the **ice thickness**. Initial constraints on this observation can be derived from reverberation timing and wave velocity within the ice shell. The ice thickness can be further constrained using the characteristic harmonic frequency of the Crary wave and using the estimated P (compressional) and S (shear-horizontal and shear-vertical) wave velocities in the ice.

With the ice thickness constrained, the next key quantity to be determined is the **location of seismic events** that can be measured using P and S arrival times. The **ocean depth** can be measured by identifying multiples within the ocean coda of body waves, by estimating the time of travel for two-way reflected phases.

Table 6
Potential Scientific Objectives of a Future Icy Ocean World Seismometer and Seismic Observables That Address It

Scientific objective	Seismic observable	Signal strength	Distance range
Tectonic activity	Location of seismic events	strong	global
Ice thickness	Resonant frequency of Crary phase	strong	global
	Transition frequency between Rayleigh and flexural surface wave	intermediate	global
	Reverberations in body wave coda	strong	teleseismic
	Autocorrelation of ambient noise	strong	ambient noise
Ocean depth	Reverberations in body wave coda	strong	teleseismic
	Autocorrelation of noise	intermediate	ambient noise
Ocean chemistry (from sound velocity in water)	Reverberations in body wave coda	strong	teleseismic
High-pressure ice phases	Coda of Sn waves	strong	teleseismic
	Scholte waves	strong	teleseismic
	P to *S* ratio	intermediate	teleseismic, depends on focal mechanism
Core diameter	Autocorrelation of noise	weak	ambient noise
	Autocorrelation of seismogram	intermediate	>100°

Figure 1.2: Table 6 adapted from Stähler et al. [2017]:Potential Scientific Objectives of a Future Icy Ocean World Seismometer and Seismic Observables That Address It

1.3.2 Seismology as a Key Astrobiological Tool

Seismological inferences of subsurface structure has astrobiological implications for Titan, as seismology is the key to uncovering Titan's deep interior which is important for understanding the habitability of Titan. In particular, I am currently studying thermal and seismic profiles of high- pressure ice (ice underneath Titan's ocean). The existence of high-pressure ice is of much interest as it has many astrobiology implications. There could exist high-pressure ice underneath the ocean's of icy moons, that could be determined using spectral analysis (Stähler et al. [2017]). In particular, the existence of high-pressure ice could limit the amount of water-rock interactions that could provide crucial nutrients for potential life (Vance et al. [2018b]).

1.3.3 Titan

Titan is of much interest as it is one of the largest moons of in the Solar System and contains both an atmosphere and a subsurface ocean. On it's surface there are sand dunes, mountains,

methane lakes,and even water ice. Beneath the surface there is thought to be a 45-120 km thick (Vance et al. [2018b], Stähler et al. [2017], Panning et al. [2018]) ice shell, and beneath that there is a >80km deep ocean (Stähler et al. [2017]).

What is currently known about Titan has been constrained from data from the *Cassini-Huygens* probe (Vance et al. [2018b]). Using Schumann-resonance, the first estimates of the ice-shell were given (the mean ice-thickness has been constrained to be about 55-80km) (Béghin et al. [2012]). Due to Titan's high gravitational moment of inertia, a metallic core is not permitted within the compositional models (Vance et al. [2018b]).

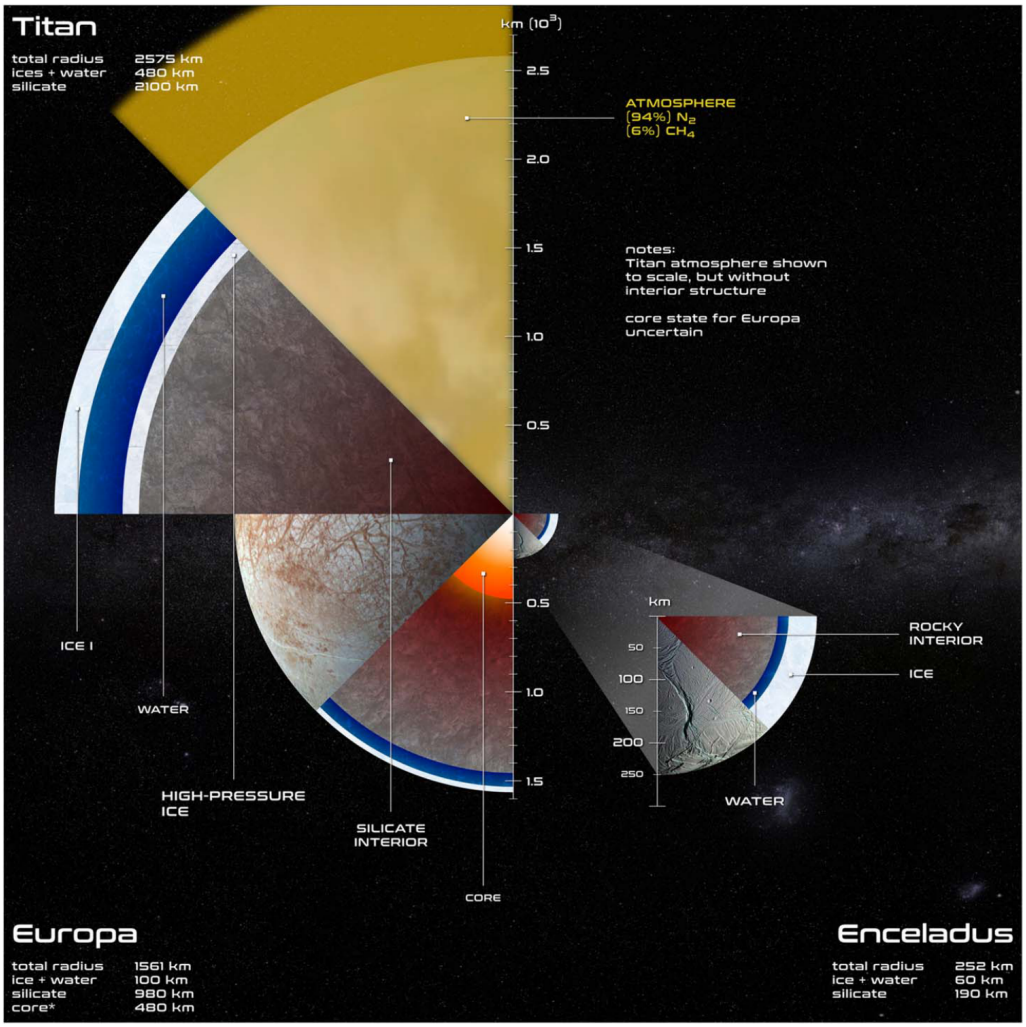

Figure 1.3: Interior structure of Titan, Ganymede, Europa, and Enceladus from Marusiak et al. [2021] based upon models from Vance et al. [2018b].

Still, since the *Cassini-Huygens* mission was only able to image Titan's surface, many questions remain (Marusiak et al. [2021]). The dynamics and internal structure of the ice shell is not well understood (Marusiak et al. [2021]). However the use of a suite of geophysical and seismic instruments will uncover much of what is unknown about Titan in the common decade (ie. the Dragonfly mission). To constrain various aspects of Titan, much work has been done using the data from the *Cassini-Huygens* mission, and much more work remains ongoing in preparation for the upcoming Dragonfly mission. Focusing on the observable feature of seismology on Titan, the main sources of seismic events are thought to be ice cracking due to the tidal cycles of Titan from Saturn (Marusiak et al. [2021]). Both the hydrocarbon lakes and atmosphere of Titan will also contribute background seismic noise, analogous to Earth's background seismic noise due to Earth's oceans and atmosphere (Gutenberg [1947], Dybing et al. [2019], Marusiak et al. [2021]).

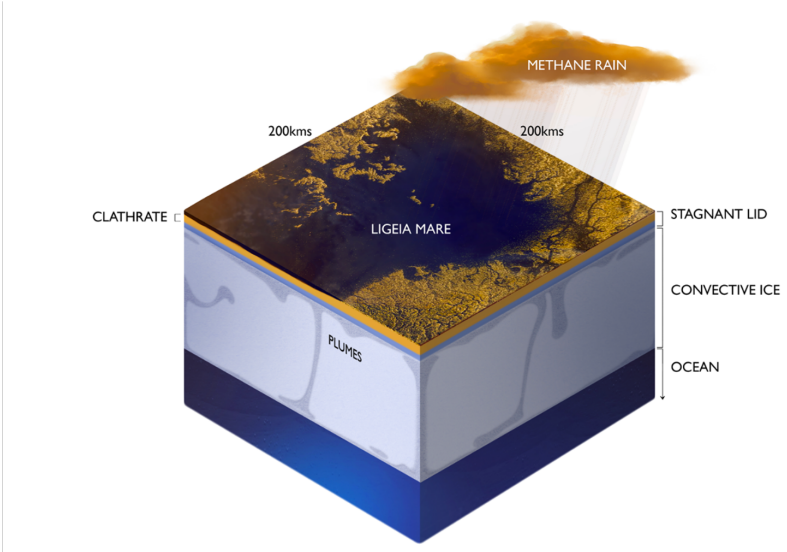

Figure 1.4: Image from Kalousova and Sotin (2020) illustrating the methane cycle and a stagnant methane clathrate lid on top of convective ice.

1.3.4 Methane Clathrates on Titan

We know that there are a plethora of different hydrocarbons on Titan, but among these methane is the most abundant, making up $> 6\%$ of the atmosphere, with the most abundant molecule being nitrogen N_2. We also know from the *Cassini-Huygens* mission that there is an abundance of water on Titan, although not in liquid form on the surface but underneath the surface. With the surface temperature of Titan being $\approx 94K$, methane– which is usually in gaseous form on Earth's surface– exists in liquid form on the surface of Titan, where the primary element of Titan's hydrological cycle is methane (e.g. methane lakes, rivers, and rain).

Experimental studies have shown that under Titan temperatures and pressure liquid methane and water ice will form methane clathrate hydrates, also known as methane clathrates. Methane clathrates are cage like molecular structures made of water molecules that host a single methane molecule inside. They are discussed more in depth in Chapter 2 and Marusiak et al. [2022]. It is commonly thought that the abundance of atmospheric methane is the result of outgassing from Titan's interior, which episodically replenishes the atmospheric methane that is observed in Titan's atmosphere (Tobie et al. [2006]).

The presence of clathrates within the ice shell can affect the ice shell thermodynamics and methane cycle on Titan (Lunine and Stevenson [1985], Mousis et al. [2015]). In comparison to pure water ice, methane clathrates have a lower thermal conductivity (about 1/5 that of water ice), but higher viscosity (20 times higher than water ice Ih), density, and specific heat (Lunine and Stevenson [1985], Helgerud et al. [2003, 2009], Hand et al. [2006], Waite et al. [2007]). This in turn influences the thermal structure, density, and dynamics of the ice shell (Kamata et al. [2019], Kalousová and Sotin [2020b], Čadek et al. [2021]). Understanding where and how the presence of clathrates affects Titan's ice shell is a topic of much research (ex. Lunine and Stevenson [1985], Mousis et al. [2015], Kalousová and Sotin [2020b], Vu et al. [2020], Carnahan et al. [2021], Marusiak et al. [2022]) and the focus of Chapters 2 and

3 of this thesis.

1.4 NASA's Dragonfly Mission

NASA's Dragonfly mission is currently planned to launch in 2027 and land on Saturn's moon Titan in the mid-2030s (Barnes et al. [2021b]). The rotorcraft itself is a dual-quadcopter that would hold many instruments, including a seismometer and two geophones, within the DraGMet (Dragonfly Geophysics and Meteorology) instrument package, to measure ground motion (Lorenz et al. [2021b]).

Dragonfly's targets are the equatorial dunes and Titan's Selk Crater (Soderblom et al. [2010]), and the main science goals of the mission center around determining the history and evolution of prebiotic chemistry on Titan, as well as processes of Titan's surface geology, and its interior composition. An exhaustive list of Dragonfly's science goals exists in Barnes et al. [2021b].

1.4.1 Dissertation Focus Statement

Utilizing the knowledge of wave propagation through various media (e.g. rock, ice, and water) while varying depths/pressures (seismology), the interior structures of icy ocean worlds will be revealed. For my dissertation I use wave-form modeling techniques to analyze and catalog potential interior structures of icy moons (focusing on Titan) for upcoming and potential icy moon exploration missions.

CHAPTER 2

METHANE CLATHRATES

Preface: I present first the paper Marusiak et al. [2022] of which I am a coauthor. I contributed to this work by running the models using the spectral element method based software: *AxiSEM* (Nissen-Meyer et al. [2014]), and generating broadband seismograms with *Instaseis* (van Driel et al. [2015]), presented and discussed in the later part of this chapter in a section called "Investigating Detection of Methane Clathrates with Varying Source Depths on Titan". Namely, the paper includes two of the three models that I simulated, as well as only the most shallow of the four source depths that I simulated. I also contributed through discussion of science implications throughout the writing process. In the amended section I present these models in full, and briefly discuss the detectability of a shallow event by some known extraterrestrial seismometers.

2.1 The Effects of Methane Clathrates on the Thermal and Seismic Profile of Titan's Icy Lithosphere

This open-access, copyrighted paper was published by the American Astronomical Society in their *Planetary Science Journal* in July 2022 (Marusiak et al. [2022]). A few small changes for formatting purposes have been made, but otherwise, the work is presented as is.

2.1.1 Author List

Angela G. Marusiak (1), Steven Vance(1), Mark P. Panning (1), **Andrea S. Bryant** (2), Marc A. Hesse (3,4), Evan Carnahan (3,4), Baptiste Journaux (5)

1. Jet Propulsion Laboratory, California Institute of Technology, 4800 Oak Grove Drive Pasadena, CA 91109, USA

2. University of Chicago, Department of Physics, Chicago, IL, USA

3. Institute for Geophysics, Jackson School of Geosciences, The University of Texas at Austin J.J. Pickle Research Campus, Bldg. 196, 10100 Burnet Rd. (R2200), Austin, TX, 78758 USA

4. Oden Institute of Computational Engineering, The University of Texas at Austin J.J. Pickle Research Campus

5. University of Washington, Department of Earth and Space Sciences, Seattle, WA 98915, USA

2.2 Abstract

We investigate the effects of methane clathrates on Titan's thermal and seismic structure. The Dragonfly mission is planned to arrive at Titan in 2033 with a payload that includes a seismic package. The seismic instruments are tasked with recording seismic events and recovering the internal structure. Here, we explore whether differences in thermal and seismic profiles between a pure water ice shell and an ice shell with a clathrate lid could be detectable with seismic instrumentation. Due to their higher viscosity and lower thermal conductivity, clathrates reduce the conductive lid thickness thus altering the thermal profile. The differences between seismic velocities of clathrates and pure water ice, coupled with changes in the thermal profile, indicate the clathrate lid will create lower seismic velocities, particularly for the upper 10 km of the surface ice shell. The differences in P and S velocity at the surface are 2.9 and 4.5%, respectively, and reach up to 8.4% (for both P and S) at a depth of 9.6 km. Due to changes in thermal profile, the seismic attenuation of the ice shell will change such that clathrates will suppress surface wave amplitudes relative to the pure water ice model. The clathrate lid will further create minor changes ($\leq 2.0\%$) in the surface wave dispersion curves. Dragonfly, or other future seismic investigations, could provide evidence

for or against the presence of a clathrate lid by constraining the thermal and seismic profile of Titan's ice shell, by measuring the relative amplitudes of the surface to body waves, or by constraining the surface wave dispersion with high accuracy and precision.

2.3 Introduction

Titan, Saturn's largest moon, is of great interest for several reasons. Like other icy ocean worlds, such as Jupiter's Europa or Saturn's Enceladus, Titan has an icy shell overlying a subsurface ocean (Sotin et al. [2021]). Titan's subsurface ocean may provide the requirements for life to currently exist. Beneath the subsurface ocean, could lie an additional layer of high-pressure ices such as Ice V and Ice VI (Journaux et al. [2020b]). Titan is unique compared to other icy ocean worlds, due to its thick methane-rich atmosphere (Niemann et al. [2005]). Temperature and pressure conditions at the surface allow for liquid hydrocarbons to stably exist (Stofan et al. [2007]). In addition to its presence in Titan's atmosphere, and on its surface, methane may also be present within Titan's icy lithosphere in clathrate structures (Choukroun et al. [2010]).

Methane clathrates are non-stoichiometric compounds with methane molecule hosted inside a cage-like structure of hydrogen bounded water molecules. For the remainder of the paper, we will use the term *clathrates* to refer to methane clathrates. Other forms of clathrates possibly found inside Titan in smaller amount, such as ethane and carbon dioxide clathrates, have similar bulk and seismic properties, so we use measurements made on methane clathrates to calculate the clathrate layers' seismic properties. Due to their large stability range, it has been hypothesized that clathrates should remain stable throughout Titan's hydrosphere and cryosphere, and inside the liquid water ocean (Lunine and Stevenson [1985, 1987], Choukroun et al. [2010]). For this reason, CH_4 clathrates could play a major role in Titan's methane cycle (Mousis et al. [2011], Atreya et al. [2006], Choukroun and Sotin [2012], Tobie et al. [2009]). Clathrates forming in Titan's interior and migrating

upward would subsequently dissociate when reaching the surface, releasing methane into the atmosphere. In addition to contributing to Titan's methane cycle, clathrates may also influence the dynamics of the surface ice shell. Indeed, clathrate thermal and bulk transport properties vary significantly from those of pure water ice. Notably, the thermal conductivity of clathrates is ≈ 0.5 W/m/K compared to water ices 2.5 W/m/K, while the viscosity is nearly 20 times higher for clathrates than pure water ice Ih (Waite et al. [2007], Helgerud et al. [2003, 2009], Hand et al. [2006]). Due to the important differences in transport properties compared to ice Ih, clathrates will likely alter the conductive ice shell thickness (Kalousová and Sotin [2020b], Kamata et al. [2019]), thermal profile, and heat flux through the ice shell. Convection in the ice shell will affect how materials are exchanged between the surface, ice shell, and subsurface ocean, and could have implications for the habitability of the ocean. A thinner, warmer ice shell, would allow for material to be more easily exchanged between the ice and the ocean. Furthermore, previous studies (e.g. Hemingway et al. [2013], Čadek et al. [2021], Carnahan et al. [2022]) have invoked or shown that clathrates can help explain Titan's topography and density in the ice shell.

Future missions, such as NASA's Dragonfly mission (Barnes et al. [2021a]), will investigate Titan's surface and interior to assess the potential habitable environments. Dragonfly's payload includes a seismic package which has the goal of constraining Titan's seismicity and internal structure (Lorenz et al. [2019]). Here, we model the effects methane clathrates have on Titan's thermal and seismic velocity profile to assess if a mission, such as Dragonfly, could help constrain the presence of methane clathrates within Titan's ice shell through seismology.

2.4 Methods

Previous studies investigated how a clathrate lid or the presence of clathrates may alter the thermal profiles of icy ocean worlds (Kalousová and Sotin [2020b], Kamata et al. [2019]). These 2D numerical studies solve for thermal convection with set depths for total ice thick-

ness. Here, we construct radial models of Titan's ice using the PlanetProfile (Vance et al. [2018b, 2022]) open-source software package, integrating the numerical results of (Kalousová and Sotin [2020b]) to include a 10 km clathrate lid at the top of a 100 km total thickness outer shell. We create a set of geophysically consistent models based on input parameters including moment of inertia, mass, total radius, and temperature at the ice-ocean boundary. We update PlanetProfile to allow for calculations using clathrate properties instead of pure water ice. This additional capability allows for computing the bulk and seismic properties of the resulting icy shells, and direct comparisons between the icy shell compositions and structures.

For the purposes of this comparative study, we maintain the same ocean and silicate compositions, surface conditions, and ice-ocean temperatures for both models we describe below. We set the surface temperature to 94 K and the surface pressure to 0 MPa. The ocean composition is set at 10% $MgSO_4$ (Vance et al. [2018b]). The silicate interior is roughly 48.82% SiO_2, 28.3%c MgO, 11% FeO, 8% Al $_2$ O_3, and 3% CaO. PlanetProfile uses $Perple_X$ (Connolly [2009]) to determine the equation of state for the silicate interior. We assume no metallic core. The modeled mineral assemblages do not include lower density minerals such as phlogopite that might explain the low density of Titan's interior (Néri et al. [2020]), so the total mass of each Titan model exceeds the actual mass but would only affect calculations at the very center of Titan. This discrepancy does not affect the physical parameters of the ice, which assumes depth-dependent gravity based on the actual mass of Titan. We set the ice-ocean temperature to 260 K which creates ice shells of roughly 100 km (Figure 2.1). To determine ice shell thickness, we calculated the pressure at which the ocean would freeze, given the ice-ocean temperature and ocean composition. The architecture of the PlanetProfile code builds the planet from the surface down, thus the ice shell thickness is determined by the depth at which the pressure from the overlying ice reaches the freezing pressure of the ocean. Since clathrates are slightly denser than water ice Ih, the clathrate

lid reduces the ice shell thickness, but by less than one kilometer. Once the thickness and boundary temperatures are set, we use the methods of Deschamps and Sotin [2001] to determine if convection occurs, and if it does, what are the resulting conductive and convection thicknesses and temperature profile. This approach is straightforward for pure water ice. We modify the approach for the clathrate lid as follows.

When the ice shell includes a clathrate lid, we use the values of heat flux (Q) and temperature of the convective layer(T_{conv}) from Kalousová and Sotin [2020b] to guide our approach. We benchmarked our pure water model against their pure water model to ensure they were in close agreement, justifying our use of heat flux and convective temperatures for the clathrate lid model.For simplicity we assume a 2D geometry, rather than spherical when calculating heat flux. We determine the overall thickness of the conductive lid using Fourier's law (Equation 2.1), where k, is the thermal conductivity, and $\frac{dT}{dZ}$ is the thermal gradient between the surface and the convective temperature.

$$Q = k\frac{dT}{dZ} \tag{2.1}$$

Because clathrates have a thermal conductivity of ≈0.5 W/m/K and pure water ice has a thermal conductivity value closer to 2.5 W/m/K, we split Equation 2.1 into two calculations. The first calculation (Equation 2.2) determines the temperature at the base of the clathrate lid (T_{clath}) using the heat flux, thermal conductivity of clathrates (k_{clath}), surface temperature (T_{surf}), and the thickness of the clathrate lid (h_{clath}).

$$T_{\text{clath}} = \frac{Qh_{\text{clath}}}{k_{\text{clath}}} + T_{surf} \tag{2.2}$$

$$h_{\text{ice}} = \frac{(T_{\text{conv}} - T_{\text{clath}})k_{\text{ice}}}{Q} \tag{2.3}$$

We then use T_{clath} along with the convective temperature (T_{conv}), and thermal conductivity

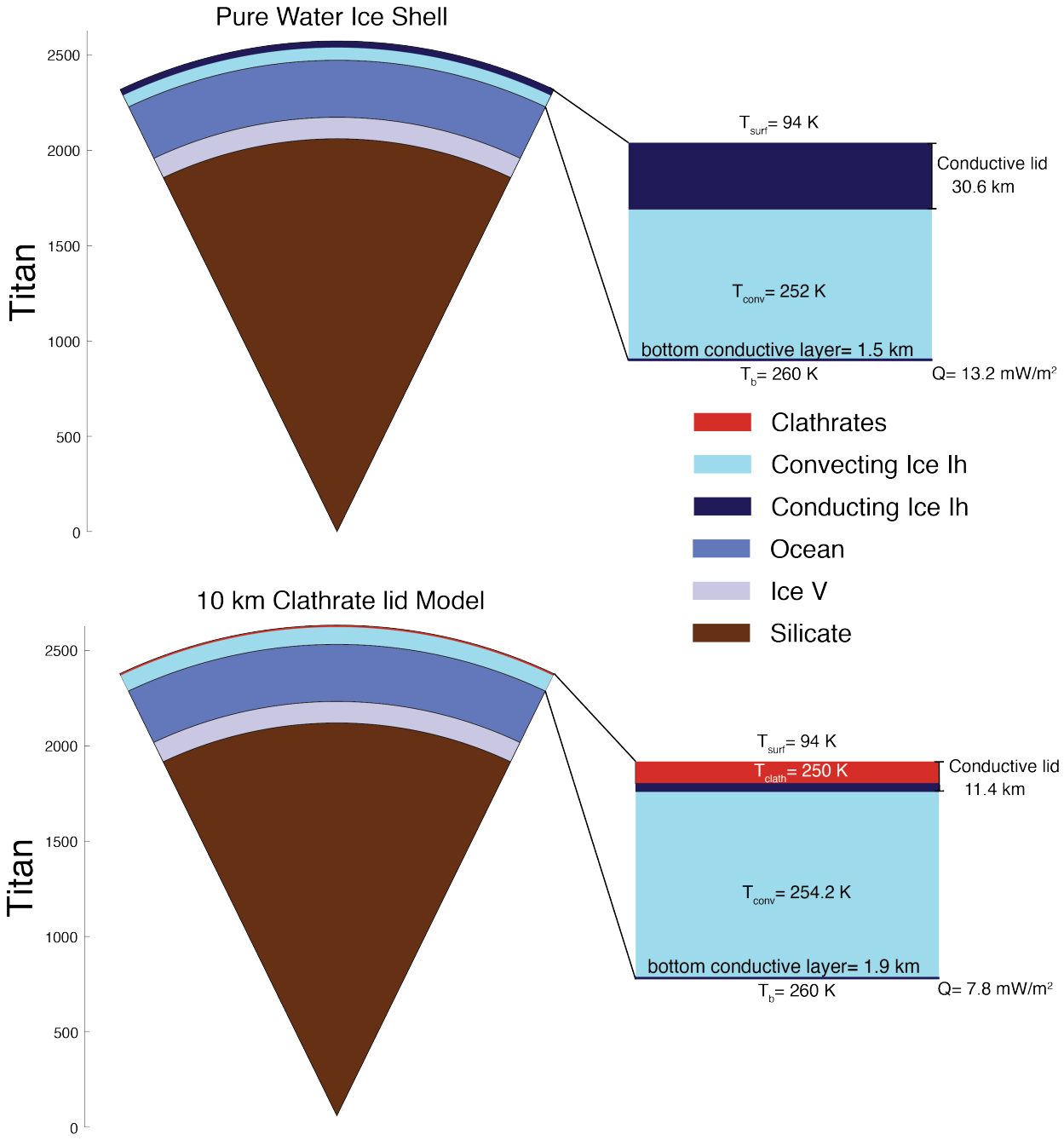

[tbp]

Figure 2.1: (Top) Wedge diagram of internal structure for a purely water ice shell. (Bottom) Diagram of internal structure with a 10 km clathrate lid. The figures are to scale, such that the thin clathrate lid (red) represents only a small fraction of Titan's cryo- and hydrosphere. The temperatures at the boundaries have been labeled, along with the layer thicknesses.

of ice (Andersson and Inaba [2005]) to determine the thickness of the conductive ice (h_{ice}). The total conductive lid thickness (e_{TBL}) is the sum of h_{ice} and h_{clath}. At the base of the ice shell there is a second conductive boundary layer between the convecting ice and the liquid ocean. We use Equation 2.3 to determine the thickness of this layer by finding the temperature difference between T_{conv} and the temperature at the ice ocean interface.

Once the pressure and temperature profile of the icy shell is determined, the bulk properties are calculated. We use the SeaFreeze library (Journaux et al. [2020a]) to calculate the pressure and temperature dependant properties of pure water ice phases (density, heat capacities, thermal expansion, seismic velocities). We use Helgerud et al. [2009] to determine bulk and seismic properties of clathrates based on pressure and temperature. With this approach we produce thermal and seismic velocity profiles for the two models, one with a pure water ice shell, and a second with a 10 km thick clathrate lid overlying a 90 km thick pure water ice shell. We select 10 km for the clathrate lid, as it represents a large lid thickness in which clathrates are still completely contained within the conductive portion of the ice shell which simplifies our calculations and models. Kalousová and Sotin [2020b] showed the conductive lid thickness and heat flux are highly dependent on grain size for clathrate lids smaller than about 10 km, thus by using a 10 km ice shell we do not have to make assumptions about grain size.For thin ice shells, the grain size determines convection rigor, which can further reduce the stagnant lid thickness. Thicker ice shells are less dependent on convection rigor, grain size, and viscosity but more sensitive to the effects of thermal insulation. Lastly, and most importantly, a 10 km lid has been shown to produce the greatest change in thermal profile (due to a thinning of the stagnant lid, and increase in convective temperature), thus we can measure the maximum effect on seismic velocities and resulting ground motions. We only alter the composition of the surface ice shells, meaning we assume any high-pressure ices beneath the ocean are pure water ices (e.g. Ice V, Ice VI).

Once we produce PlanetProfile seismic velocity profiles, the files are used as inputs for

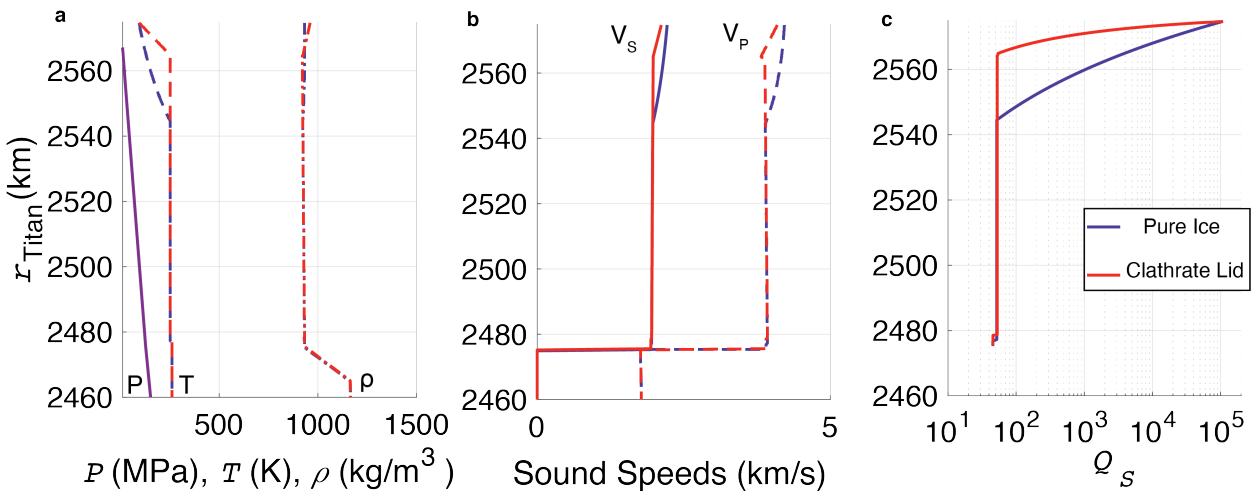

Figure 2.2: (a) Seismic velocities of a purely water ice shell (blue) compared to a 10 km clathrate lid (red). (b) The pressure profile (purple) is nearly the same for both models, but the temperature (dashed) and density (dotted) lines vary between the models. (c) Attenuation profiles also vary with depth. The difference in thermal profile creates the changes seen in the seismic and attenuation profiles. (The data used in this figure are available as the Data behind the Figure).

AxiSEM and InstaSEIS (Nissen-Meyer et al. [2014], van Driel et al. [2015]), open source codes which create seismic waveforms. To generate the waveforms, we set a dominant period of 2 seconds, a moment magnitude (M_w) of 3.1, source depth of 3 km, and a time length of 3600 s which was sufficient to investigate seismic phases that pass through the ice shell, ocean, and any reflections off the interfaces between the surface ice, ocean, high-pressure ices, and silicate interior. The chosen magnitude represents a plausible event size (Hurford et al. [2020]), but is completely arbitrary as we are comparing seismic events without any background noise and without instrument responses added. Receivers are placed across Titan's surface spanning 180 degrees and spaced every 1 degree, allowing us to investigate seismic events from nearly any distance with high spatial resolution. No noise is added to the waveforms, to allow more direct comparison of the arrival times and waveforms. We use the open-source code TauP (Crotwell et al. [1999a]) to calculate the predicted arrival times of seismic phases.

2.5 Results

We investigate how a model with a clathrate lid compares to a pure water ice shell model. We find that clathrates will significantly reduce the thickness of the conductive lid from $\approx$ 30.7 km to $\approx$ 10.5 km. Due to the reduction in the conductive lid thickness, the thermal profiles for pure water ice compared to a clathrate lid are significant (Figure 2.2 a).

Seismic velocities within the icy shell are largely controlled by temperature, such that seismic velocities decrease with increasing temperature at at rate of $\approx$ 2.5 km/s/K for compressive waves and 1.5 km/s/K for shear waves. Thus, changes in the thermal profile result in changes in the seismic profile (Figure 2.2 b). At surface conditions where both models have the same pressure and temperature, clathrate seismic velocities are 2.9% lower for shear (V_S) and 4.6% lower for compressive (V_P) velocities compared to pure water ice (Figure 2.3). Due to the higher temperature gradient, the seismic velocity gradient is also larger for a clathrate lid than for pure water ice. This change causes the differences in velocities between the two models to increase with depth, maximizing at a depth of $\approx 10km$, and then to decrease and eventually reach nearly zero once both models have pure water compositions and both are convecting at similar (within three degrees) temperatures. The clathrate lid also creates a small discontinuity at the clathrate-water ice interface, where the seismic velocity show a slight increase before continuing with a negative velocity gradient. At its maximum, the difference in velocities between the models reached $\approx$ 8.4% for both P and S waves.

Temperature not only affects seismic velocities, but also seismic quality factors (Q_s), the inverse measurement of attenuation (Figure 2.2 c). Following the approach of Cammarano et al. [2006], attenuation in the ice shell depends on temperature, such that warm ice will attenuate more seismic energy than cold brittle ice will. For the pure water ice model, Q_s is relatively high for the upper thirty kilometers. The high Q_s allows surface waves to retain high amplitudes even at great distances (Figure 2.5). For the clathrate lid model, Q_s decreases rapidly within the upper ten kilometers. This reduction in Q_s, greatly reduces

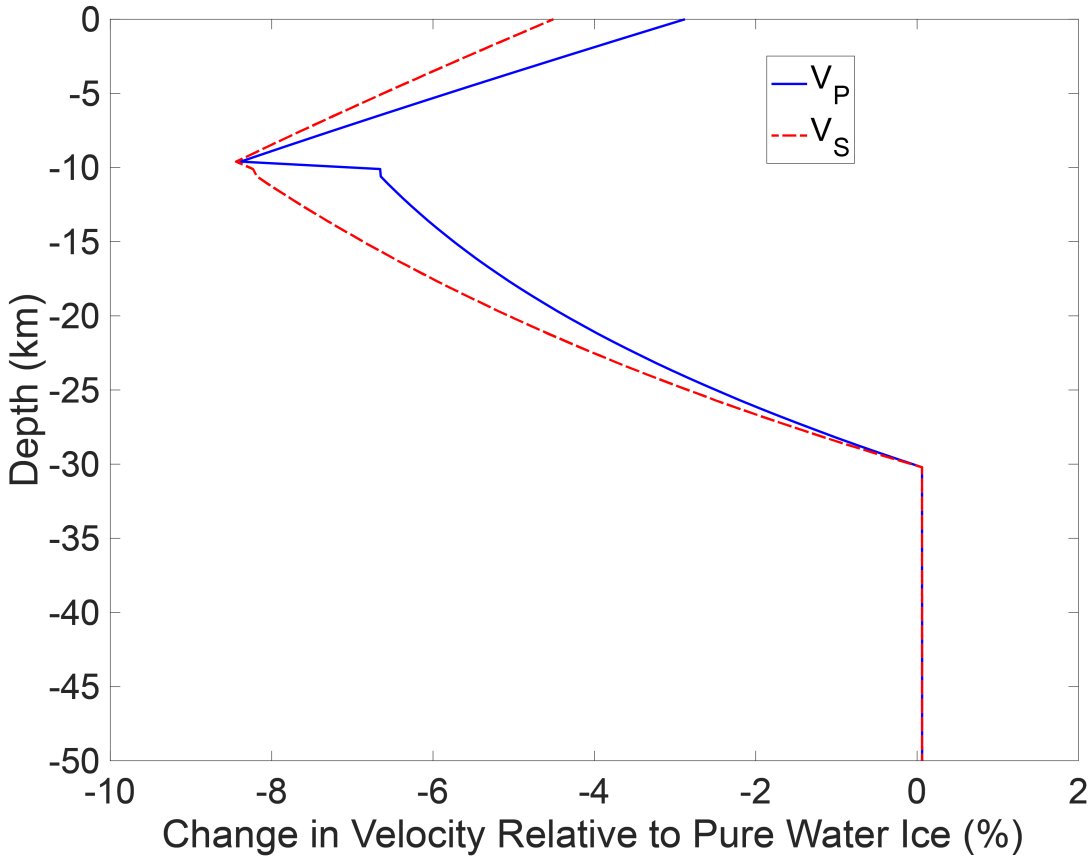

Figure 2.3: Change in velocity for P waves (blue) and S wave (red) with depth. At the surface, both internal structure models have the same pressure and temperature but clathrates have smaller seismic velocities. The differences are exacerbated down to the depth of the conductive lid where the differences reach over 8%. Once the temperatures, pressures, and compositions are near identical again, the seismic velocities are near identical.

surface wave amplitudes as distance between the event and receiver increases. The suppression of surface waves means a pure water ice model will produce average ground acceleration values up to 75 times greater than the clathrate lid model (Figure 2.4). Because clathrates act to suppress surface waves, while pure water ice maintains high amplitude surface waves, the amplitudes of body waves relative to surface waves could be used to identify a thin conductive lid, thus pointing to the presence of clathrates within the lid.

Changes in seismic velocity structure create changes in observable distances and arrival times for key seismic phases. For example, at a distance of 20 degrees, the clathrate lid

delays the arrival of P waves reflecting off the ice-ocean interface by 2 seconds, at 30 degrees the S reflection is likewise delayed by ≈ 1.5 seconds. It is worth noting that differences on the order of a few seconds are typical uncertainties seen by the InSight Mars Quake Service (MQS, Giardini et al. [2020]) so differences of a few seconds may be difficult to detect. See Section 2.6 for further details.

To further investigate the effects on surface waves, we invoke the open-source code, Mineos (Masters et al. [2011]), to investigate surface wave dispersion. We supply the Mineos code with the two interior structure models from PlanetProfile. We look at both spheroidal and torodial modes with angular orders up to 3000 and frequencies up 200 Hz. We show in Figure 3.2 that there are slight differences in the dispersion characteristics between pure ice and clathrate-lid models. However, the differences between clathrate model values and pure ice model values are within 2% of each other, indicating that surface wave dispersion could be another tool to determine whether or not clathrates are present in Titan's surface ice shell, but would require very high precision and accuracy in measurements.

2.6 Discussion

Using PlanetProfile with updated parameters from Kalousová and Sotin [2020b] we show that clathrates will reduce the thickness of the conductive lid, thus altering the thermal profile of Titan. Because seismic velocities and quality factors depend on temperature, a clathrate lid overlying pure water ice will produce different seismic responses than a model composed purely of water ice. At most, the seismic velocities in the clathrate lid will be reduced by 8.4% compared to pure water. On Earth, the average seismic velocity is well known (Dziewonski and Anderson [1981], Kennett and Engdahl [1991]) and tomographic studies have been able to discern variations down to a few percentages (≤ 5) (Anderson and Dziewonski [1984], Grand et al. [1997]). However, previous planetary missions like InSight and the Apollo seismic experiments have not benefited from numerous and dense

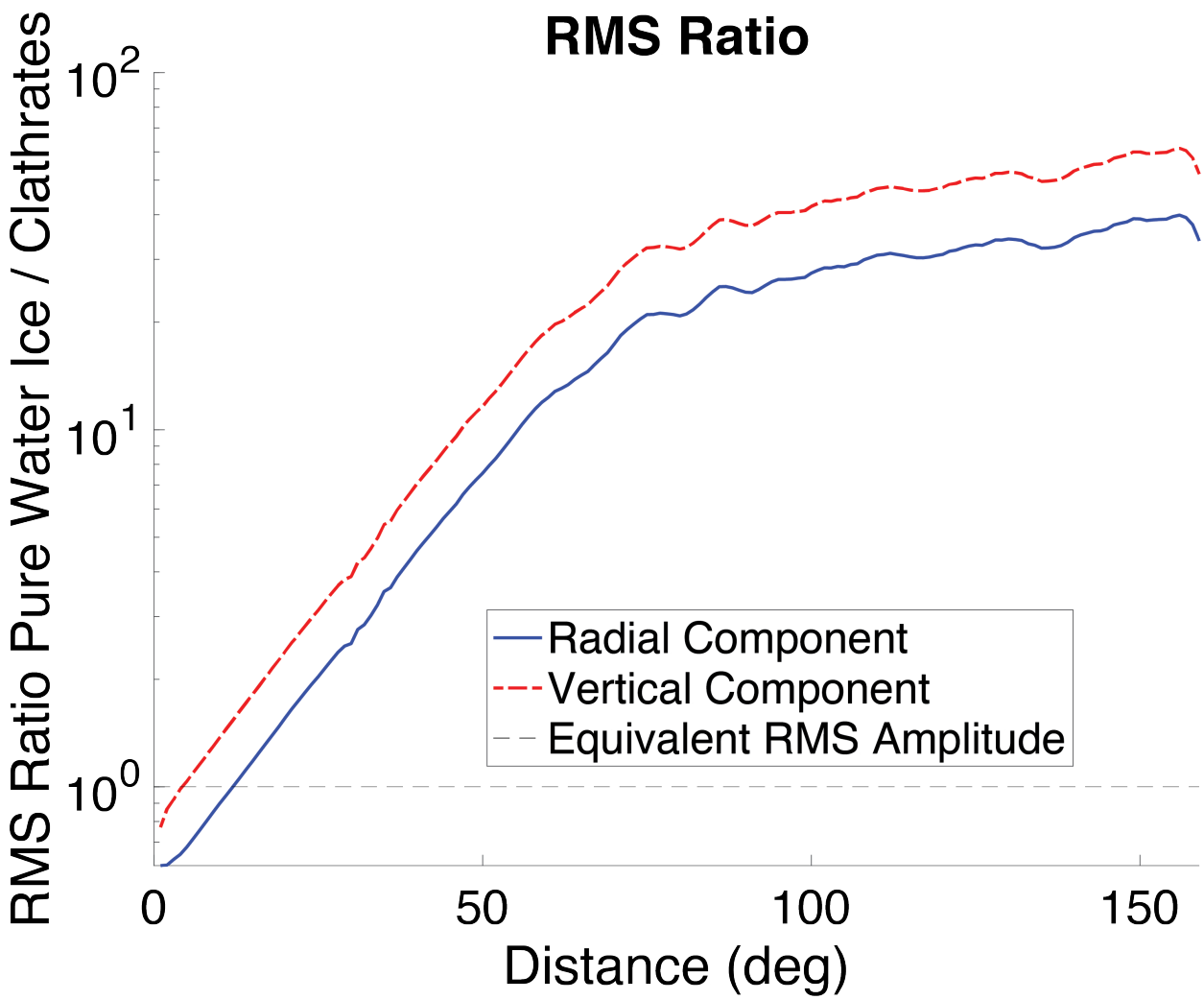

Figure 2.4: Root mean square (RMS) comparison of pure water ice shell to clathrate lid waveforms. The RMS rati o for the radial (blue) and vertical(red) components are plotted versus distance. Values greater than 1.0 (dashed gray) indicates the clathrate lid model has greater amplitudes than the pure water ice model.

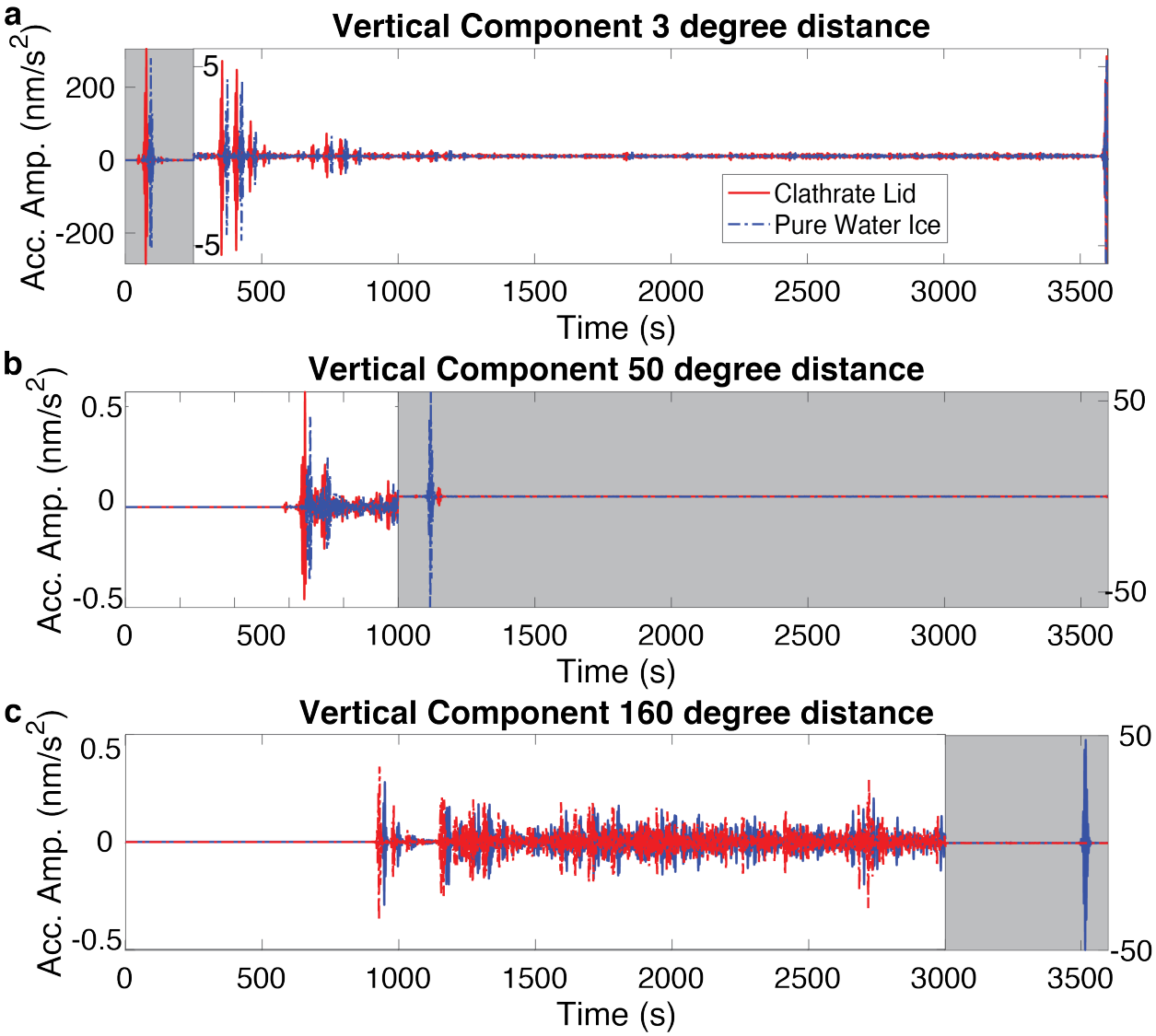

Figure 2.5: Vertical component of a M_w 3.1 event at epicentral distances of (a) 3 degrees, (b) 50 degrees, and at (c) 160 degrees. Pure water (blue) is compared to a clathrate lid (red). To show both body and surface waves, the gray shaded areas have different y-axis limits. In the first plot, the clathrate lid model has higher amplitudes than the pure water ice model. In the bottom two plots, the pure water ice model has greater amplitudes for surface waves but comparable amplitudes for body waves.

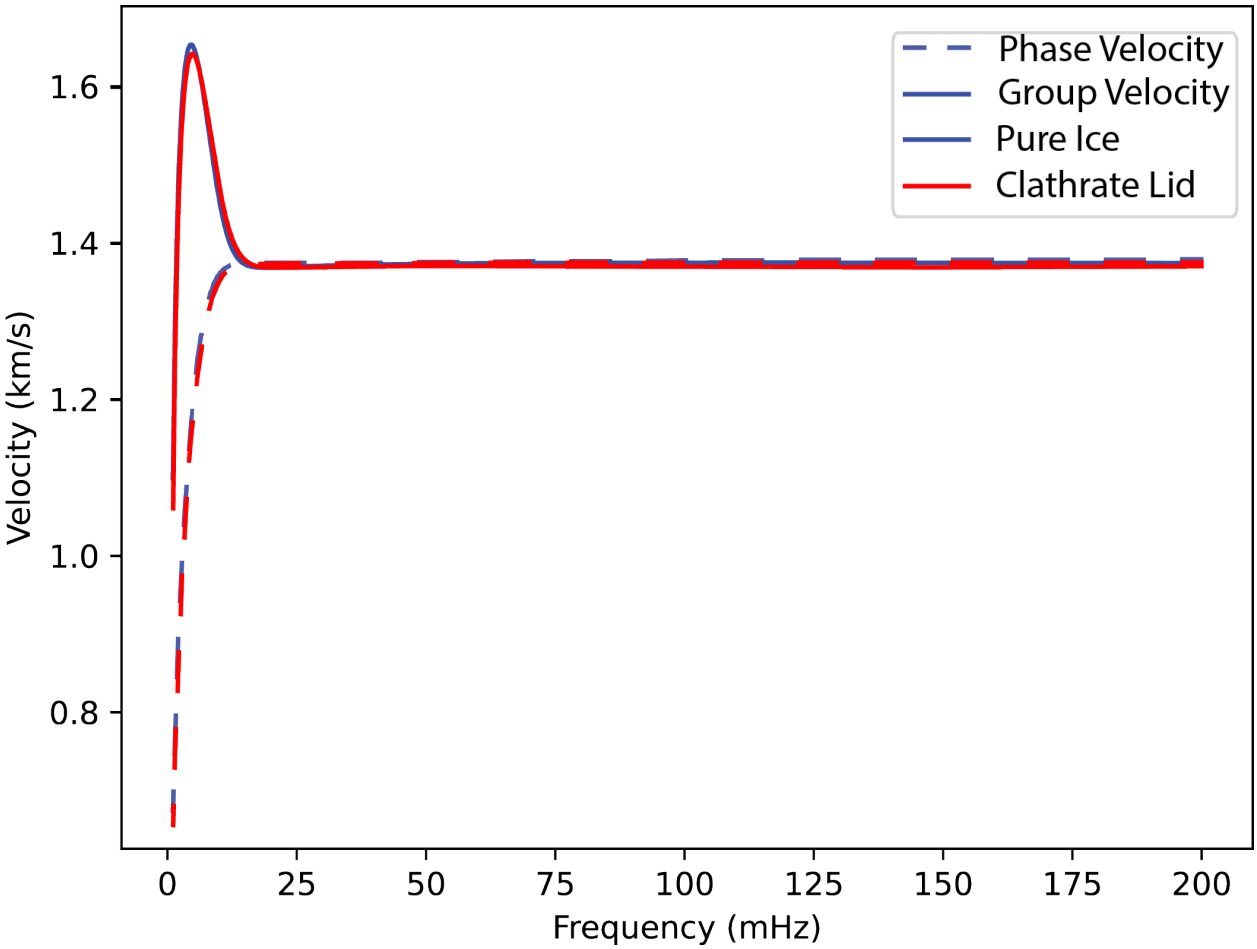

Figure 2.6: We compare the dispersion curves for group (solid) and phase (dashed) velocity using the pure ice model (blue) and the clathrate-lid model (red). The differences are subtle and minor.

seismic arrays nor frequent teleseismic events that occur on Earth. Due to the limited numbers of stations and scarcity of large events, the inferred internal structures for the Moon (Garcia et al. [2019]) and Mars (Knapmeyer-Endrun et al. [2021], Khan et al. [2021], Stähler et al. [2021]) have uncertainties in velocities that exceed 10%, and corresponding errors in boundary locations on the order of several kilometers. To distinguish between the models presented here, a seismic investigation would need to recover internal structure with uncertainties less the 8%, ideally less than 5%. It may be possible to reach those levels of uncertainty, but it would require recording numerous high-quality seismic events for which the source location could be derived, and the seismic phases need to be well constrained. The

InSight MQS team typically reports uncertainties in seismic phase arrivals ranging from ≈ 1 second up to tens of seconds for some reflection phases. The locations and depths also have uncertainties on the order of several degrees in epicentral distance and several kilometers in depth, even for the highest quality events.

In addition to arrival times of body waves, the surface waves will also be affected by the presence of a clathrate lid. The increased attenuation of the comparatively warmer ice will reduce the amplitudes of surface waves traveling through Titan's clathrate lid compared to those traveling through colder, brittler, pure-water ice. Because body waves do not exclusively travel through the surface ice layers, the amplitudes of body waves for both models are comparable. The relative amplitudes of surface waves and body waves may help indicate if a clathrate lid is present, particularly at longer distances. In the shallow parts of the ice shell, the temperature-based model of seismic attenuation from Cammarano et al. [2006] predicts high Q values, but as discussed in Panning et al. [2018], attenuation in very low temperature ice is not well-constrained. If the cold ice has a much lower quality factor, the difference between the two models would be reduced. Surface waves can also be suppressed if the source event has a deep source.

If the quality of waveforms is sufficiently high, the arrival times and amplitudes of seismic phases may help indicate if clathrates are present. Figures 2.5 and 2.4 indicate there are subtle differences between the body waves, but significant differences in surface wave. Surface wave dispersion could also be implemented, but the differences between the two models are subtle. However, these waveforms and Mineos models include no added background noise, precisely known location and timing of the event, and assume Titan is radially consistent with no porosity or lateral heterogeneity. The atmosphere, Titan's lakes, and surface roughness will create seismic background noise and create scattering effects (Stähler et al. [2019], Lorenz et al. [2021b]). Topography along the ice-atmosphere and ice-ocean boundary can also alter the relative arrival times of seismic phases. The thermal profile of Titan might also be

altered by organic sands, which can lower the thermal conductivity more than clathrates can (Schurmeier and Dombard [2018]). The sands may mimic the effects of clathrates, thus making it hard to distinguish between the materials. Lastly, physical and/or chemical heterogeneity within Titan's ice shell will also create variations in travel times and waveform amplitudes. The anomalies may be caused by changes in porosity, changes in concentration or depth of the clathrate lid, organic sand infilling craters, or entrained liquid water or methane. For these reasons, the differences in the waveforms of the two models may be trivial and non-unique once background noise and the above factors are considered.

For a seismometer to constrain the presence of clathrates within Titan's ice shell, numerous high quality events need to be recorded. The arrival times and waveforms can be used to recover the seismic velocity profile of Titan, which can inform on the thicknesses of the conductive lid. If the seismic velocity structure can be recovered with high precision, it might be possible to determine whether or not clathrates are present. A better understanding of Titan's current internal structure, thermal profile, and composition will help inform how Titan might have evolved to its current state and place constraints on Titan's history.

2.7 Conclusions

Methane clathrates will insulate the icy shell of Titan. Compared to a shell composed of pure water ice, an ice shell with a clathrate lid will have a reduced conductive lid thickness and smaller seismic velocities. The difference in seismic velocities could reach up to $\approx 8.4\%$. Changes in the seismic velocity will result in changes in arrival times and amplitudes of seismic phases. However, these changes are subtle and would require high-quality seismic events. Background noise, heterogeneity, and topography may make it difficult to pick arrival times and will introduce uncertainty in the seismic velocity profile. If the seismic profile is known with $\leq 5\%$ uncertainty, or if the conductive lid thickness and total ice thickness is well constrained, seismology can help constrain whether clathrates are present in Titan's

surface ice shell.

2.8 Acknowlegments

A part of the research was carried out at the Jet Propulsion Laboratory, California Institute of Technology, under a contract with the National Aeronautics and Space Administration (80NM0018D0004). Copyright 2022. We thank two anonymous reviewers for their constructive remarks that helped improve this manuscript.

2.9 Data Availability Statement

The interior structure models were made using PlanetProfile v1.2, which is available through Github (https://github.com/vancesteven/PlanetProfile)(DOI:10.5281/zenodo.6323610). Additional software, Axisem, InstaSeis, and Mineos are also open source and available for download through the Computational Infrastructure for Geodynamics software page (https://geodynamics.org/cig/software/). The resulting interior structure models, seismic waveforms, and dispersion curves will be made available on NASA's Open Data Portal (https://data.nasa.gov/Space-Science/Interior-Structure-Models-and-Modelled-Seismic-Res/awki-gbbc).

2.10 Addendum: Investigating Detection of Methane Clathrates with Varying Source Depths on Titan

In addition to the findings on Marusiak et al. 2022 (aforementioned in this chapter) I will present some of my findings of the changes to the models with depth for the following models (Figure 2.7). Using the interior structure models as inputs, I simulated four source depths (Table 2.1) and illustrated in Figure 2.8, or titanquake hypocenters for each interior structure model. Waveform propagation is simulated using AxiSEM (Nissen-Meyer et al. [2014]), the

spectral element solver, to model the global wavefield of Titan for each of the source depths. The source depths fell into two regimes, namely shallow quakes and deep quakes. The shallow quakes take place within the top ice layer, at 3km (within the clathrate layer, if present) and 25km (within the pure water ice), while the deep quakes take place within the high-pressure ice and the silicate interior, or 411km and 525km, respectively.

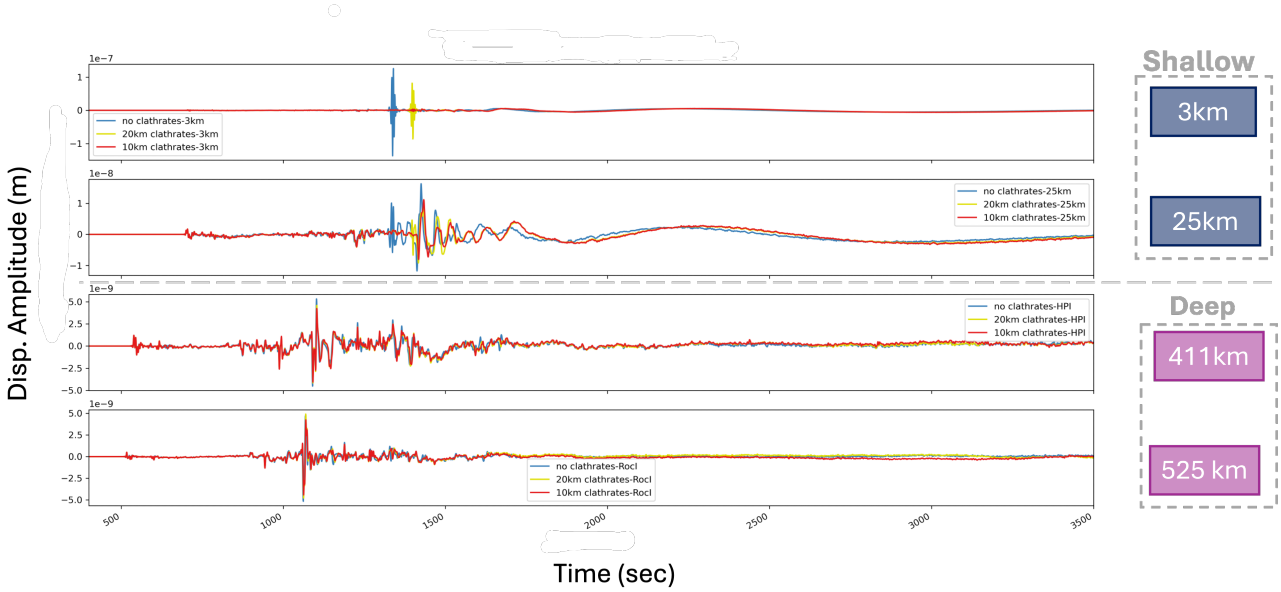

Figure 2.7: Seismograms recorded over one hour, with a vertical orientation at 61 degrees. The seismograms represent different layers: a 100 km pure water layer (blue), a 10 km methane clathrate lid (red), and a 20 km methane clathrate lid on pure water ice shells (yellow), all above a 10%$MgSO_4$ ocean (Vance et al. [2018b], Marusiak et al. [2022], Styczinski et al. [2023a]). The sources are located at depths of 3 km, 25 km, 411 km, and 525 km (top to bottom) (Table 2.1, Figure 2.8).

Source Depth	**Layer**
3km	ice shell
25km	ice shell
411km	high pressure ice
525km	rocky (silicate) interior

Table 2.1: Source depths modeled and corresponding layers

2.10.1 Methodology

I generated three, spherically-symmetric interior structure models using PlanetProfile—a MATLAB software used for constructing thermodynamically self-consistent one-dimensional interior structure models (Journaux et al. [2020a]). These interior structure models all contain a 100 km thick ice I layer with varying clathrate thickness, a pure water ice shell containing no clathrates, and clathrate-lids thicknesses of 10km and 20km respectively.

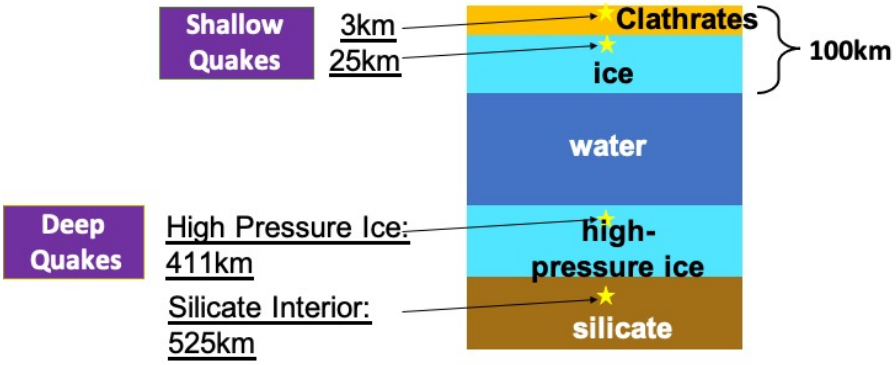

Figure 2.8: Schematic of the Source Depths Simulated with AxiSEM and Instaseis. Shown is the schematic for a 20km clathrate lid. Note the two quake regimes: Shallow (3km and 25km) and Deep (411km and 525km).

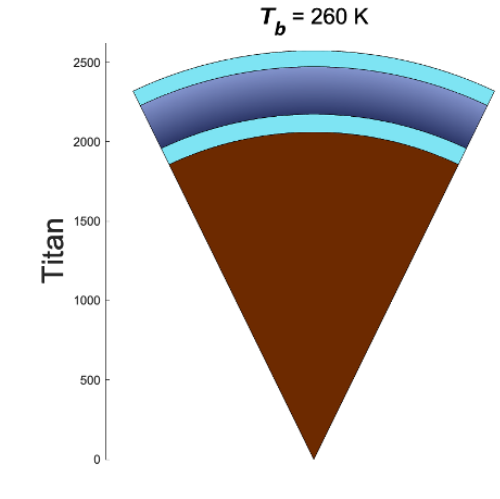

Figure 2.9: Output from *Planet Profile* (Journaux et al. [2020a], Styczinski et al. [2023a])– 100km ice shell, the temperature at the base of the top ice shell is 260K. Seismic data obtained from this software informed *AxiSEM* (Nissen-Meyer et al. [2014]).

The Python package *Instaseis* (van Driel et al. [2015]) was used to reconstruct seismograms for hypothetical source and receiver location from the AxiSEM models. The *TauP* software package was used to calculate theoretical arrival times (Crotwell et al. [1999b]).

2.10.2 Results & Discussion

Deep vs. Shallow Events

Of all the twelve model runs (from 3 different structural models and 4 different source depths), the shallow events produced the largest amplitudes. The most notable feature in the shallow events was a large Rayleigh pulse, although this varied as a function of the different attenuation structure of the models due to different thermal profiles due to the lower thermal conductivity of clathrates. Models run with a high level of seismic attenuation (low Q values) lacked the large Rayleigh pulse. We found that the seismic amplitudes differed within several orders of magnitude depending on the source depth (Figure 2.11).

I also present the complete seismograms for all the source depths (Table 2.1, Figure 2.8) in Figure 2.7. There is can be seen that as expected the 3km quakes have the highest ground displacement amplitudes, the 25km quake are an order of magnitude less in peak amplitude ($\approx 1.5e^{-8}m$). The sources within the high pressure ice and rocky interior have peak ground displacement amplitudes, 2 orders of magnitude lower, both $\approx 5e^{-9}m$. The deeper quakes (high pressure ice and rocky interior) do have earlier arrival times overall, as demonstrated by the P waves arriving just after 500 seconds and the Rayleigh wave just after 1000 seconds for the deeper event. In contrast, the shallower events from within the ice shell have P wave arrival around 700 seconds and and the Raleigh waves around just before 1500 seconds, also with a flexural wave (that is seen better in the 25km deep event).

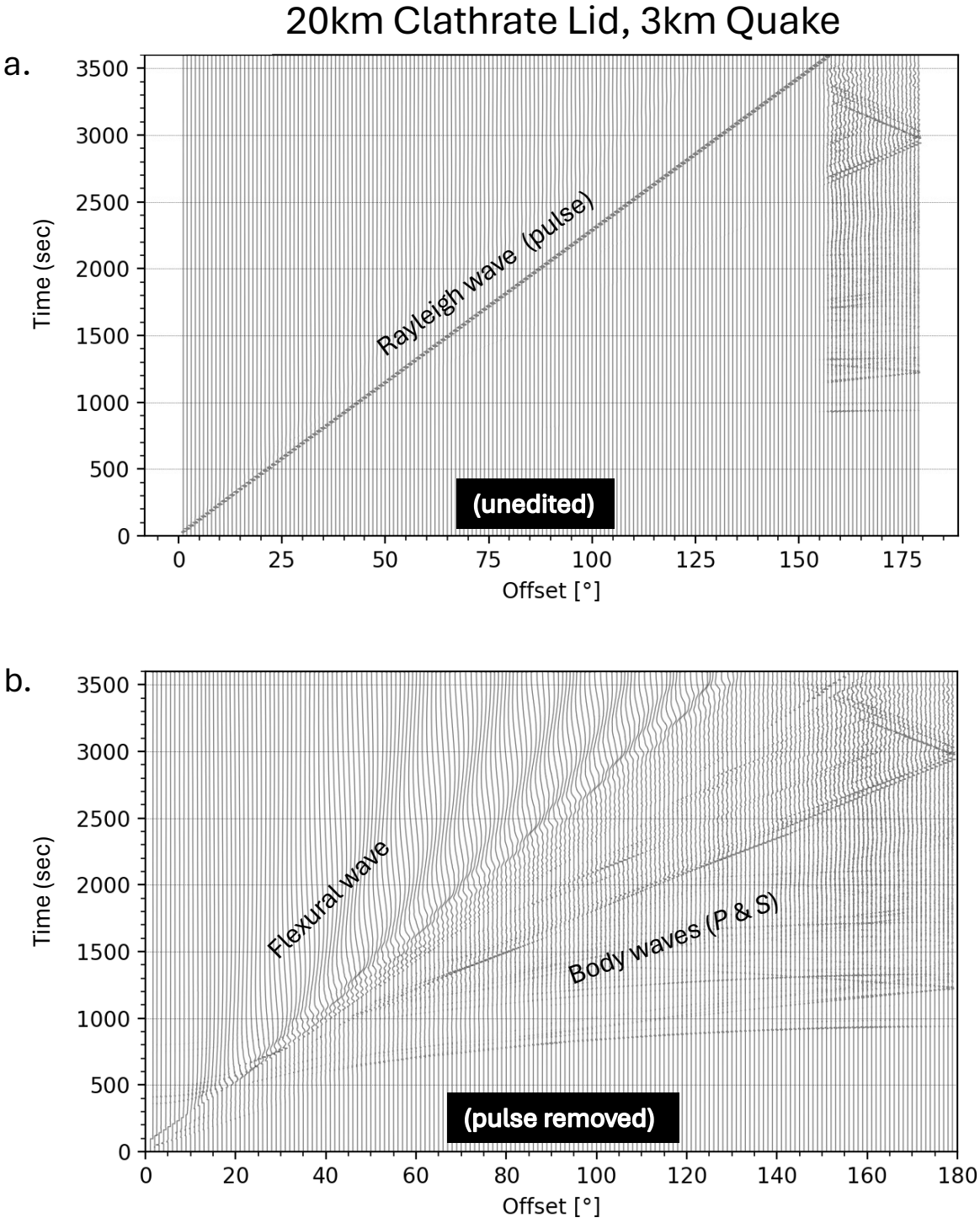

Figure 2.10: A strong Rayleigh pulse seen within a record section from a Titan model with a 20km clathrate lid, with the titanquake originating 3km from the surface (original data). a. unedited, b. the Rayleigh wave (pulse) has been cut out of the seismograms to show the body waves and surface waves.

Clathrate Lids

In agreement with (Marusiak et al. [2022]), we found that P and S wave sound speeds slightly decrease in the presence of methane clathrates versus pure ice. Surface waves therefore travel slightly slower in the presence of clathrates versus pure ice. This is clearly seen in the Figure 2.12 where a Rayleigh pulse is seen first within the pure-ice seismogram (blue), while the Rayleigh pulse is seen within the 20km clathrate-lid (magenta) at a later time and also at a lower displacement amplitude.

The Rayleigh pulse becomes small in the 10km clathrate-lid due to a very thin thermal lid (Figure 2.12: orange). The thinner thermal lid leads to a higher temperature and lower Q, and therefore results in reduced seismic amplitudes, particularly seen in the Rayleigh pulse.

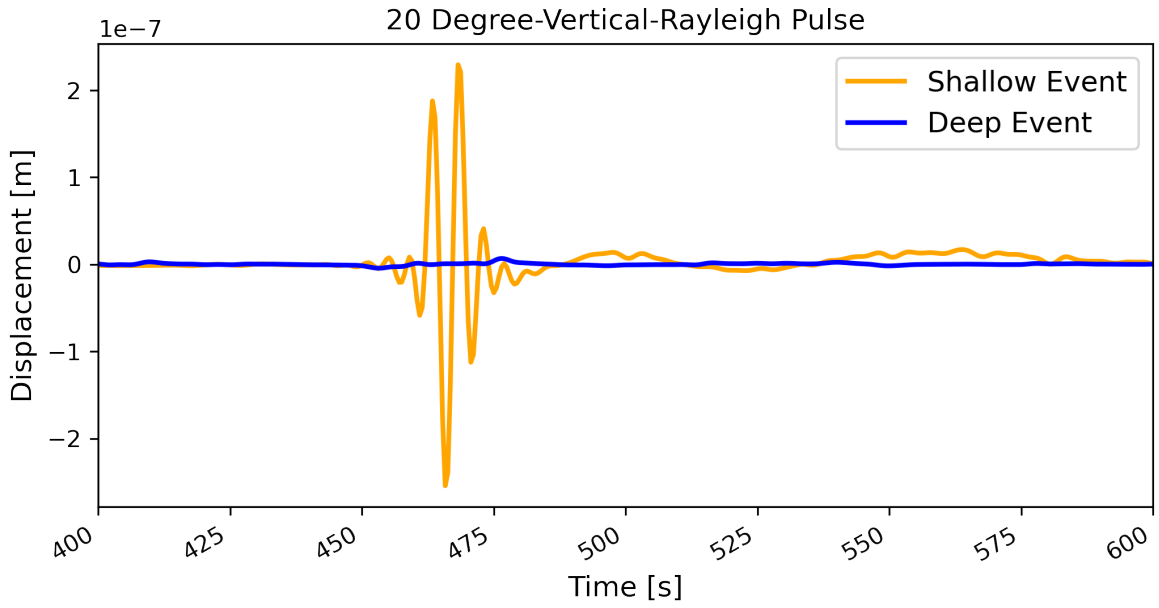

Figure 2.11: Displacement [m] versus Time [s] for a 20 Degree titanquake, Vertical Component. Both seismograms correspond to events that lack a clathrate lid. The Shallow Event is a 3km quake and the Deep Event is a 525km quake within the rocky interior of Titan. The time interval is from 400 to 600 seconds in order to zoom in on the Rayleigh pulse present within the Vertical component.

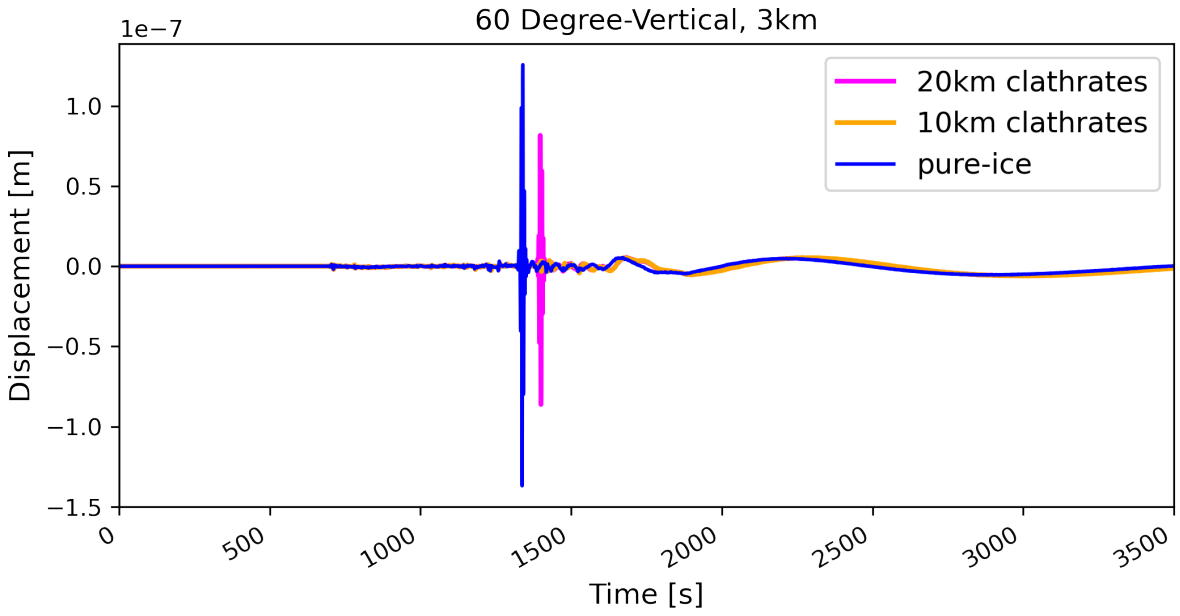

Figure 2.12: Displacement Amplitude [m] versus Time[s] for a 60 Degree, Vertical Component, 3km source depth titanquakes for 20km and 10km clathrate-lid (magenta and orange, respectively), and pure-ice (blue). Total seismogram duration is 1 hour, 3600 seconds, with the last 100 seconds clipped due to edge effects.

Probabilistic Power Spectral Density

I plot the probabilistic power spectral density (PPSD) for a simulated 3km deep quake within a 100km total ice shell thickness with 20km of methane clathrates on the surface, under Titan-like temperatures and pressures, based upon the mass & moment of inertia measurements taken by the *Cassini* spacecraft (Lopes et al. [2019], Hayes et al. [2018], Lebreton et al. [2009]). Plotted in Figure 2.13, in the background is the probability density function amplitude of the power of the ground acceleration from a magnitude 3 event at a depth of 3 km generated from 180, 1 hour long segments, each separated by one Titan distance degree, ,(45 km). I report comparisons to the following seismological instruments: the Trillium compact seismometer, STS2 seismometer, a 10Hz geophone, the SP Imperial seismometer used in the InSight mission on Mars, and the JAXA PSS seismomometer. The peak signal and the mean power spectral density of the sample is also shown. The PPSD includes an Earth noise model as well.

We see that the highest amplitude events would be detectable by a JAXA PSS seismometer (similar to the one that will be on Dragonfly), with a sensitivity of events between $\approx 3 - 12$ second periods or between frequencies of $83 - 333$ mHz.The STS2 seismometer is the most sensitive (being sensitive to the mean PSD). Could detect frequencies down to about ≈ 7 mHz and up to ≈ 384 mHz. In contrast, a 10 Hz geophone would most likely not be able to detect this event.

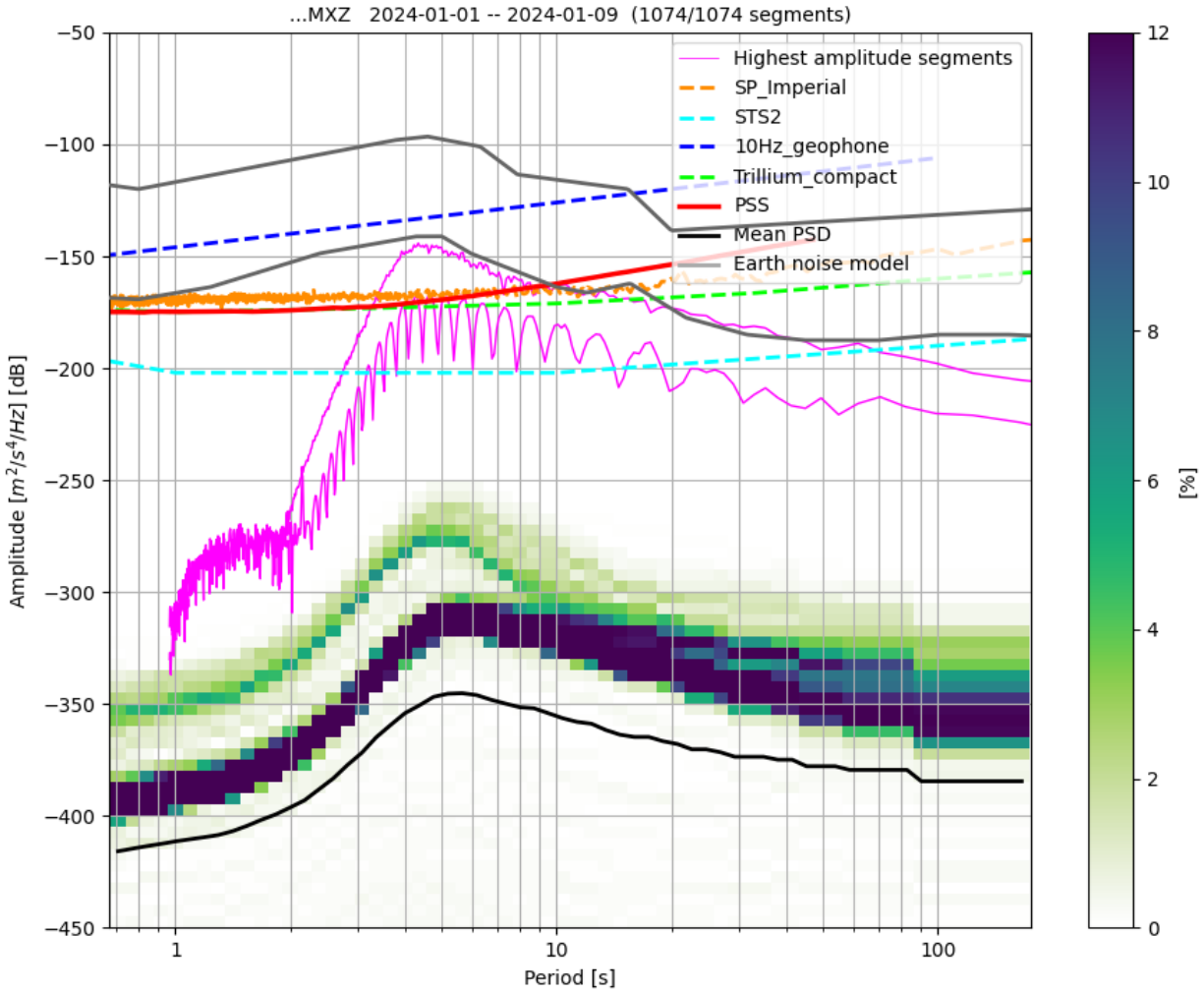

Figure 2.13: A PPSD for a simulated 100km ice shell (total thickness) with the top 20km being methane clathrates, 3km source depth. The background colors are the probability density function amplitude of the power of ground acceleration generated from 180, 1 hour long segments, each separated by one Titan distance degree, $\approx 45km$. Dashed lines: (lime) Trillium compact seismometer (Ringler and Hutt [2010]), (teal) STS2 seismometer, (blue) a $10Hz$ geophone (Rodgers [1994]). Solid lines: (black) the mean probabilistic spectral density (PSD) of the models, (orange) SP Imperial seismometer, (red) JAXA PSS seismometer, (gray) Earth noise model, (pink) highest amplitude segments from the seismograms. Done according to (Panning et al. [2018]).

CHAPTER 3

LONG PERIOD SEISMOLOGY IN THE PRESENCE OF A CLATHRATE-LID ON TITAN

3.1 Preface

In this chapter I present a paper in which I am the first author and in which I created every figure as well wrote/accepted edit suggestions for the words. The writing was edited most heavily by my coauthors Angela Marusiak-Schools, an assistant research professor at the University of Arizona as well as, my Jet Propulsion Laboratory (JPL) (dissertation) advisor Mark Panning. I also acknowledge Marshall Styczinski's help in editing, especially in regards to formatting. This work began on a sunny day at JPL, I was pondering what further types of analysis could be done to determine methane clathrates on Titan, the focus of the first chapter.

3.2 Long Period Seismology on Titan in the Presence of a Methane Clathrate Lid

This paper was submitted for publication by the American Geophysical Union in their *Earth and Space Science* journal in April 2024.

3.2.1 Author List

Andrea S. Bryant (1), Mark P. Panning (2), Angela G. Marusiak (3)

1. University of Chicago, Department of Physics, Chicago, IL
2. Jet Propulsion Laboratory, California Institute of Technology, Pasadena, CA
3. University of Arizona, Lunar and Planetary Laboratory, Tucson, AZ

Andrea S. Bryant, asbryant@uchicago.edu is the corresponding author

3.2.2 Key Points

- Based on simulations, the Rayleigh wave signal is dominated by the first overtone at frequencies > 20 mHz
- Given likely measurement uncertainty, it is unlikely that we can resolve clathrate layers in thick ice shells of icy ocean worlds
- We resolve the frequency range of flexural waves transitioning to a Stoneley wave (mode) in the fundamental mode, and see a Rayleigh wave in the first overtone for a 100 km ice shell on Titan for a $M_w = 3$ quake

3.3 Abstract

Previous 1-D spherically symmetric seismic modeling studies have shown that in the presence of a clathrate lid on Titan significant thermal profile differences result, particularly in comparison to a pure water ice shell. In turn, these thermal differences would lead to notable changes in the waveform amplitudes and seismic phase arrival times. In this study we investigate the feasibility of using surface waves dispersion to explore the structure of Titan's ice shell. We investigate the ability to measure and observe the frequency-dependent signals ($0.003 - 0.100$ Hz) and their utility in being able to detect existence of a methane-clathrate lid. We find that we are unlikely to resolve the clathrate-lid's existence using long-period techniques, and this could be a limitation for studying very thick ice shells ($>\approx 20$ km) of icy ocean worlds. We did resolve the frequency range of flexural waves transitioning to a Stoneley wave (mode) in the fundamental mode, and see a Rayleigh wave in the first overtone for a 100 km ice shell on Titan for a simulated quake.

3.4 Introduction

Titan is of much interest as it is one of the largest moons of in the Solar System and contains both an atmosphere and a subsurface ocean. On its surface there are sand dunes of organic material and methane lakes. The ice shell is thought to be $45 - 120$ km thick (Mitri and Showman [2008], Deschamps et al. [2010], Vance et al. [2018b], Durante et al. [2019]), and beneath the thick ice is an ocean greater than 80 km in depth (Stähler et al. [2017], Sotin et al. [2021], Sohl et al. [2003], Grasset et al. [2000]). On Titan, seismology is a potentially powerful tool that may uncover many of Titan's secrets including but not limited to; the ocean depth and chemistry, ice thickness, presence or lack thereof of high-pressure ice phases, and silicate interior properties. Insights into these scientific parameters have broader implications for studies of astrobiology and habitability of the Titan system, especially given Titan's unique surface conditions (being the only body beyond Earth in the Solar System to currently have long-lasting liquid on its surface) (Stofan et al. [2007], Lopes et al. [2007], Hayes [2016]).

Much knowledge about Titan has been obtained from data from the *Cassini–Huygens* mission to the Saturnian system (Lopes et al. [2019], Hayes et al. [2018], Lebreton et al. [2009]). Using Schumann resonance, the first direct estimates of the ice shell were given: $55 - 80$ km, in line with earlier internal structure models (Béghin et al. [2012], Tobie et al. [2005], Sohl et al. [2003], Lorenz and Le Gall [2020]). However, investigations from *Cassini–Huygens'* electric field, geophysical, and gravitational data suggest that Titan's ice shell could be anywhere from $25 - 200$ km thick (Tobie et al. [2006], Mitri and Showman [2008], Deschamps et al. [2010], Nimmo and Bills [2010], Béghin et al. [2012], Iess et al. [2012], Hemingway et al. [2013], Baland et al. [2014], Sohl et al. [2014], Durante et al. [2019]). Due to Titan's high gravitational moment of inertia factor (0.341) (Durante et al. [2019]), a metallic core is not expected from compositional models (Vance et al. [2018b]). A diverse abundance of organics have been shown to be present in Titan's surface and atmosphere, from *Cassini–Huygens* and Earth-based measurements (Barnes et al. [2021a], Niemann et al.

[2005], Cordiner et al. [2015, 2018], Janssen et al. [2016], Hörst [2017], Lai et al. [2017], Thelen et al. [2019, 2020], Nixon et al. [2020]). In particular, organics created in the atmosphere can settle over Titan's bedrock composed of water–ice (Barnes et al. [2021a], Rodriguez et al. [2006], Barnes et al. [2007], Soderblom et al. [2007], Le Mouélic et al. [2008], Janssen et al. [2009, 2016], Hayne et al. [2014], Neish et al. [2015], Lopes et al. [2019]).

Since the *Huygens* probe was only able to directly image Titan's surface and give rough estimates of the interior structure, many questions remain outstanding (Marusiak et al. [2021], Elachi et al. [2005], Porco et al. [2006], Iess et al. [2014]). For example, the dynamics and internal structure of the ice shell are still not well understood (Marusiak et al. [2021], Carnahan et al. [2022]). However the use of a geophysical suite including seismic instrumentation may uncover key unknowns about Titan in the coming decades (i.e. the Dragonfly mission) (Lorenz et al. [2018], Turtle and Lorenz [2021]). To investigate various aspects of Titan, much work has been done using the data from *Cassini–Huygens*, and much more work remains ongoing in preparation for the upcoming Dragonfly mission. The main expected sources of seismic events are thought to be ice cracking driven by the tidal cycles of Titan from Saturn (Marusiak et al. [2021], Hurford et al. [2020]), although there remains a number of other potential seismic sources, e.g., active cryovolcanoes hidden beneath the ice (Schurmeier et al. [2023]). Both the hydrocarbon lakes and atmosphere of Titan will also contribute background seismic noise, similar to Earth's background seismic noise due to Earth's oceans and atmosphere (Gutenberg [1947], Dybing et al. [2019], Stähler et al. [2019]).

NASA's *Dragonfly* mission is currently scheduled to launch in 2028 and land on Titan in the mid-2030s. *Dragonfly* is largely an astrobiological mission, with the search for prebiotic chemistry as an overarching theme of its mission goals (Lorenz et al. [2018], Turtle and Lorenz [2021], Barnes et al. [2021a]). It's target landing site is near Selk crater (80 km diameter), a location where liquid water once mixed with surface organics (Barnes et al.

[2021a], Lorenz et al. [2021a]). The rotorcraft itself is a dual-quadcopter that will hold many astrobiology-focused instruments, including the DraGMet (Dragonfly Geophysics and Meteorology) instrument package, containing a seismometer and two geophones to measure seismicity (Lorenz et al. [2021b], Barnes et al. [2021a]).

Seismology is a robust tool that will reveal details of interior structures of planets where it otherwise would have been difficult or non-unique. Seismometers were placed on the Moon during the Apollo landings and measured thousands of deep and shallow moonquakes that revealed secrets of the lunar interior (Nakamura et al. [1982], Nunn et al. [2022, 2020]). Additionally, data from the *InSight* lander revealed the interior of Mars including the core, crust and upper mantle compositions (Stähler et al. [2021], Knapmeyer-Endrun et al. [2021], Khan et al. [2021], Banerdt et al. [2020]). More plans are in the works for what we can learn about the Solar System bodies from seismology (Sun et al. [2023]).

It has been argued that seismology is the preeminent tool to determine "vital signs" on icy ocean worlds (Marusiak et al. [2021], Vance et al. [2018a]). Unlike Earth, where rock is the primary medium in the crust, ice is the dominant surface material on these bodies. There are specific seismic phases that are distinct to ocean world environments (e.g. flexural and Crary waves). On Earth, Love and Rayleigh waves dominate surface wave observations.

One of the most important seismic observations for understanding the internal composition of icy ocean worlds is the ice thickness. Initial constraints on this observation can be derived from body wave measurements based on P and S reverberation timing within the ice shell, in addition to the depth dependent epicenter. The ice thickness may be further constrained using the characteristic harmonic frequency of the Crary wave and the recovered P- and S-wave velocities in the ice. Panning et al. [2006] also proposed that surface waves may be a good tool for estimating ice shell thickness, as the fundamental mode Rayleigh wave has a characteristic group velocity maximum associated with a transition from a flexural wave at low frequencies to something more similar to a Rayleigh wave in a half-space at

higher frequencies (Table 3.1, Figure 3.1). In this study we see that transition zone between $2.1 - 13.7mHz$, for a 100 km (Figure 3.1) Titan-like ice shell.

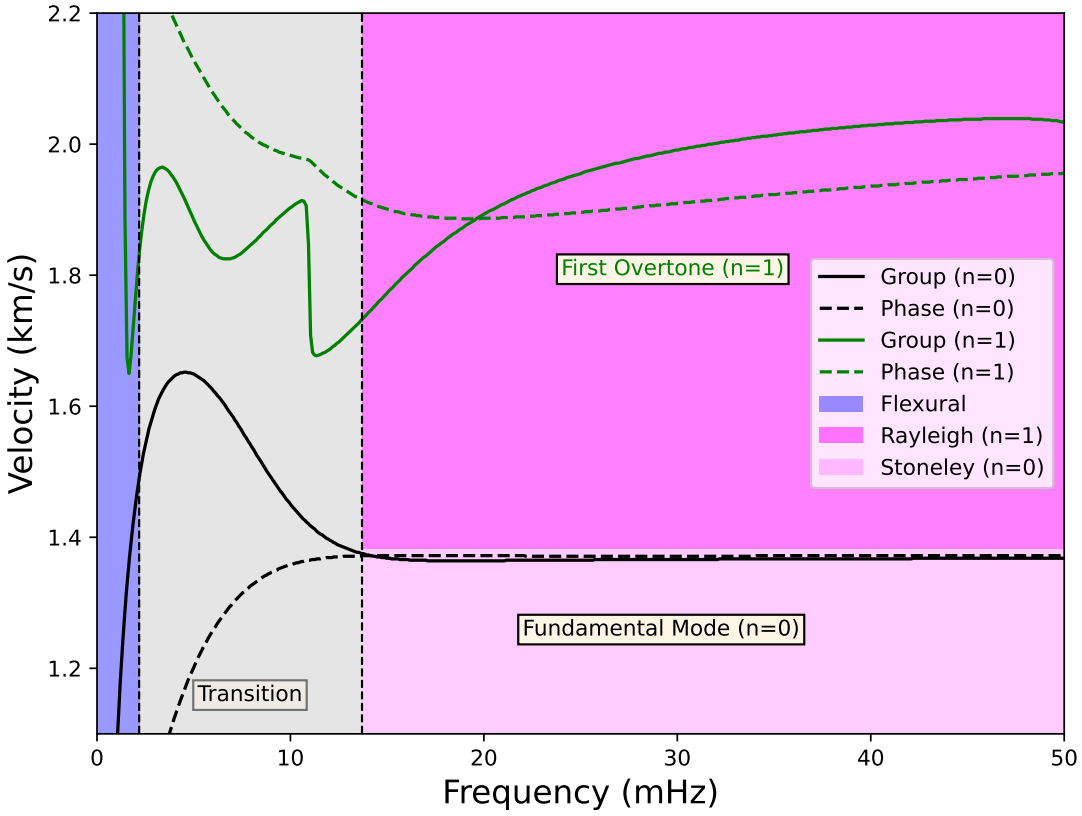

Figure 3.1: Illustration of the transition between the flexural wave and Stoneley mode in the fundamental mode, and a Rayleigh wave in the first overtone. Calculated for a Titan model with a 100 km thick ice shell. The transition zone for a 100 km pure water ice shell is between 2.1 mHz and 13.7 mHz. This trend is also the same for the 10 km and 20 km methane clathrate lid models.

This study explores the use of seismic wave dispersion (long-period seismology) as a means to learn more about Titan's interior, and in particular we investigate if it is feasible to distinguish between the various clathrate models (no clathrate, 10km and 20km clathrate lid) using this method. The phase and group velocities are both dependent on the frequency. Because dispersion is related to the properties of the medium, *Dragonfly's* seismometer may

Mode (n)	d & λ	Wave Type	v_p, v_g & f
0	$\lambda > 2\pi d$	Flexural wave (entire ice shell)	$v_g = 2v_p$ $v_g \propto \sqrt{f}$
0	$d < \lambda < 2\pi d$	Transition between flexural & Stoneley waves	
0	$\lambda < d$	Stoneley waves (ocean/ice shell interface)	$v_p = 0.87 v_{\overline{P},ocean}$
1	$\lambda < d$	Rayleigh wave (surface, non-dispersive)	$v_g = v_p$

Table 3.1: Mode (n) and wavelength dependence of waves for a 100 km thick ice shell under Titan-like conditions, following Panning et al. [2006] and Stähler et al. [2017].
Variables: d = ice shell thickness, λ = wavelength of surface wave, v_p = phase velocity, v_g = group velocity, f = frequency, $v_{\overline{P},ocean}$ = the P-wave velocity of the ocean. Here $n = 0$ corresponds to the fundamental mode branch, and $n = 1$ corresponds to the first overtone.

record surface wave dispersion to explore Titan's interior. Due to the Rayleigh surface wave being a prominent feature of the seismograms for a simulated quake, we will focus on measuring Rayleigh wave group velocities. We only investigate the vertical component as the Dragonfly seismometer is only sensitive in the vertical component (Lorenz et al. [2021a]). There are expected to be horizontal component geophones on Dragonfly, but the sensitivity will be lower while the noise is expected to be higher (Lorenz et al. [2021b]). In the case of icy ocean worlds, surface Rayleigh waves are short period waves that don't interact with the bottom of the ice shell (Table 3.1) and can be described with the usual retrograde elliptical motion, as seen on Earth. In contrast to Rayleigh waves that only see the top of the ice shell, longer period flexural waves are full-layer, or affect the entire depth of the ice shell. However, they are only seen at low frequencies. In this study, Rayleigh waves are the prominent surface wave (Table 3.1) at < 14 mHz and above. It is also important to note that the velocity gradient is very small with depth, so Rayleigh waves have very little dispersion in ice shells (Stähler et al. [2017]).

3.5 Methods

We use two models from Marusiak et al. [2022] including one with no clathrates and one with a 10 km clathrate lid integrated according to the numerical results of Kalousová and Sotin

[2020a]. Marusiak et al. [2022] demonstrated relatively minor changes in seismic ground motions and arrival times when comparing the 10 km-thick methane clathrate lid to an ice shell of water ice ($\leq$ 2.0%). In this study we have modeled a 20 km-thick clathrate lid as well. Models consist of spherically symmetric interior profiles created with *PlanetProfile* (Vance et al. [2018a], Styczinski et al. [2023a]). *PlanetProfile* creates thermodynamically self-consistent models that match orbital constraints on mass and moment of inertia. In the case of Titan, mass and moment of inertia were measured during the *Cassini–Huygens* mission (Fortes [2012]). The surface temperature was set to 94 K (Jennings et al. [2016]) and the the temperature at the base of the ice shell, (T_b), was approximately 260 K for all the models. Model values for T_b are selected to set the ice shell thickness based on the pressure-dependent melting point of the ocean fluid Journaux et al. [2020a]. While different ice shell thicknesses will strongly affect the long-period data in icy ocean worlds (Kovach and Chyba [2001], Panning et al. [2006], Stähler et al. [2017], Marusiak et al. [2021]) we chose to look at only one thickness, 100 km, to isolate any specific effects of clathrate layer presence. All ice shells we modeled have a total thickness of 100 km, varying only in thickness of the methane clathrate lid. Only methane-type clathrates were considered for this study as atmospheric methane has been hypothesized to be episodically replenished via outgassing of the methane clathrates present within the top ice layer (Tobie et al. [2006]). For this reason it is thought that methane clathrates will insulate Titan's icy shell.

Using the outputted models from PlanetProfile, we then inputted them in the open-source spectral-element code *AxiSEM* (`www.axisem.info`) to create three-dimensional (3D) global seismic wavefields in an anisotropic, visco-elastic media (Nissen-Meyer et al. [2014]). In addition, we used *Instaseis,* also open-source (`www.instaseis.net`) to extract seismograms for arbitrary source–receiver configurations from the databases generated with *AxiSEM* (van Driel et al. [2015]). Although originally designed for Earth, *AxiSEM* and *Instaseis* have been adapted for arbitrary spherically symmetric models of other planets and icy ocean worlds.

Using the output 1D seismic wave velocity profiles from *PlanetProfile* as input, dispersion curves and normal modes (eigenfrequencies and eigenfunctions) ((Woodhouse [1988]) were computed using a version of the code *Mineos* (Masters et al. [2011], Panning et al. [2018]) (Figure 3.2). This code also computes synthetic seismograms using normal mode summation in a spherically symmetric planetary model. The complete seismogram of Titan can beexpressed as a sum of the normal modes, with the proper corresponding excitation factors, similar to normalization coefficients (Shearer [2019]). Eigenfunctions for an given eigenfrequency can be written as

$$u(r) = [{}_nU_l(r)e_r + {}_n\, V_l(r)\nabla_1 - {}_n\, W_l(r)(e_r \times \nabla_1)]Y_l^m(\theta, \phi), \tag{3.1}$$

where n is the radial order, l the angular order, m the azimuthal order, and Y_l^m is the spherical harmonic (Table 3.2). Normal modes where generated considering both spheroidal and toroidal dispersion data (Masters et al. [2011]). As mentioned in introduction section, this study presents theoretical dispersion curves generated for spheroidal modes, in accordance with the sensitivity specifications that Dragonfly's DraGMet seismometer will have (being sensitive to only the vertical component) (Figures 3.1 and 3.2) (Lorenz et al. [2021a]). Under the assumption of radial symmetry, the eigenfrequencies and eigenfunctions are not dependent on l or m, and depend only on radius:

$$\nabla_1 f(\mathbf{r}) = \partial_\theta f(\mathbf{r})\mathbf{e}_\theta + (n\theta)^{-1}\partial_\phi f(\mathbf{r})\mathbf{e}_\phi, \tag{3.2}$$

with mode normalization

$$\int_0^{r_T} \rho(r)({}_nU_l^2(r) + l(l+1)_nV_l^2(r))r^2dr = \int_0^{r_T} \rho(r)l(l+1)_nW_l^2(r)r^2dr = 1. \tag{3.3}$$

where r_T is the radius of the Titan, 2575 km. We look at angular orders up to $l = 3000$,

and frequencies up to 150 mHz, although we sample the envelopes at lower frequencies (up to 100 mHz).

Variable	Definition
r, r_T	radius, Titan radius
n	radial order
l	angular order
ρ	density
m	azimuthal order
$f(r)$	eigenfrequency
${}_nW_l(r)$	toroidal eigenfunction
${}_nU_l(r)$,${}_n V_l(r)$	spheroidal eigenfunctions
$Y_l^m(\theta, \phi)$	spherical harmonics

Table 3.2: Definitions of major terms from equations 3.1, 3.2, and 3.3 used for calculating theoretical dispersion curves as well as the normal modes Woodhouse [1988], Masters et al. [2011], Panning et al. [2018]

Individual overtone modes ($n \geq 0$) were isolated from the normal-mode-summed code in order to identify which mode branch of the Rayleigh wave is dominant. For this reason, we focused mainly on lower-order modes, as the surface-waves are contained in this parameter space, whereas the body waves are contained mainly in the larger-n modes.

We measured group velocity using the seismograms from both methods. This was done to test the validity of comparing *Mineos* and *AxiSEM/ Instaseis* since both use different methods of calculating the seismograms; AxiSEM calculated in the time domain, while the normal mode summation is performed in the frequency domain. In order to directly compare the *AxiSEM/ Instaseis*-generated seismograms to the full normal-mode-summed seismograms, generated with *Mineos,* we narrow-band-pass filtered both between $20 - 100$ mHz. Using the *AxiSEM/Instaseis*-generated seismograms, we calculated the group velocities at 25, 50, 75, 100, 125, 150 epicentral distance degrees from the source. For each distance we pick the peaks for 3, 5, 10, 20, 40, 60, 80, 100, and 100 mHz center frequencies, with a 15% edge taper. The seismograms were low-pass filtered at 250 mHz initially, then narrow-band-pass filtered at 15% of their respective center frequencies.

We also present the results of the envelope picking for observations using the *AxiSEM/ Instaseis*-generated synthetic seismograms in comparison with *Mineos* data (Figure 3.5). In the first panel of Figure 3.5 we see the mean group velocity measurements (from *AxiSEM/ Instaseis*) for the range of the distances and center frequencies, as well 1-σ (standard deviation of the number of samples, normalized to N-1, where N is the number of samples per center frequency) away for each of the three structural models with varying clathrate thicknesses.

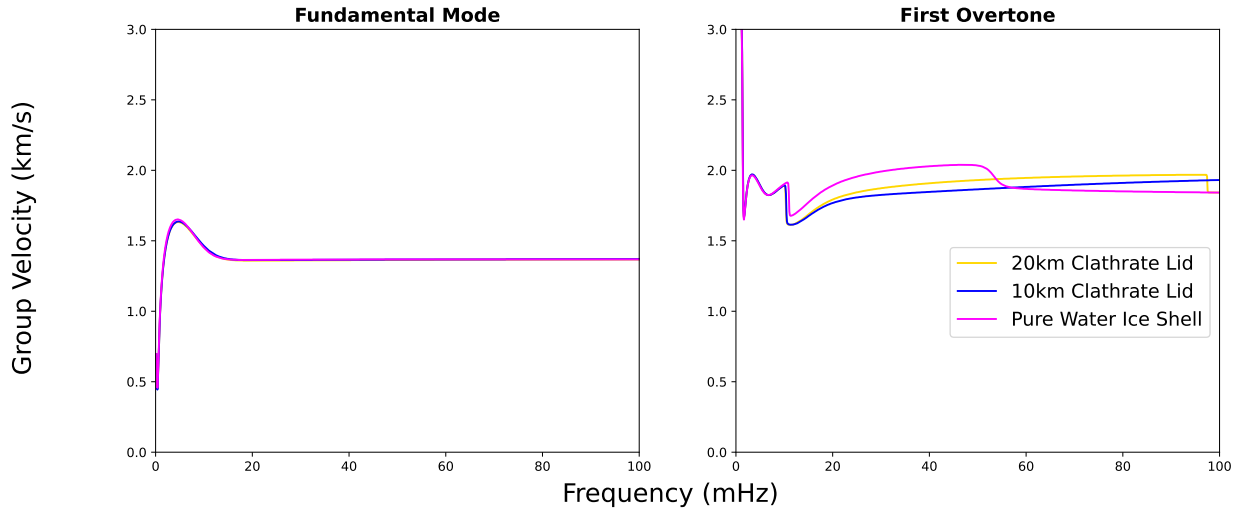

Figure 3.2: Theoretical dispersion curves, containing group velocity measurements as a function of frequency for all models, produced using *Mineos* v1.0.2 (Masters et al. [2011]). Model dependent differences in the group velocities can only be seen in the first overtone, above $\approx$ 15 mHz.

3.6 Results

In the fundamental mode, we note that a Stoneley mode (an interface wave propagating at the solid-fluid interface at the base of the ice shell) rather than a Rayleigh mode is dominant for wavelengths less than the thickness of the ice shell, and the flexural wave is dominant for wavelengths greater than $2\pi d$, where d is the thickness of the ice shell (Panning et al. [2006], Stähler et al. [2017], Table 3.1, Figure 3.1). While this Stoneley mode behavior of

the fundamental mode was not discussed in previous modeling of long-period ocean world seismic wave propagation (e.g., Panning et al. [2006]), it is apparent in the modeling of the Titan ice shells due to several factors discussed in this section. In particular, this can be seen through analysis of the relative amplitudes of the fundamental mode branch and the first overtone, the predicted group velocities of the mode branches, and the shape of the mode eigenfunctions with depth. In the fundamental mode, there is a transitional region between d and $2\pi d$ where the flexural mode transitions to the Stoneley mode. This contribution is partially demonstrated in the normal mode displacement seismograms(Figure 3.3a,c,e); these seismograms were generated for a $M_w = 3$, double-couple event at 3km depth so the Stoneley mode is not visible at this depth. The Stoneley mode is at the bottom of the ice shell and not seen in the seismograms feature surface waves generated from a 3 km depth quake (Marusiak et al. [2022])(Figure 3.4).

We present the theoretical dispersion curves (group velocity as function of frequency) for different modes for the three different interior structure models (Figure 3.2). The fundamental mode models are nearly indistinguishable from one another, with the group velocity values having the greatest difference of 2.5% for the 10 km and pure water ice shell models, where thermal profiles differ the greatest leading to differences in seismic attenuation and amplitude (Marusiak et al. [2022]). For the higher overtones ($n > 0$), group velocities across all models are nearly indistinguishable for frequencies below $\approx$ 2050 mHz. There is considerable frequency dependent group velocity variation above this threshold across the models due to the thermal conductivity-driven seismic attenuation seen in the various thermal lid thicknesses of this study. For moons with thicker ice shells, surface Rayleigh waves are expected to be mostly non-dispersive, thus $v_p \approx v_g$, where v_p is the phase velocity and v_g is the group velocity (Table 3.1). Stähler et al. [2017] predicts a characteristic Rayleigh wave velocity of approximately $1.8 km/s$, assuming a compression wave velocity ($v_{P,ice}$) of $4 km/s$, and a shear wave velocity ($v_{S,ice}$) of $2 km/s$, with $v_g \approx v_p = 0.9194\, v_{S,ice}$, but our prediction

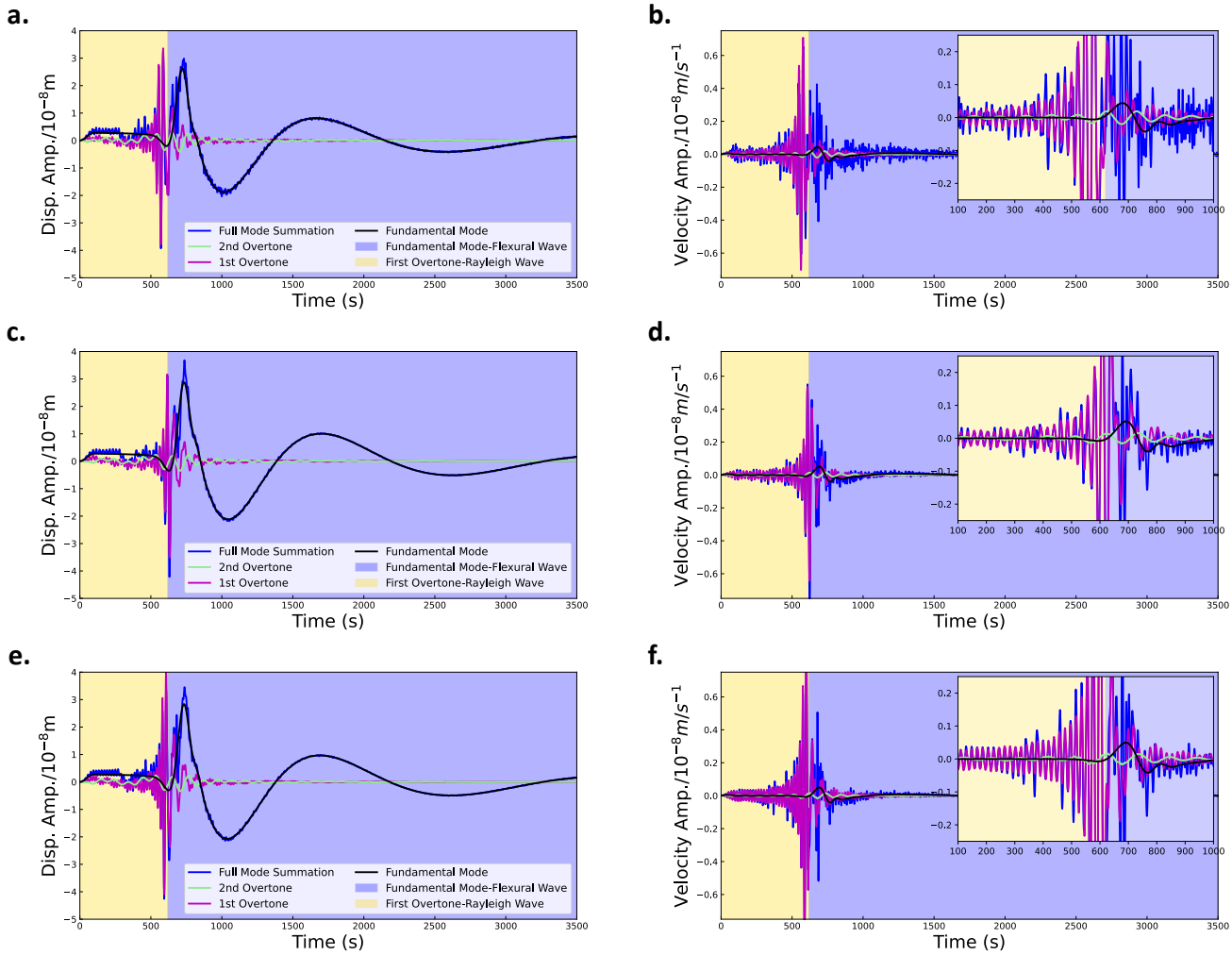

Figure 3.3: Isolated normal modes generated using *Mineos*, at a distance of 25° . Plotted for all three interior structure profiles, at 3 km depth. The modes plotted include the fundamental mode, as well as overtones 14. Insets to the right zoom into the fundamental and second overtones as the complete seismogram of summed normal modes up to $n = 999$ is seen to be dominated by the first overtone. (a-b) 0 km methane clathrate lid (pure water 100 km ice shell), (c-d) 10 km methane clathrate lid ice shell, and (e-f) 20 km methane clathrate lid ice shell. All models are plotted with displacement (left: a, c, e), and velocity (right: b,d,f).

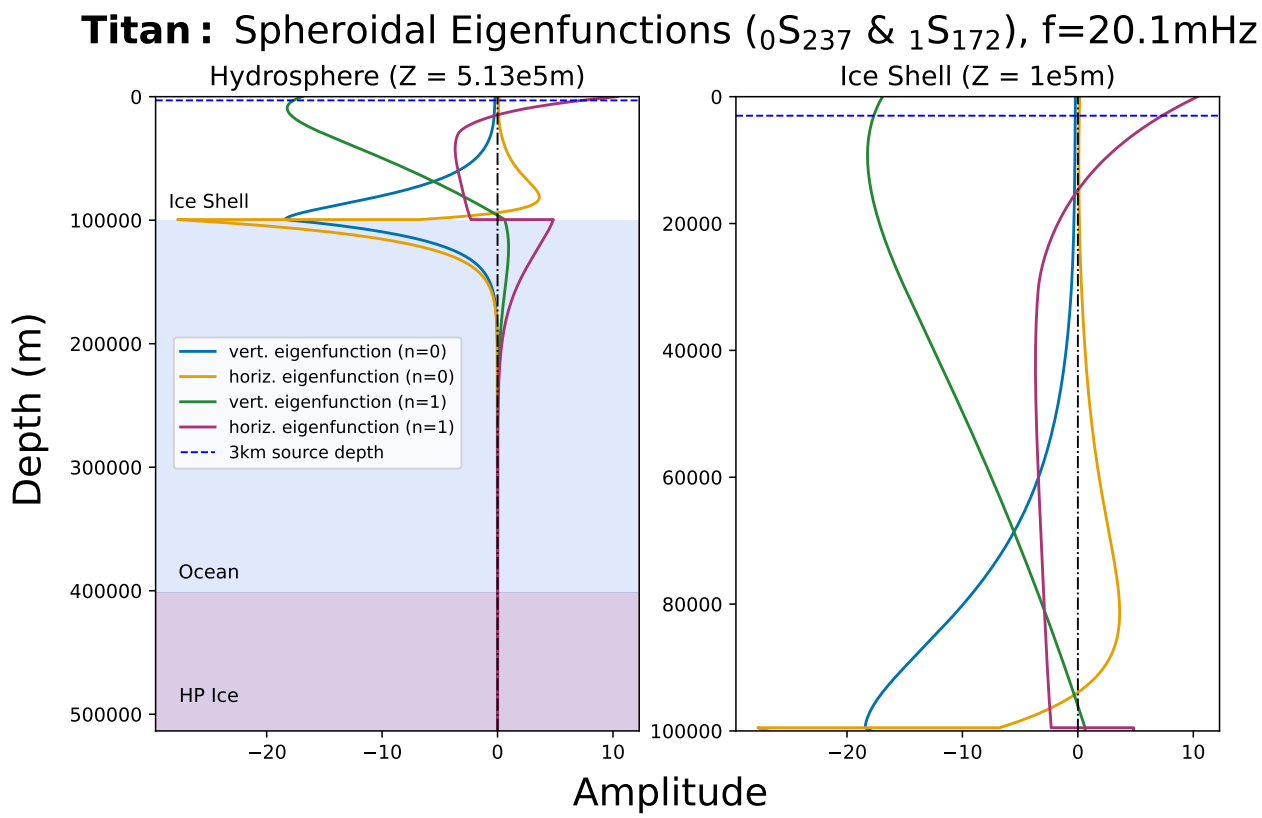

Figure 3.4: Vertical and horizontal eigenfunctions for a frequency of 20.1 mHz for both the fundamental mode ($n = 0, l = 237$) and first overtone ($n = 1, l = 172$). Seen in the fundamental mode is the Stoneley mode with high amplitudes at the base of the ice shell, and in the first overtone the Rayleigh wave is shown ($n = 1$). On the left side is the full Titan hydrosphere (total thickness of 513 km, including the ice shell, ocean, and underlying high pressure ice). On the right side the is a 100 km Titan ice shell in greater detail. The blue dashed line is plotted at 3 km depth, where the source in this study and Marusiak et al. [2022] is located.

shows a fundamental mode group velocity of approximately $1.4km/s$ and a first overtone group velocity of approximately $1.8km/s$ (Figure 3.2). The lower velocity predicted for the fundamental mode is, however, consistent with a Stoneley mode, which is controlled by the P velocity in the ocean (Stähler et al. [2017]).

There is overlap of the $\pm 1\sigma$ region for either method with the fundamental mode, especially below $\approx$ 20 mHz for calculated group velocities from the mean times given from the peak of the envelopes of the narrow filtered data. However, it is important to note that various interior models are indistinguishable from each other based upon using dispersion measurement techniques alone. The average group velocity measurements for both (*AxiSEM* and *Mineos*) are centered around the first overtone value, but we see that the $\pm\sigma$ of calculated center frequency dependent group velocity also overlaps with the fundamental mode (Figure 3.5).

Comparing the band-passed filtered seismograms (between 20-100 mHz) of the *AxiSEM/ Instaseis* and normal mode summation generated *Mineos* models, the pure water ice shell and the 20 km clathrate lid model are the most similar, and the 10 km clathrate lid has the overall lowest amplitude (Figure 3.6). This is due to the thermal profiles of the models; the pure-water-ice shell and the 20 km clathrate lid models have the most similar thermal profiles, due to the stagnant lid thickness being similar, whereas the 10 km clathrate lid has the smallest conductive lid (Marusiak et al. [2022], Kalousová and Sotin [2020a]). The conductive, stagnant lid thickness plays a major role in the seismic amplitudes, as it influences the seismic attenuation (and its inverse, seismic quality factor), driving the amplitude differences between the Rayleigh wave (the most prominent feature in the seismograms) that we see in all of the models (Marusiak et al. [2022]; this study: Figures 3.6 and 3.3).The Rayleigh wave can be seen in the first overtone, as opposed to the fundamental mode which was the expected dominant mode for dispersion measurements (Panning et al. [2006], Stähler et al. [2017]).

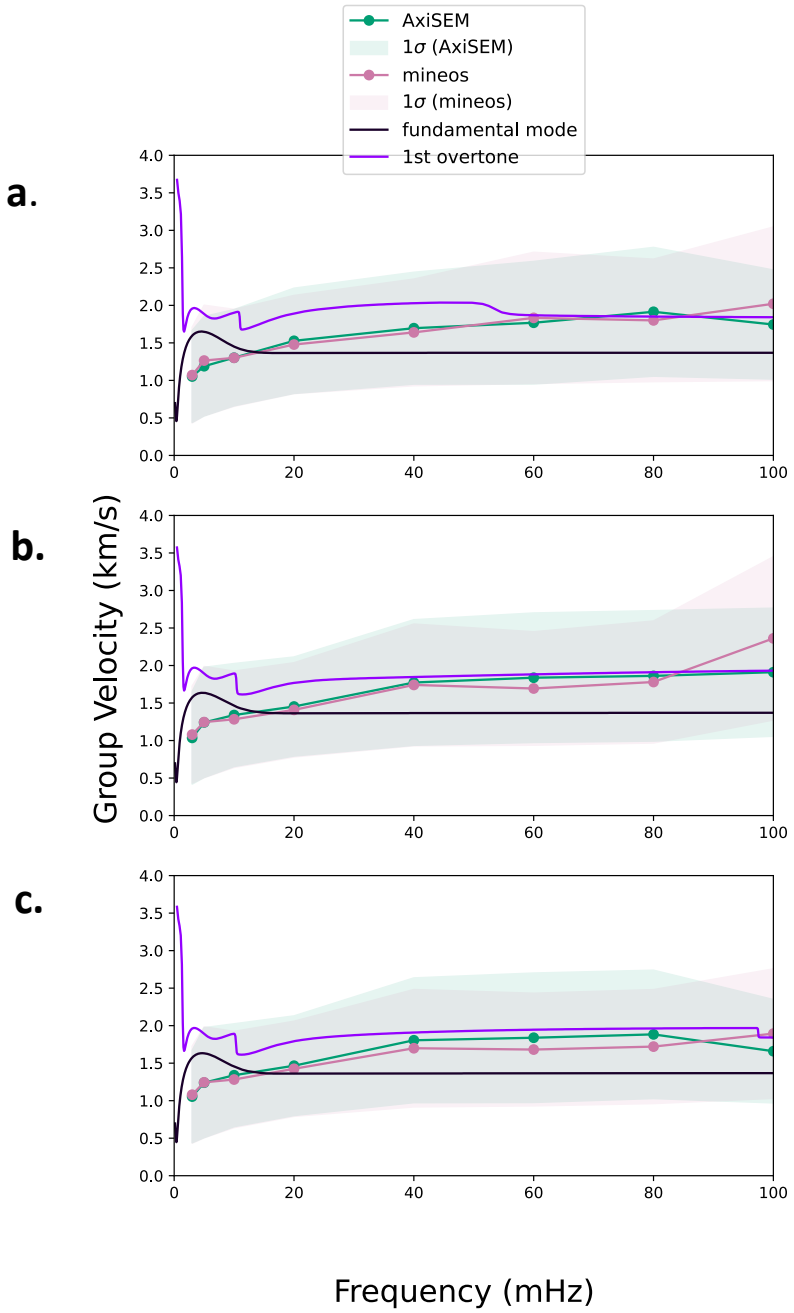

Figure 3.5: Data points: calculated group velocities from the mean times of the peaks of the envelopes of the filtered seismograms; averaged over a range of distances: $25 - 150$deg epicentral distance, and center frequencies: $3 - 100$ mHz. Also denoted is one standard deviation (1σ, normalized to N-1) of the samples. Overlaid fundamental mode and first overtone theoretical *Mineos* dispersion curves from *PlanetProfile* velocity models: (a) 0 km methane clathrate lid (pure water 100 km ice shell), (b) 10 km methane clathrate lid ice shell, and (c) 20 km methane clathrate lid ice shell.

We see clear separation of the mode information, except for the unseen Stoneley wave (Figure 3.4) carried by the fundamental mode at frequencies larger then $\approx$ 14 mHz. And the fundamental mode also carries the flexural wave, but at very low frequencies, below $\approx$ 3 mHz. The first overtone, carries the high amplitude Rayleigh wave above $\approx$ 14 mHz,(Figure 3.3). In Figure 3.3, in line with Figure 3.1, we have denoted the areas of the seismogram where the Rayleigh wave (first overtone) is dominant, and likewise for the flexural wave (fundamental mode) for a 25 deg seismogram (Table 3.1, Figure 3.6).

To understand the contributions that individual normal modes have on the resulting surface waves, we look at the individual normal mode seismograms (Figure 3.3) with *Mineos*, as well as plot the eigenfunctions (Equation 3.1). For all models, the fundamental mode peaks about $200s$ after the peak of the full normal mode (up to $n = 999$) seismogram (Figure 3.3). It is clear that the first overtone, rather than the fundamental mode, contains the Rayleigh wave energy at higher frequencies (Figures 3.1, 3.3, and 3.4). This is in agreement with the theoretical group velocity and is further confirmed by the eigenfunctions, where in the first overtone at 20.1 mHz. Within the ice shell we see the characteristic zero crossing of the horizontal eigenfunction, as well as the decay to zero within the ocean of the vertical eigenfunction (Figure 3.4). Because the seismic source is shallow (3 km depth) the first overtone is excited instead of the fundamental mode, as the fundamental mode is a Stoneley mode excitable (and detectable) only for deep sources and receivers near the boundary of the ice shell and the subsurface ocean.

Delving deeper into the eigenfunctions, we see vertical and horizontal motions of the long period flexural wave in the fundamental mode. At a frequency of 1.86 mHz, the flexural wave is the dominant surface wave seen in the ground displacement seismograms. The near constant vertical motion is seen in the blue in the vertical eigenfunction, decaying to zero in the ocean. Seen in the horizontal eigenfunction, is the oscillating compression and extension, the characteristic motion of the entire flexing of the ice shell (Figure 3.7).

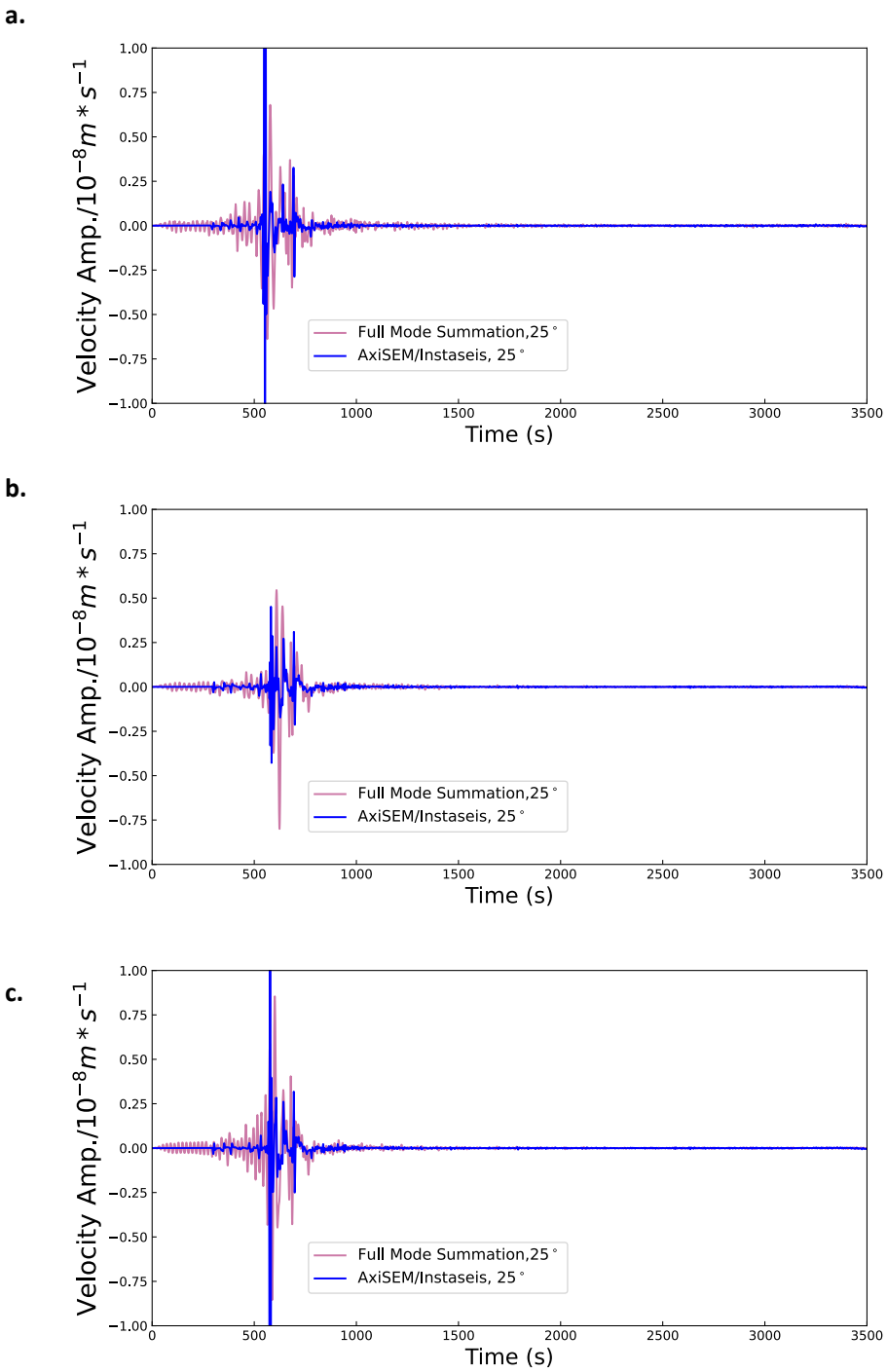

Figure 3.6: Band-passed filtered velocity *AxiSEM/Instaseis* and *Mineos* normal mode summed seismograms: (a) 0 km methane clathrate lid (pure water 100 km ice shell), (b) 10 km methane clathrate lid ice shell, and (c) 20 km methane clathrate lid ice shell. Here the seismograms are in phase, however there is a notable difference in amplitude between the two-types of seismograms. All seismograms filtered from 20100 mHz

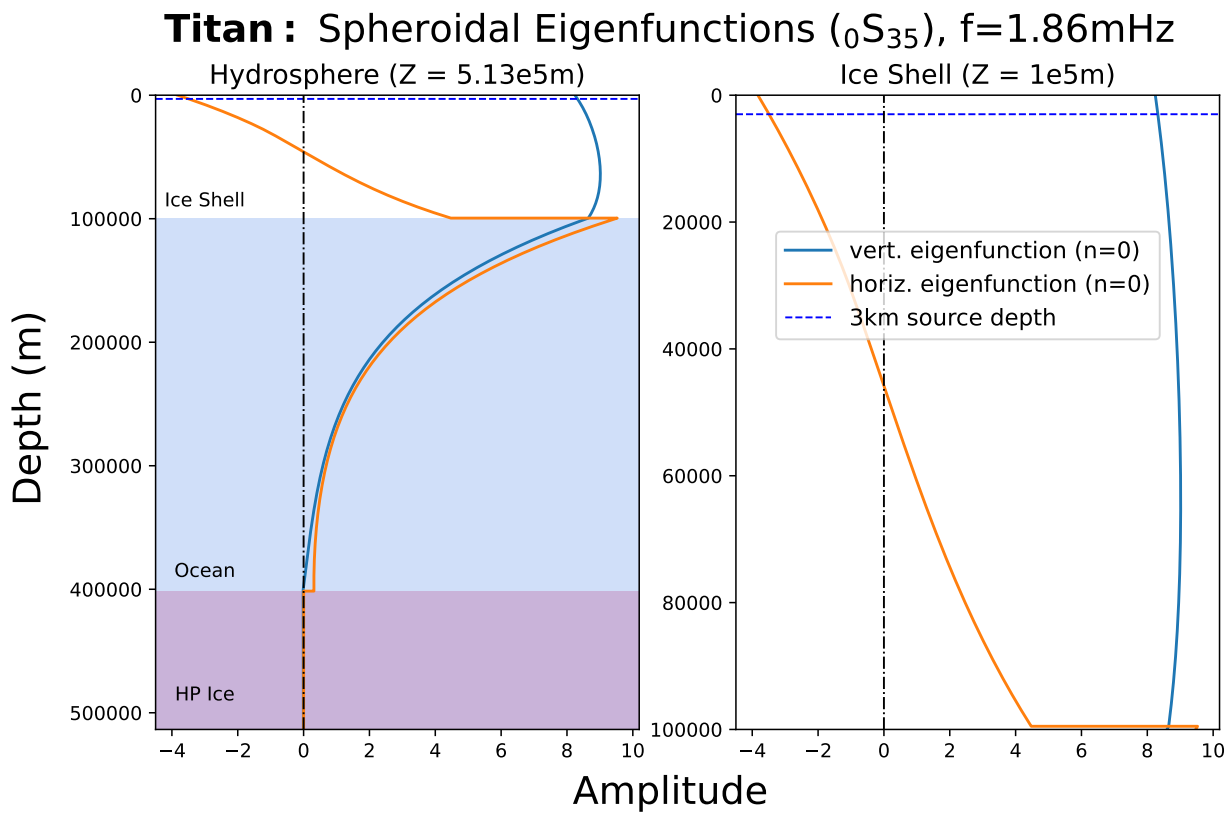

Figure 3.7: Vertical and horizontal eigenfunction amplitudes for the entire hydrosphere (region from the surface to the top of the mantle) at 1.86 mHz, for the fundamental mode where the flexural wave is the dominant feature ($n = 0, l = 35$). The model shown is a pure water 100 km, Titan ice shell. As in Figure 3.4, the blue dashed line at 3 km represents the depth of the source used in this study and Marusiak et al. [2022], with the complete Titan hydrosphere on the left panel, and the 100 km ice shell on the right panel.

3.7 Discussion

Our models are the same as Marusiak et al. [2022], with an additional 20 km clathrate model, which actually serves as an intermediary model given that it has a thicker stagnant lid/conductive region than the thinner 10 km clathrate model, and thus its thermal profile is more similar to the pure water ice shell. The thermal profile has large implications for the seismic attenuation based on the choice of the thermodynamic model chosen for this study from Kalousová and Sotin [2020a]. Newer models have been released (Carnahan et al. [2022]) that demonstrate more clathrate convection models—including models with clathrates at the bottom of the ice shell which could have large consequences for the thermal profile of the ice shell and chemical composition of the ocean.

To build off Marusiak et al. [2022], we study long-period/surface-wave seismology to investigate measurable differences that enable seismic data to constrain possible interior structure models. The advantage of using long-period seismology, especially in the case of a single-station seismometer, is that it could enable direct resolution of the ice shell thickness better than using body-wave seismology alone, particularly in the event that we are not able to clearly identify body waves but have large amplitude surface waves, e.g. Panning et al. [2006]. Maguire et al. [2021] found, at least in the case of flexural wave dispersion, thicker ice shells require extremely sensitive broadband seismometers. In the case of Europa, using group velocity measurements with periods of $25250s$ (frequencies ranging from 0.0040.04 Hz) we can infer Europa's ice shell thickness using the Bayesian inversion method implemented by Maguire et al. [2021][not used in this study]. But it is important to note that the ability to constrain the ice shell thickness becomes steadily more inaccurate when using events from large epicentral distances. Europa also has an ice shell estimated to be $5 - 30$ km (Anderson et al. [2004]), a fraction of Titan's estimated ice shell thickness $25 - 200$ km (Tobie et al. [2006], Mitri and Showman [2008], Deschamps et al. [2010], Nimmo and Bills [2010], Béghin et al. [2012], Iess et al. [2012], Hemingway et al. [2013], Baland et al.

[2014], Sohl et al. [2014], Durante et al. [2019], Barnes et al. [2021a]). The thicker ice shell shifts relevant flexural wave signals to lower frequencies ($\leq\approx 2mHz$), increasing the challenge of measuring the relevant surface waves with a less sensitive seismometer such as that proposed for Dragonfly. Dragonfly will host a seismometer similar to the Lunar-A seismometer (Yamada et al. [2015]), which has a peak sensitivity around $1-2$ Hz (Panning et al. [2020]), more suited for detecting body wave signals. In order to increase the frequency sensitivity to long-period surface waves, it would require a more sensitive (and therefore more massive) seismometer, such as the broadband InSight VBB seismometer (Lognonné et al. [2019]).

There are several sources of uncertainty for using surface waves to determine the ice shell thickness. The interior models used in this study are spherically symmetric which is simplified when compared to reality. Repeating this study in a heterogeneous, three-dimensional interior model (e.g., Marusiak et al. [2023]), with added noise model could yield more realistic, Titan-like results. However, modeling in three dimensions on a global scale, and adding in complex noise sources are computationally expensive and non-uniquely determined. We choose to investigate differences in surface waves under a simplified scenario.

A recent Enceladus seismology study by Marusiak et al. [2023] focused on Crary waves instead of Rayleigh waves. This is due to thinner ice shells ($<$ 20 km) having resonance frequencies that match the predicted theoretical models. However, in the case of thicker ice shells ($>$ 20 km), these authors found that theory and observations began to diverge. The Crary wave method was useful for predicting the mean ice shell thickness for a uniform, spherically symmetric model, but when compared to non-uniform, heterogeneous ice shell model (with topography) the predicted dispersion curves diverged. Marusiak et al. [2023] also inferred that for thicker ice shells($>$ 20 km, as seen in this study) strong Rayleigh waves are produced as well as more body waves that are dependent on the distance from the seismic event.

We see that the dispersion measurements are dominated by the first overtone. The uncertainties (1σ) of our measurements are greater than the variation of the group velocities for each model at various distances and frequencies. Thus we are unable to use surface wave dispersion to distinguish clathrate models from one another based upon the current models (Figure 3.5). Future investigations of using long period seismology to investigate icy ocean worlds that could contain clathrates might consider looking at worlds with thinner ice shells (eg. Europa or Enceladus). For example, Panning et al. [2006] used the multiple filter technique (MFT) (Dziewonski et al. [1969]) to extract group velocity curves from a single measurement, even in the absence of location and absolute velocity information. However, Panning et al. [2006] also showed that when using this MFT method for flexural or Rayleigh wave propagation, error estimation increases with ice shell thickness. The frequency of the distinctive peak changes very little for ice shells greater than 40 km.

There are remaining discrepancies between the *AxiSEM/Instaseis* seismograms in comparison to *Mineos* (Figure 3.6). Ideally, both methods of generating seismograms should agree, especially since both use the same radial velocity profiles generated by *PlanetProfile*. The *AxiSEM/Instaseis* method uses Green's functions in the time domain, while *Mineos* uses normal mode summation in the frequency domain. We see that the seismograms are in phase, but not exactly identical in amplitude. Here we look at the velocity instead of the displacement, as data collected with the Dragonfly seismometer will be used to infer surface wave velocities. It is possible that differences arise from poor numerical resolution of the mode calculations within *Mineos*, which is highly tuned for performance in Earth-like models, as demonstrated by the difficulty in calculating modes at frequencies greater than 150mHz, the upper limit used in this study. However, we do see that both methods do show a great deal of consistency, as there is good agreement in calculating the group velocities (Figure 3.5).

Looking again at the ground displacement plots (Figure 3.3), we can see the flexural

wave clearly, however in the real seismic data the seismometer will not be sensitive to this lower frequency ($\approx\geq 2mHz$) information. Visualizing this modal decoupling in this manner is more useful in pinpointing why this phenomenon occurs when there is a thick ice shell (e.g.100 km as seen in this study).

3.8 Conclusions

While *Mineos* dispersion predictions suggest differences between clathrate models, these differences are smaller than the uncertainty of the measurements we were able to make on synthetic data in this study. Thus we predict it would be difficult to detect clathrates lids using long period seismology on Titan. Of course this does not preclude using long period seismology at all on Titan, just further investigations of features in the ice would have to be conducted.

Future studies could include investigating clathrates at different depths, varying the composition of the ocean, or adding heterogeneities to the ice shell. Although these additions will only complicate the seismograms more, they will also make them more realistic for the comparison to real seismic data that will be received from Dragonfly in the mid-2030s. This research also applies to other icy ocean worlds where clathrates could exist.

3.9 Data Availability Statement

The *PlanetProfile* v1.2.0 interior structure models (generated with MATLAB) are available on Github (`https://github.com/vancesteven/PlanetProfile`). The open source software packages, *AxiSEM* v1.3 (Nissen-Meyer et al. [2014]), *Instaseis* (van Driel et al. [2015]), *Mineos* v1.0.2 (Masters et al. [2011]), and *TauP* (`http://www.seis.sc.edu/TauP/`) (Crotwell et al. [1999b]) are all open source and available for download. Interior structure models will be made available on NASA's Open Data Portal.

3.10 Acknowledgments

The authors would like to thank the Dragonfly Guest Investigator Program, members of the Jet Propulsion Laboratory's Moons Geology and Geophysics group especially Marshall Styczinski and Steve Vance. A. Bryant thanks Steve Meyer and Sunny Park at the University of Chicago for many helpful conversations. A part of the research was carried out at the Jet Propulsion Laboratory, California Institute of Technology, under a contract with the National Aeronautics and Space Administration (80NM0018D0004). A. Bryant was also funded partially by the Dragonfly Guest Investigator Program through the Johns Hopkins Applied Physics Laboratory.

CHAPTER 4

HIGH PRESSURE ICE

4.1 Preface

In this chapter I present the last paper of my dissertation focusing on detecting high-pressure ice on Titan. This work was written by myself with editing done by Mark P. Panning, and based upon the thermodynamic underpinnings of the work done by Baptiste Journaux at the University of Washington, with his code *SeaFreeze*. The idea for this work was the fruit of a conversation with Baptiste over how discovering high-pressure ice on Titan could hold a lot of significance for astrobiologists who are searching for signs of life of Titan, either extant or in its earliest stages. This study assumes a hydrosphere (top ice shell, ocean, and any phases of high-pressure ice beneath the ocean) composed completely of pure water, with no solutes. These are modeled using *PlanetProfile* (Vance et al. [2018b], Styczinski et al. [2023a]) and *SeaFreeze* (Journaux et al. [2019, 2020a]).

4.2 Seismic and Thermal Profiles of High-Pressure Ice in Titan's Hydrosphere

4.2.1 Author List

Andrea S. Bryant (1,2), Mark P. Panning (2), Baptiste Journaux (3) Angela G. Marusiak (4), Marshall J. Styczinski (5)

1. University of Chicago, Department of Physics, Chicago, IL
2. Jet Propulsion Laboratory, California Institute of Technology, Pasadena, CA
3. University of Washington, Department of Earth and Space Sciences, Seattle, WA
4. University of Arizona, Lunar and Planetary Laboratory, Tucson, AZ

5. Blue Marble Space Institute of Science, Seattle, WA

Corresponding author: Andrea S. Bryant , asbryant@uchicago.edu

4.2.2 Key Points

- We identify key phases to investigate high-pressure ice within a Titan-like ice world
- Models with high-pressure ice show specific reverberations that are distinct from models that do not contain high-pressure ice

4.3 Abstract

Due to the cold temperatures on Titan's surface water ice is stable however pressure and temperature on Titan increase with depth. This causes various ice phases that are not normally seen on Earth, where water ice exists almost entirely as ice Ih. Depending on the temperature and pressure conditions, various phases of ice could exist and be detectable with seismology. If present, this ice could serve as a barrier between the potentially nutrient-rich deep interior of Titan and the water rich ocean where life may exist. We produce thermodynamic self-consistent models of Titan and then numerically simulate seismic wave propagation. We use the resulting seismograms to isolate potential seismic observations that are diagnostic of the presence of high-pressure ice.

4.3.1 Plain Language Summary

We model various crystalline structures (phases of ice different from Earth's surface) of ice beneath the subsurface ocean of a hypothetical Titan-like world using numerical modeling. These phases could be present on Titan where there is much evidence to expect that there is an ocean much deeper than Earth's ocean covered by thick ice, separating if from the surface. We model how such ice phases affect the kind of measurements way could make

with a seismometer on the surface of Titan in order to understand how we may be able to identify such layers.

4.4 Introduction

The existence of high-pressure ices could limit the amount of water–rock interactions that would provide crucial nutrients for potential life in icy ocean worlds (Vance et al. [2018b]). Exploring the astrobiological potential of Saturn's moon Titan is a key goal of the the upcoming *Dragonfly* mission, where the rotorcraft will search for signs of prebiotic chemistry, potential biosignatures, and habitability (Barnes et al. [2021a]). High-pressure ices are a geophysical phenomena not occurring naturally on Earth, outside of the laboratory, but are expected in a number of bodies across the Solar System including Callisto, Ganymede, and Titan (the focus on this study) (Journaux et al. [2020b]).

We created thermodynamically self-consistent models of Titan, with *PlanetProfile* (Vance et al. [2018b], Styczinski et al. [2023a]) including water properties calculated with *SeaFreeze* (Journaux et al. [2020a]) to vary the temperature at the base of the ice shell and how this induces the presence or absence of high-pressure ice or not. We constrained the approximate transition temperature at the base of the ice shell where high-pressure ice forms and generate models near this transition in order to determine diagnostic seismic features associated with the onset of the high-pressure ice.

Next, in order to determine whether or not the high-pressure ice generates distinct phases, we take a 100 km thick ice shell, which includes a layer of high-pressure ice at the base of the ocean, and simply manually remove the high-pressure ice layer and replace it with liquid water so the only difference is the presence or absence of high-pressure ice. We then use the *AxiSEM* (Nissen-Meyer et al. [2014]) and *Instaseis* (van Driel et al. [2015]) generated-seismograms computed through the two models to isolate differences only due to the high-pressure ice. We do observe differences associated with the presence of the high-pressure ice,

Table 4.1: Model specifications. T_b is the temperature at the base of the ice shell. The lowest T_b has the thickest ice shell as well as multiple layers of high-pressure ice. The highest T_b has no high-pressure ice, and also the thinnest ice shell of the models.

Ice Shell Thickness	T_b	**High-Pressure Ice Present**
89.9 km	$262.66K$	No
95 km	$261.94K$	Yes
100 km	$261.2K$	No*
100 km	$261.2K$	Yes
130 km	$256.5K$	Yes (phases V & VI)

*Identical to the 100km model, but with the high-pressure ice layer removed.

and we analyze what body wave paths are associated with these differences.

We also look at a range of models with ice shell thicknesses ranging from $89 - 130$ km (Table 4.1), including models ranging from no high-pressure ice to two phases of high-pressure ice below the ocean.

The aim of this paper is to investigate potential key seismic signals for detecting high-pressure ice, beneath Titan's ocean. The significance of the detection of these seismic phases is to be able to detect whether or not high-pressure ice exists using a seismometer like the one on the *Dragonfly* mission that will land in the mid 2030s.

4.5 Methods

We generated five, spherically-symmetric interior structure models using *PlanetProfile*, an open source generator of spherically symmetric planet profiles, used for constructing 1D interior structure models (Vance et al. [2018a], Journaux et al. [2020a], Styczinski et al. [2023a]). *PlanetProfile* uses *SeaFreeze* for the calculation of the water properties, as this study focuses on the hydrosphere (Journaux et al. [2020a]). We model slight variations in the thickness of the top ice shell, high-pressure ice, and in the case of the coldest model—we see two phases of high-pressure ice (Table 4.1).

All models are generated to be thermodynamically self-consistent, with one exception. Namely, the 100 km model without the presence of high-pressure ice is generated to be

identical to the one with high-pressure ice, but with the high-pressure ice layer manually replaced with liquid water.

We conduct a number of tests (previously mentioned in the introduction section of this paper) in order to investigate whether or not we would be able to detect the pressure of high-pressure ice on Titan with a single station seismometer, as will be the case for the *Dragonfly* mission (Barnes et al. [2021a]).

We look at models of the same surface ice shell thickness with and without a high-pressure ice layer. In the model without high-pressure ice, we omit the layer by altering the velocity model files to match the ocean layer above with pressure and compressive seismic velocities increasing with depth, with the shear velocities within the layer set to zero.

Using the interior structure models as inputs, we then simulate four source depths, or titanquake hypocenters for each interior structure model. Waveform propagation is simulated using AxiSEM (Nissen-Meyer et al. [2014]), the spectral element solver, to model the global wavefield of Titan for each of the source depths. We model various source depths in order to determine the differing seismic signals from shallow quakes and deep quakes. The source depths are 1 km and 10 km within the brittle upper region of the ice shell, respectively, and at 470 km within the upper mantle (assuming a solid core, Table 4.2). We assume the mechanism for the upper region of the ice shell to use a double couple mechanism and the deeper source, upper mantle also a double couple however due to tidal deformation (Pou et al. [2024]).

We look into two different regimes of titanquakes, within the ice shell's cooler and brittle conductive layer (top layer in contact with Titan's 94 K surface). The source depths here are 1 and 10 km. We also investigate whether or not we can detect the quakes within Titan's silicate interior, with a source depth of 470 km. Due to slight variations in the depths of the hydrosphere for each of our models, which varies due to the need to match observed moment of inertia with varying temperature and therefore density profiles, this resulted in quakes in

Table 4.2: Description of source depths for simulated seismic events explored in this study.

Depth	Layer description
1 km	top of brittle conductive layer of ice shell
10 km	bottom of brittle conductive layer of ice shell
470 km	within Titan's silicate interior for all models

Table 4.3: Examples of phases that could be used to identify the existence of high-pressure ice on an icy ocean world (e.g. Titan). In the first column is nomenclature from Stähler et al. [2017], and the second column is the same phase but using *TauP* (Crotwell et al. [1999b]) nomenclature for a hypothetical icy ocean world with a 100 km thick ice shell and a 400 km thick ocean. The third column provides descriptions of the phases.

Stähler	TauP	Description
$PFPFP$	P100P400P400P100P	A wave that starts within the ice layer, crosses the ocean, travels through the crust and potentially mantle, turned and went back through ocean to surface
$PFoFP$	P100Pv400P	A wave that starts within the ice shell reflects off the from the ocean floor and travels back through ocean to surface
$PFoF^eFoFP$	P200Pv400pˆ100Pv400p100p	Wave that starts within the ice shell topside reflection off ocean bottom, bottom-side reflection off ice shell, topside reflection off ocean bottom and back through ocean to surface

a range of $3 - 27$ km beneath the starting depth of the silicate mantle (Table 4.2).

The software package Instaseis (van Driel et al. [2015]) was used to reconstruct seismograms for hypothetical source and receiver locations from the AxiSEM models. The TauP/ObsPy software package was used to calculate theoretical arrival times (Crotwell et al. [1999b], Beyreuther et al. [2010]).

I present the nomenclature used to describe waves off of key boundaries. For this study we focus on P waves bouncing off of key boundary layers (example phases shown in Table 4.3).

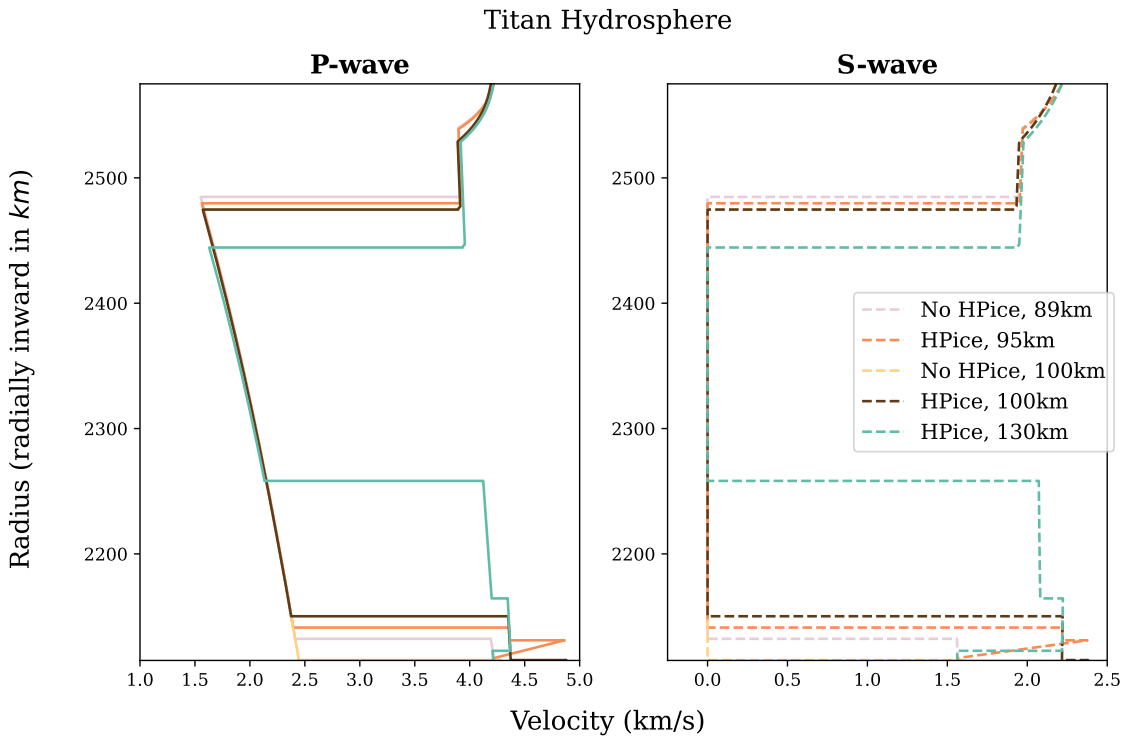

Figure 4.1: P wave velocities (left panel) for all models, and S wave velocities (right panel) for all models (Table 4.1). Radius plotted radially inward from the surface, and plotted is the entire Titan hydrosphere (ice shell, ocean, and depending on the model, high-pressure ice).

4.6 Results

4.6.1 Profiles of All Models

We present the P and S wave velocities of the hydrosphere of each model (Figure 4.1). The ice shells, oceans and high-pressure ice layers can be clearly seen as a function of depth. Accordingly, we also show the density and attenuation (Q) profiles of all the models (Figure 4.2). All the models have a pure water ice shell and ocean, so density differences result from the pressure and temperature dependence of water properties, as well as the type (ice phase) of high-pressure ice which is thermodynamically stable at each depth. While all models match the observed mass and moment of inertia for Titan, varying the temperature profile controls the presence and thickness of high-pressure ice layers.

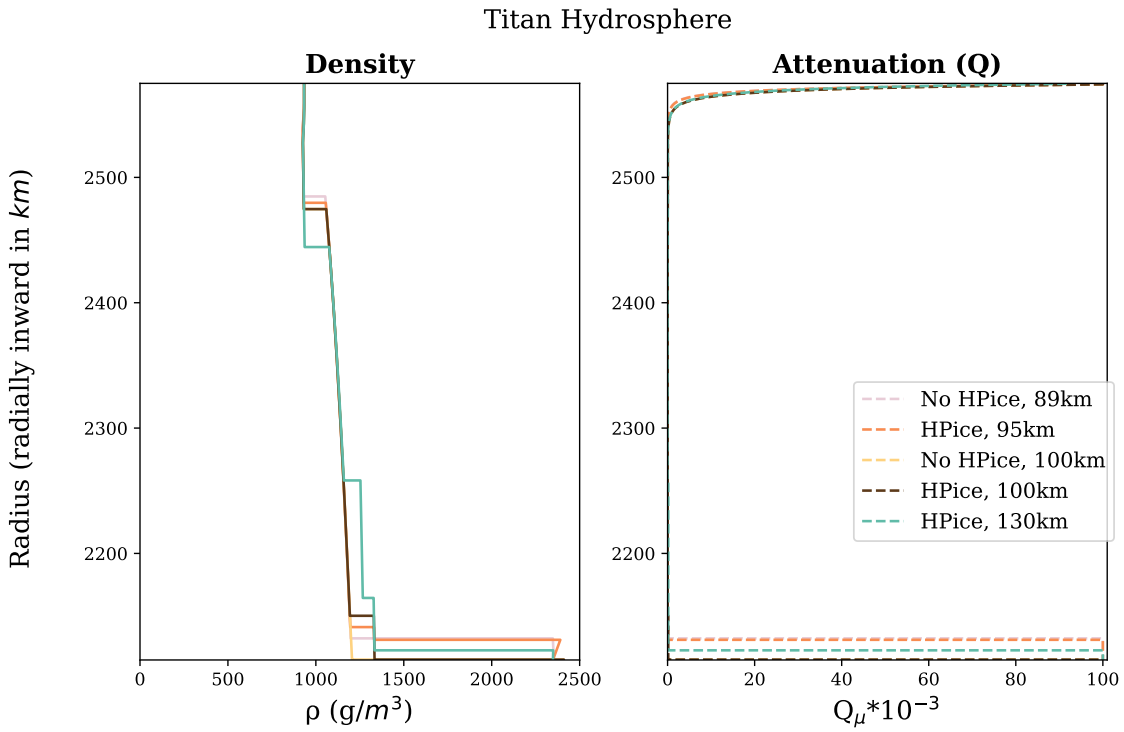

Figure 4.2: Density profiles (left side) and quality factor (Q) profiles (right side). The differences in attenuation seen mainly within the conductive region of the ice shell in contact with the surface.

4.6.2 Mid-Thickness Ice Shell Models: Looking for Specific High Pressure Ice Phases

Shallow Source Depth

For the 100 km models we manually edit out the high-pressure ice (Figure 4.3). The only differences between the models in in the ≈35 km of ice beneath the ocean. We identify phases (Figure 4.4) that interact with the high-pressure ice/bottom of the ocean, also seen in the 5° seismogram (Figure 4.5). Here we can see that within the top panel (model with high-pressure ice) around $500s$, that there are multiple bounces between the top and bottom of the high-pressure ice ($P425Pv459p^{4}25Pv459p425p$: three P wave reverberations), also we see particular phases ($P100Pv425P$: a P wave bouncing off the top of the high-pressure ice; $P100Pv425^{1}00Pv425p100p$: a P wave bouncing between the bottom and of the ice shell and the top of the high-pressure ice) that are unique to 100 km model with high-pressure ice. For both models (with and without high-pressure ice), we see the phase $P100Pv459P$ (a reverberation off the top of the mantle). However, for the model without high-pressure ice, this occurs ≈$10s$ before the model with the high-pressure ice. Additionally, we observe $P100Pv459^{1}00Pv459p100p$, a P wave bouncing between the top and the mantle and the bottom of the ice shell (Figure 4.5). The travel times are shown in Figure 4.6, including P and S waves, which are contained within the identical top ice shells of both models.

In the last panel of Figure 4.6 we see the differences in the subtracted seismograms. Reverberations are seen following the key phases previously mentioned. The high-pressure ice models show more complicated double arrivals due to reverberations off the top of the high-pressure layer and the silicate mantle.

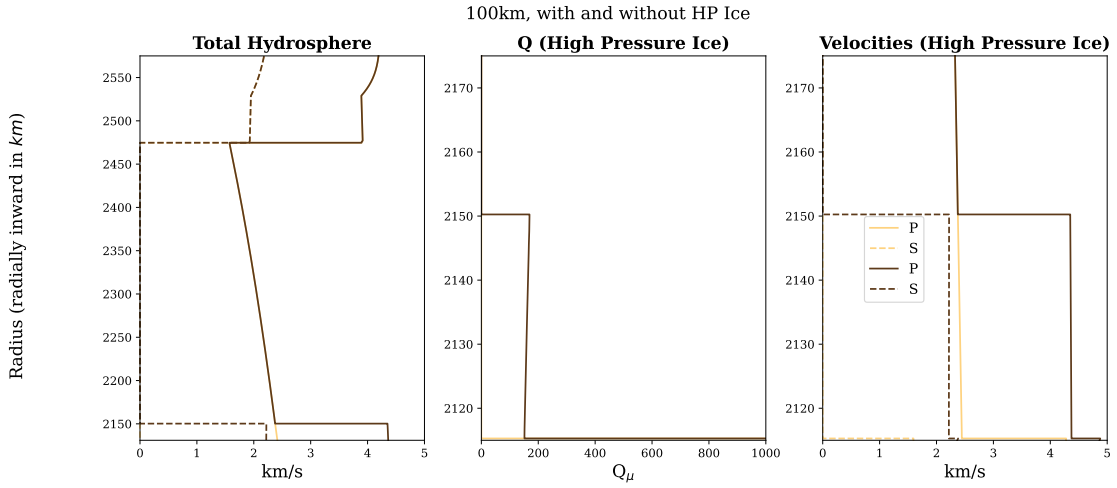

Figure 4.3: P and S velocity, and attenuation profiles for two identical 100 km thick ice shells, except in one model the high-pressure ice has been replaced with ocean.

4.6.3 Deep Sources

For the deep sources (470 km) we can detect up-going waves that pass from the silicate interior. Looking at 20° data when we looked at the travel time curves. We show predicted travel paths (Figure 4.7) and an example seismogram 4.8, both for a distance of 5 degrees. We see the same pattern of reverberations off of the high-pressure ice, as seen in in the shallower source depth seismograms. Though here we can see arrival times of additional packets of reverberations separated by approximately $300 - 400$ seconds which represent additional 2-way paths through the liquid ocean.

4.6.4 Thinner Ice Shell Comparison

In order to test the difference that the temperature at the base of the ice shell has on the formation of high-pressure ice and if those differences in seismograms were quantifiable, we directly compare a 95 km ice shell with a temperature at the base of the ice shell (T_b) being $0.72K$ cooler than the 89 km ice shell. This slight difference in the T_b can seen in (Figure 4.9) v_s and v_p profiles of the top conductive layer (≈35 km) of the ice shells; in the pink is the 89 km ice shell where there is no high-pressure ice. We can see visual differences

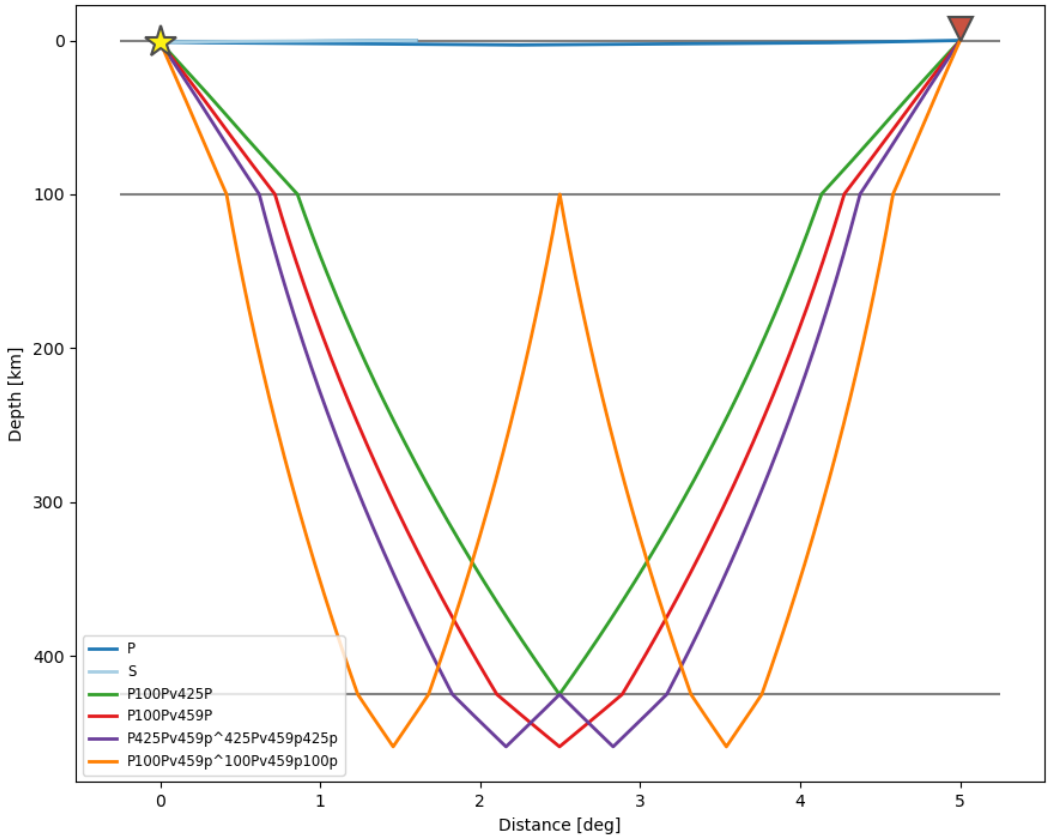

Figure 4.4: Ray path diagram for a 1 km source, 100 km ice shell (with high-pressure ice) for a receiver at 5°. Generated with TauP Crotwell et al. [1999b]. Illustrating the path of the rays for P waves traveling the ice shell, ocean, and bouncing off of the bottom of the high-pressure ice layer.

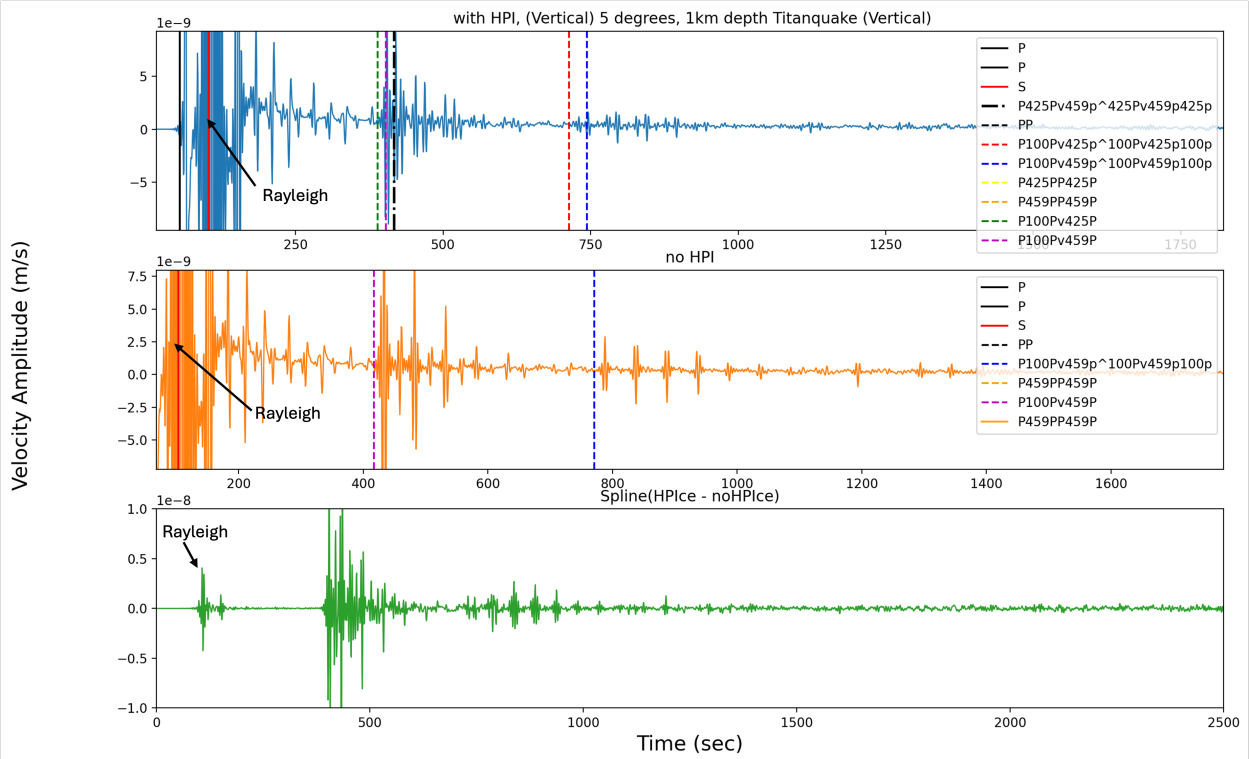

Figure 4.5: 100 km ice shell models, with and without high-pressure ice: 1 km source depth, 5° epicentral distance (top) HPI seismograms, (middle) no high-pressure ice, (bottom) spline difference of the seismograms. Phases outlined are particular phases that differ between the two models, either by arrival time or by not being present at all. Note that the amplitude of the Rayleigh pulse arriving at approximately 200 seconds, is saturated in this figure in order to see the smaller body wave reverberations diagnostic of the high-pressure ice layer.

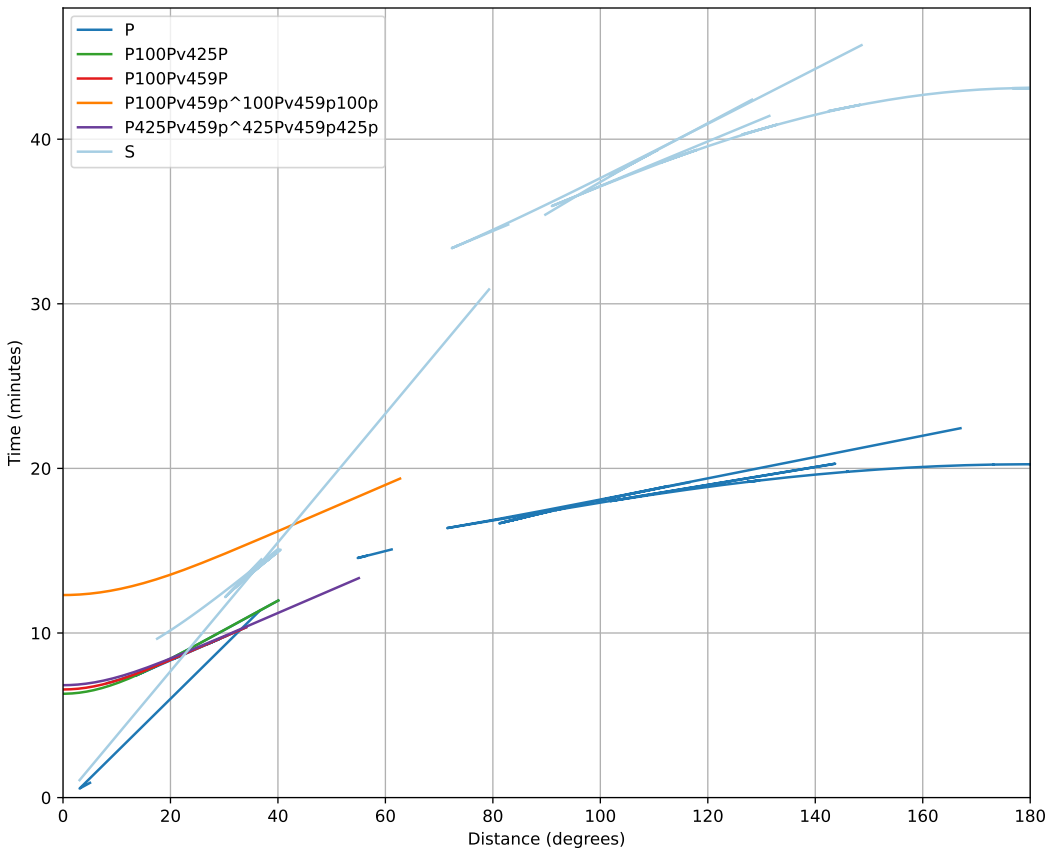

Figure 4.6: High-pressure ice travel times generated with TauP Crotwell et al. [1999b]. Phases looked at include P and S waves confined within the ice shell, and P waves reflecting off the top and bottom of the high-pressure ice layer (top at 425 km depth and bottom at 459 km depth).

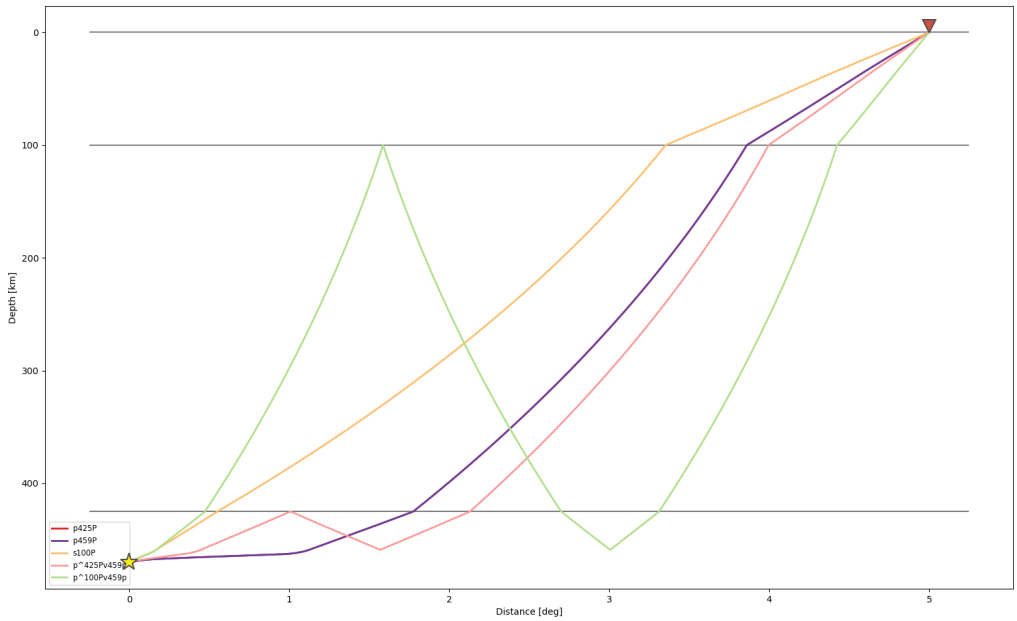

Figure 4.7: Ray Path diagram for a 470 km source, 100 km ice shell (with high-pressure ice) for a receiver at 5°. Generated with TauP Crotwell et al. [1999b]. Illustrating the path of the rays for P waves traveling from the deep source through a layer of high-pressure ice, the ocean, and ultimately to a receiver.

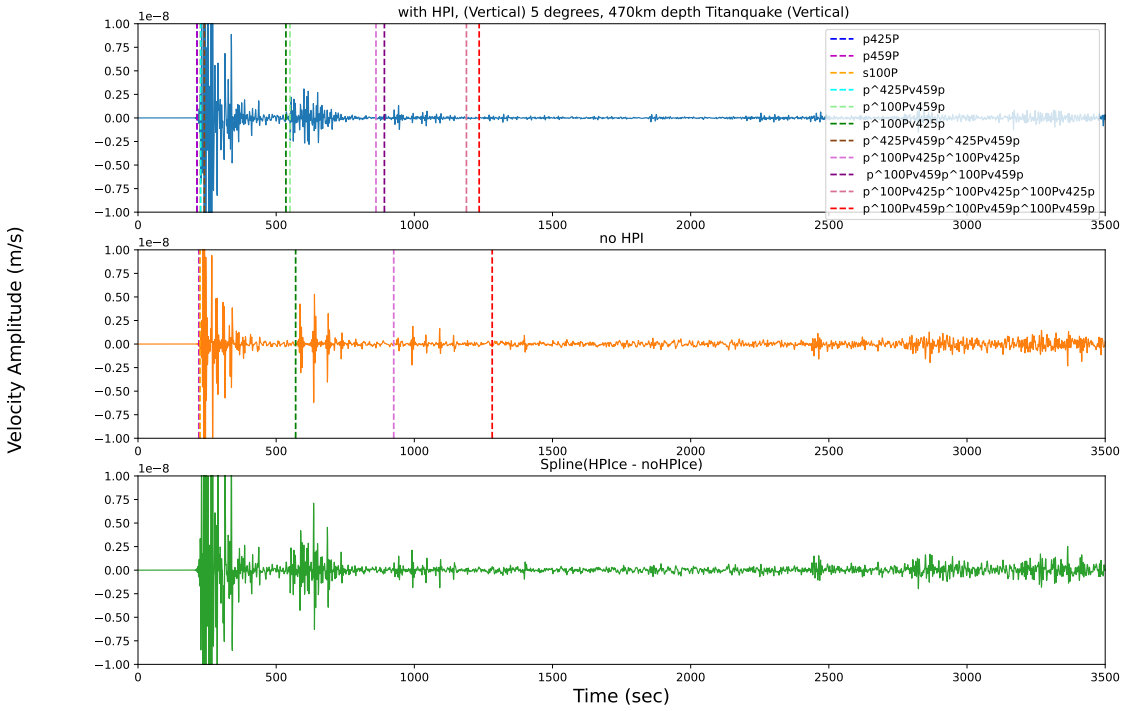

Figure 4.8: 100 km ice shell models, with and without high-pressure ice: 470 km source depth, 5° epicentral distance (top) high pressure ice seismograms, (middle) no high-pressure ice, (bottom) spline difference of the seismograms. Phases outlined are particular phases that differ between the two models, either by arrival time or by not being present at all. We see the same pattern of reverberations off the high-pressure ice but this time with up-going P waves, instead of down-going. Multiple (increasing) reverberations of decreasing amplitude are also cleared from this source depth.

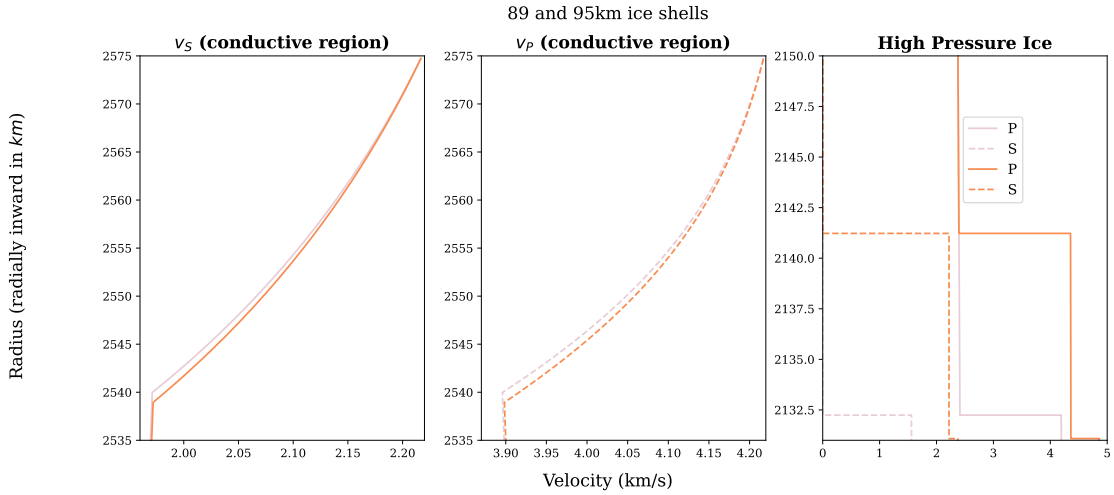

Figure 4.9: (pink) No HP Ice, 89km deep ice shell, (orange) HP Ice, 95 km ice shell, v_s, v_p within the top conductive region of the ice shell (top ≈35 km), and the bottom of the ocean (89 km ice shell model)/region of hydrosphere with high-pressure ice (for the 95 km ice shell).

in the seismograms, the reverberations from the high-pressure ice have reduced amplitudes here than the 95 km ice shell/high-pressure ice containing model (Figure 4.10). We see the usual Rayleigh wave for both models in the vertical orientation. Also we see a possible flip of polarization for 89 km ice shell particularly in the second round of highlighted reverberations from the base of the ocean (Figure 4.10).

4.6.5 Thinnest and Thickest Ice Shell Comparison

We see that the conductive region of the 130 km model extends about 10 km deeper into Titan than the 89 km region (Figure 4.11). This affects the seismic attenuation seen in 4.12, and the peak amplitude of the ground velocities, as would be measurable by the *Dragonfly* seismometer. Within the seismograms (Figure 4.13) we see specific phases between the model with high-pressure ice and model without, although the effect of the two phases of high-pressure ice is ≈5 times lower amplitude than the 89 km model with no high-pressure ice.

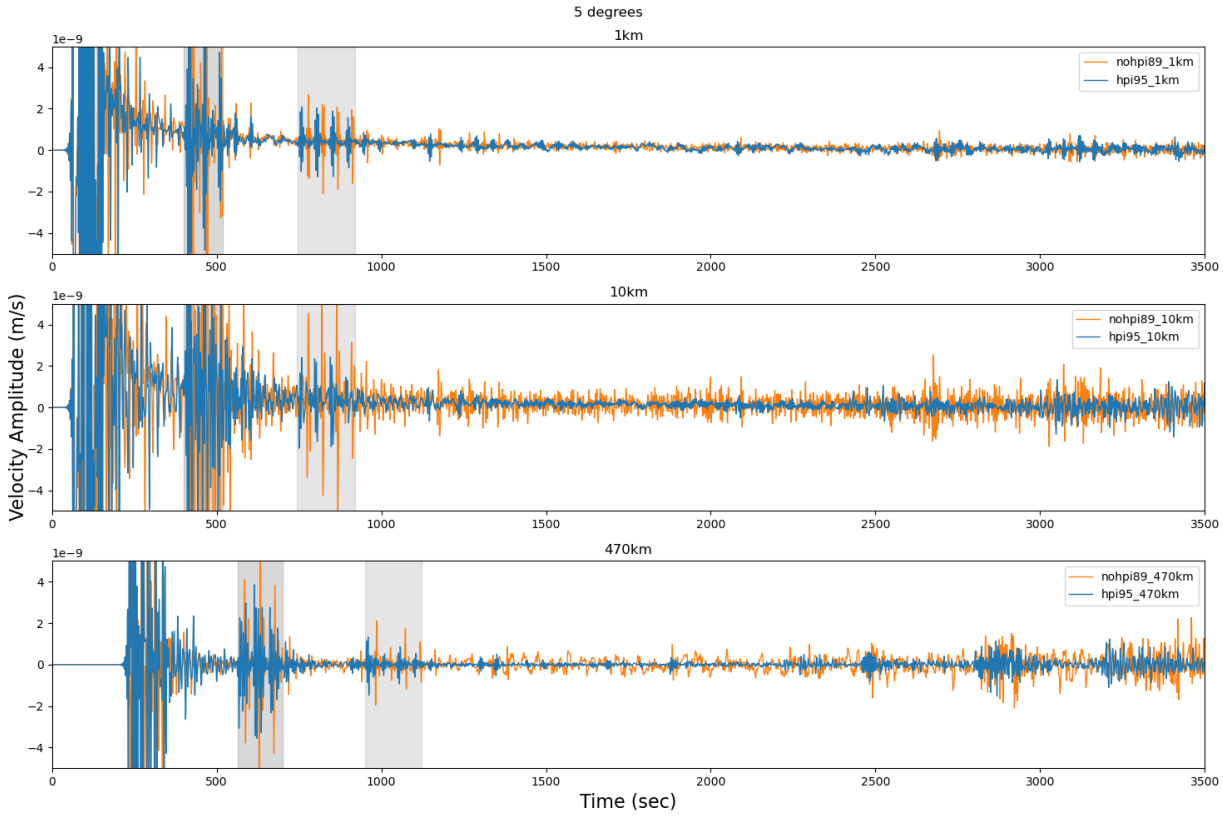

Figure 4.10: 5°, all depths, (from top to bottom: 1 km, 10 km, 470 km); comparing 89 km (no high-pressure ice) to 195 km (high-pressure ice) models. Highlighted are regions of reverberations off of the body of the ocean for both models.

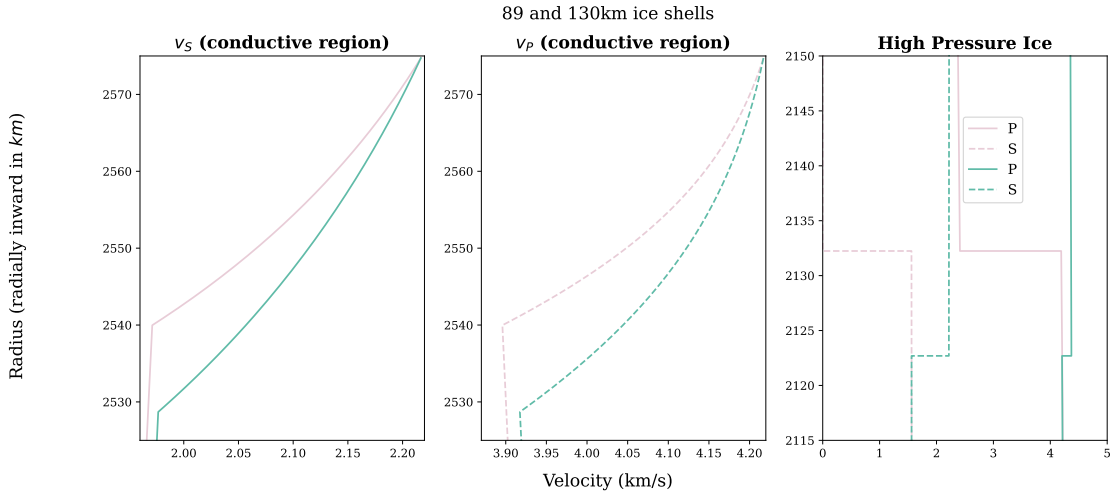

Figure 4.11: P and S wave velocities for 89 km and 130 km ice shell models. The conductive lid of the 130 km model extends ≈10 km deeper into than the 89 km model.

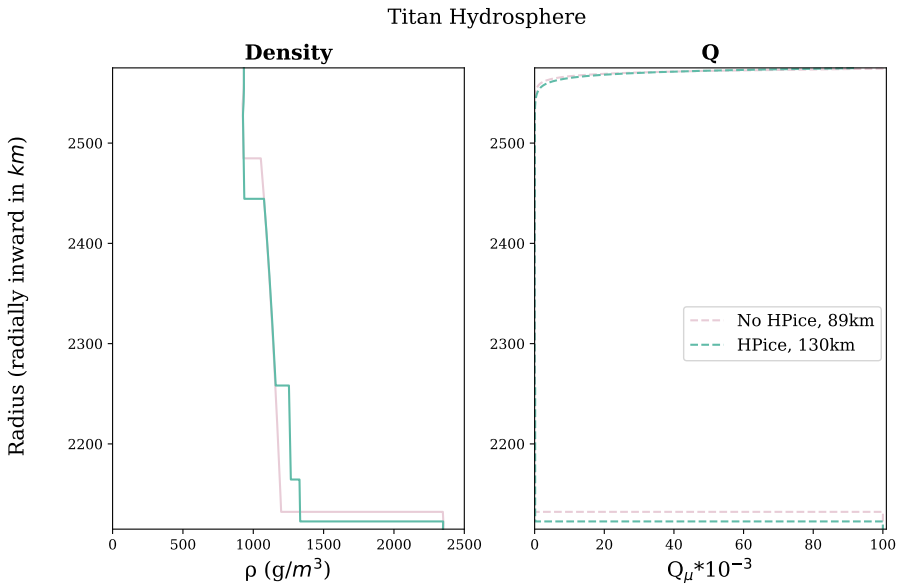

Figure 4.12: Density (kg/m^3) and $Q_\mu \times 10^{-3}$ for Titan models with 89 km of surface ice (no high-pressure ice beneath the ocean), and 130 km of surface ice (with two layers of high-pressure ice of differing ice phases beneath the ocean).

4.7 Discussion

For all of the 100 km models, studying high-pressure ice specific phases we see that extra reverberations specific to the the high-pressure ice are present for all source depths. Also when we look at the peak amplitudes at 5° (Figure 4.14) for all of the models we see that the peak amplitude for the vertical ground motion seismograms varies slightly with depth. For the shallower quakes (5°), at the top of the brittle layer (1 km source depth) the model without high-pressure ice has a ground velocity motion amplitude that is 6.19% higher than the model with high-pressure ice. At the bottom of the brittle ice layer (10 km source depth) the model without high-pressure ice has a higher peak amplitude but only 2.63% higher.These differences are primarily due to the colder models which include high-pressure ice also having a thicker cold conductive layer and therefore reduced attenuation. This is a stronger effect for the shallower source. This is, of course, only an indirect connection to the presence or absence of high-pressure ice. However the reverberative phases that reveal the

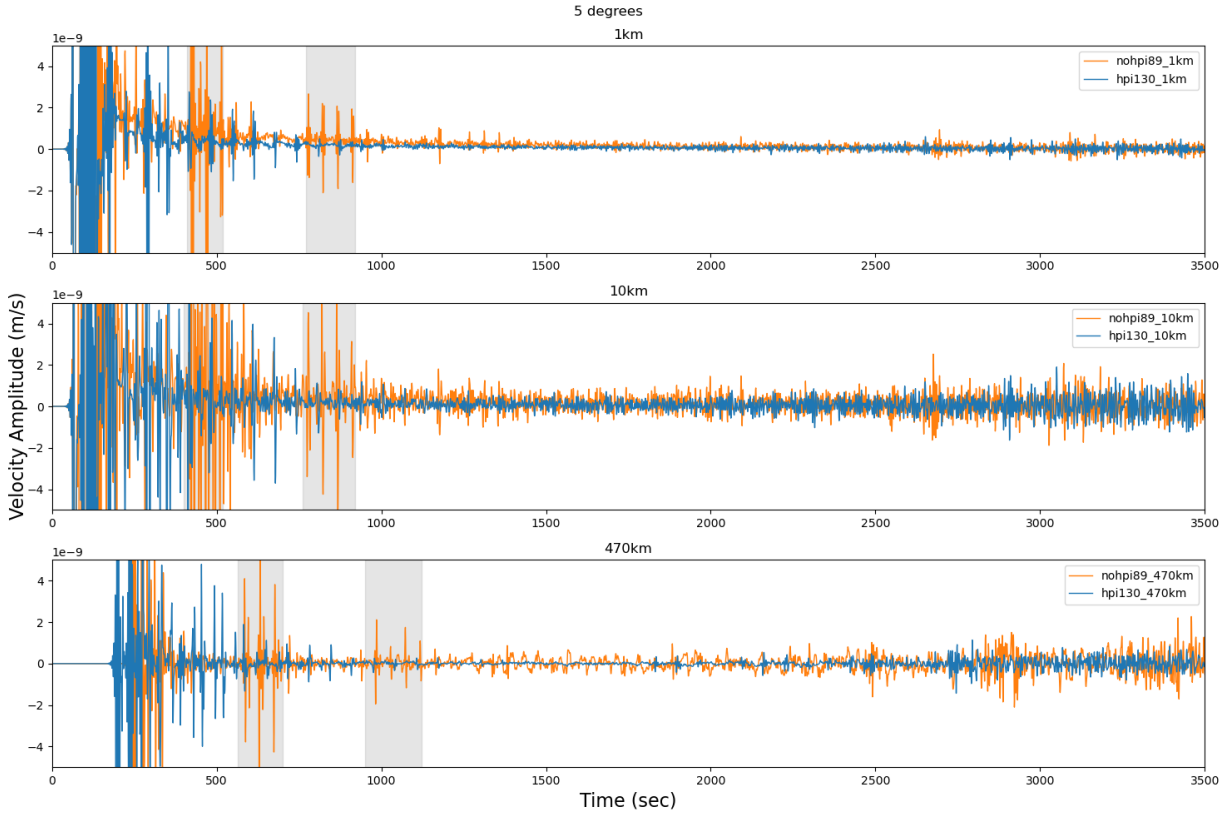

Figure 4.13: 5°, all depths, (top-bottom: 1 km, 10 km, 470 km); comparing 89 km (no high-pressure ice) to 130 km (high-pressure ice) models. Highlighted are regions of reverberations off of the body of the ocean for both models.

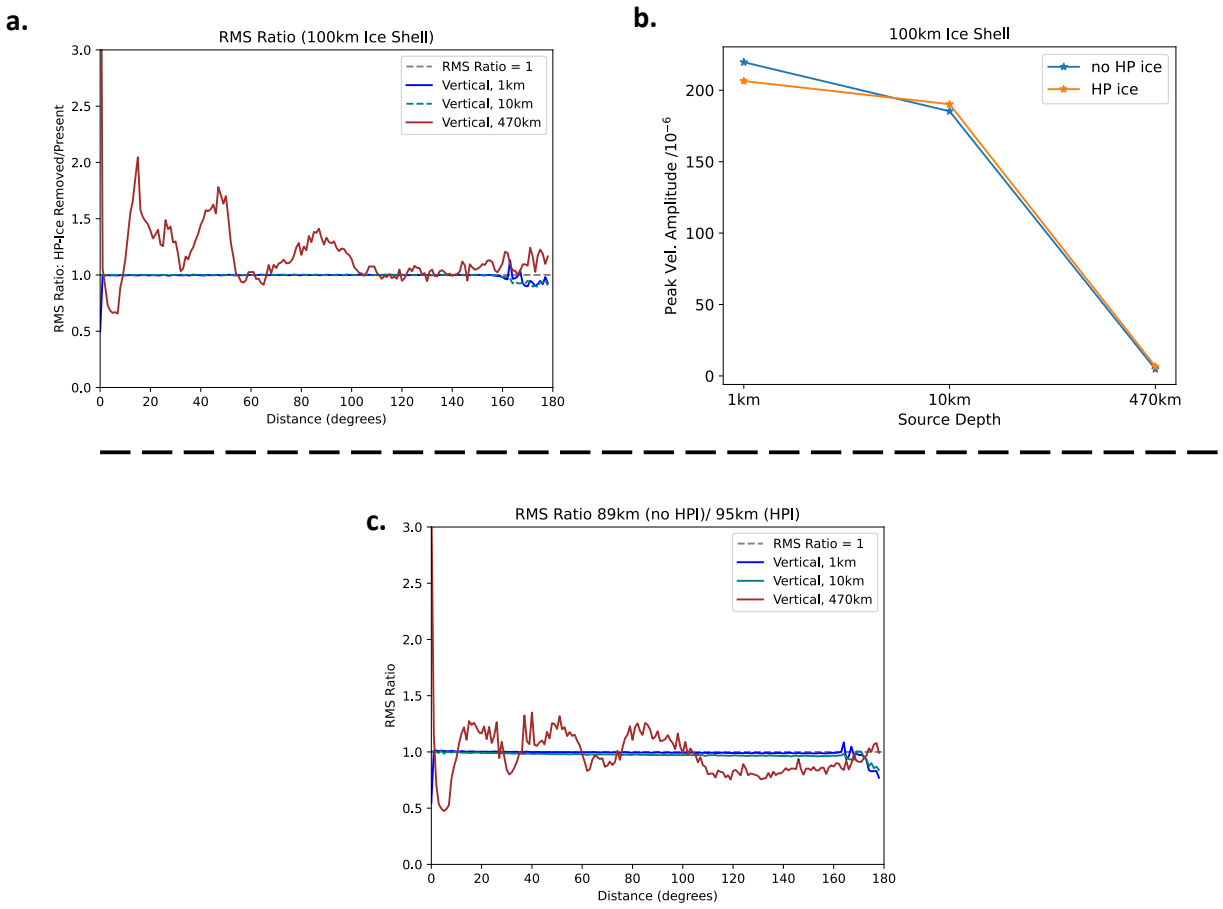

Figure 4.14: (a.) Root mean squares (RMS) of the velocities for the 100 km models, varying high-pressure ice, since the ice shell are very similar there are very small differences in the velocities for the shallow quakes, however we see much greater differences in the RMS for a deep quake (470 km source depth) when comparing a model with high-pressure ice to one without. The RMS of the velocities differs the most around 510°. (b.) Peak amplitudes vs. source depths at 5° for the 100 km ice shell models with varying high-pressure ice. (c.) RMS error of the velocities, since the ice shell are very similar there are very small differences in the velocities for the shallow quakes, however we see much greater differences in the RMS for a deep quake (470 km source depth) when comparing a model with high-pressure ice to one without. The RMS of the velocities differs the most around 510°.

high-pressure ice are three orders of magnitude smaller than the Rayleigh pulse, but possibly still detectable as they occur after the P, S and Rayleigh wave.

Also at 5°, we see the greatest peak amplitude difference for the deeper source (470 km), with the high-pressure ice having a amplitude that's 32% higher than the model without high-pressure. However, it is important to note the range of peak amplitudes at this distance differs by two orders of magnitude (≈200%), which could have a large effect on the detectability—something that this work has not addressed.

However when we look at the RMS (Figure 4.14) of the ground motion velocities of the 100 km models we see that the deeper sources (470 km) show the most amplitude variation between the models with and without high-pressure ice, although the effect varies as a function of distance for both the compared 100 km models as well as for comparison between the two closely spaced, but thermodynamically consistent models with and without the high pressure ice (Figure 4.14). This effect is only visible for the deep source because the surface waves trapped in the upper Ice Ih shell are only strongly excited by sources within the ice shell and they dominate the amplitude of those records.

One limiting factor of this study is that we look at spherically symmetric models that do not include heterogeneities, we also assume a pure water hydrosphere with no solutes or organics. Compared to what has been seen on Titan we know that this model is almost certainly oversimplified compared to what exists on Titan. We know from the *Cassini–Huygens* mission that there are dormant cryovolcanoes, mountains, rivers, lakes, as well as a rich hydrological cycle on Titan that could all be potential causes of seismic signals (at least from large events).

The composition of Titan's highly dense ocean is most likely rich in solutes, such as salts, ammonia (Mitri et al. [2014], Leitner and Lunine [2019]), or even magnesium sulfate (Vance et al. [2018b], MacKenzie et al. [2021]). Journaux et al. [2013] showed that in the case of a sodium chloride ocean there could exist patches of brine under a deep ice VI layer and a

the bedrock/mantle. It would be of much interest to investigate the ability to detect brine patches as well as the seismological effect that varying the composition of the ocean would have.

Future studies should incorporate organics of various kinds within the ice shell and throughout the hydrosphere, while varying the temperature at the base of the ice shell as well as the source depth of titanquakes to simulate more accurately what a single-station seismometer could see on Titan. Also in future studies if would be good to look with more detail, the likely magnitudes of Titan events (similar to the work done for Europa in Panning et al. [2018]) and initially extended to Titan and other tidally dominated worlds by Hurford et al. [2020]; as well as compare these results to expected seismometer sensitivity to determine whether the features discussed in this study are detectable by the *Dragonfly* seismometer.

4.8 Conclusions

We identify reverberations following body wave phase arrivals associated with reflections from the bottom of Titan's ocean as a potential diagnostic for the detection of high-pressure ice. The amplitude of most prominent feature of the shallow quakes (the Rayleigh pulse) is at most, two orders of magnitude greater than the subtle reverberations between the bottom of the ice shell an the top and bottom of the high-pressure ice—but with a very sensitive seismometer they could be detectable. Future work should investigate whether these diagnostic phases would be detectable with the *Dragonfly* seismometer.

Open Research

Some data used in this work were generated using the open-source *PlanetProfile* software hosted on GitHub (`https://github.com/vancesteven/PlanetProfile`). A Zenodo

archive of the most recent version is available at `https://zenodo.org/doi/10.5281/zenodo.844130` (Styczinski et al. [2024]). *PlanetProfile* is released under a GPL-3.0 license. The v2.3.16 release associated with this manuscript is archived at `https://doi.org/10.5281/zenodo.8098405` (Styczinski et al. [2023b]).

4.9 Acknowledgments

The authors thank the *Dragonfly* Guest Investigator Program and the Moons Geology and Geophysics group at the Jet Propulsion Laboratory. A. Bryant thanks Steve Meyer and Sunny Park at the University of Chicago for many helpful conversations. A part of the research was carried out at the Jet Propulsion Laboratory, California Institute of Technology, under a contract with the National Aeronautics and Space Administration (80NM0018D0004). A. Bryant was also funded partially by the *Dragonfly* Guest Investigator Program through the Johns Hopkins Applied Physics Laboratory.

CHAPTER 5

CONCLUSION

In this dissertation I presented a co-authored work on the methane clathrates focusing on the body waves and the surface waves. I also present work on high pressure ices on Titan and what types of seismic phases could be used to discover whether or not high pressure ice is present on Titan. At this preliminary stage of Titan seismology, I found that only a limited exploration of plausible parameter ranges was warranted; however, my results strongly suggest that with the advent of Dragonfly's arrival on Titan, Titan seismology is likely to be a powerful tool for understanding this Jovian moon's internal structure. I provide a brief summary below of the findings presented here and also some future study directions that my dissertation could serve as a launching pad for.

5.1 Seismic Models of Methane Clathrates on Titan

I presented two potential methods of detecting methane clathrates on Titan using body wave (P and S waves) and surface waves (flexural and surface Rayleigh wave dispersion) in Chapters 2 and 3.

5.1.1 Short Period: Body Wave Profiles

In Chapter 2 I presented the co-authored work, "The Effects of Methane Clathrates on the Thermal and Seismic Profile of Titan's Icy Lithosphere" (Marusiak et al. [2022]). We found some body wave arrival differences when comparing a pure water, 100km ice shell Titan model to a model with 10km of methane clathrates at the surface. There are subtle but detectable P and S wave arrival differences due to thermal gradient driven attenuation changes on Titan due to the reduced thermal conductivity of the clathrates than water ice. Also in Marusiak et al. [2022] we saw very subtle differences in the frequency content of the

seismograms between the two models. These subtle differences were investigated more in the Chapter 3.

Also in Chapter 2, I included additional work that I did to support and extend the findings of Marusiak et al. [2022]: "Investigating Detection of Methane Clathrates with Varying Source Depths on Titan".

5.1.2 Long Period: Surface Wave Profiles

The previous body wave focused study motivated my first-author submitted publication, "Long Period Seismology on Titan in the Presence of a Methane Clathrate Lid", presented in Chapter 3 of this dissertation. Both works were done in preparation for the Dragonfly mission to Saturn's moon Titan, but also as a primer for further seismic studies of icy ocean worlds within the Solar System where a thick ice shell, subsurface ocean, and thick layers of clathrates could co-exist. In particular this work explored the dominant surface waves seen in both the frequency and time domains, to provide a more complete analysis of both the body and surface waves generated by the events. In this Chapter, I, and my collaborators, investigated using low-frequency surface waves to detect surface clathrate layers on Titan. Overall, we discovered that the characteristic large amplitude Rayleigh wave can be attributed to the first overtone when looking at the frequency content contributions. However, we also found for our models with varying thickness of methane clathrate layers for a 100 km thick Titan-like ice shell, that the clathrate layers were indistinguishable using long period seismology methods as the uncertainty in the measurement of surface wave velocities exceeded the velocity differences introduced by the presence of clathrates. This does not exclude using long period methods on Titan, but it will most likely be challenging to detect clathrates lids using this method on Titan.

5.2 Seismic Models of High-Pressure Ice on Titan

In Chapter 4 we investigate key phases that would be indicative of high-pressure ice on Titan. We see that synthetic seismograms from models with high-pressure ice have a unique "double" reverberation from P waves reflecting off of the top and bottom of the high-pressure ice layer. This "double" reverberation is absent for models without high-pressure ice, as P waves reflect off the bottom of the ocean/top of the mantle. This effect is subtle, but with a sensitive enough seismometer could be detectable.

5.3 Future Directions

This work is of course non-exhaustive. We are about 10 years away from having real Titan data from Dragonfly, so there is a lot of time to continue to refine our models. The goal, as with Mars, would be to catalog as many events as is possible to be able to have a good base from which to refine what is in the interior of Titan. Of course Titan is just the beginning, as there are a number of icy ocean worlds in the Solar System (e.g. Ganymede, Europa, Enceladus and many more) each with unique water-bearing interiors that could be uncovered with seismology.

The most recent Decadal Survey (National Academies of Sciences et al. [2022]) for planetary science and astrobiology named the Uranus Orbiter and Probe (UOP) as the highest priority, and the Enceladus Orbilander as the second highest priority Flagship mission for the decade of 2023-2032 (Mackenzie et al. [2021], MacKenzie et al. [2022]). This suggests that there will be a lot of focus on these as well as the other missions such as the Europa Lander concept (Pappalardo et al. [2013], Dooley [2018], Hand et al. [2022]), or even a Venus balloon to measure quakes from the Venus atmosphere (Lognonne and Johnson [2009], Krishnamoorthy et al. [2022]). Wherever there is a solid surface to land there is an opportunity for extraterrestrial seismology to be a tool for helping to constrain the interior of said planetary

or lunar body.

We know from asteroseismology (stellar seismology), helioseismology (solar seismology), and ring (i.e., Saturn and perhaps Uranus) seismology that a seismometer on the ground is not a necessity to be able to constrain the interior structures of a planetary body using seismological methods.

There's so much to be learned with seismology across the Solar System and beyond, we've just only scratched the surface (of Earth, the Moon and Mars)! More to come in the coming decades!

REFERENCES

Keiiti Aki and Paul G Richards. *Quantitative Seismology*. 2002.

Don L. Anderson and Adam M. Dziewonski. Seismic Tomography. *Scientific American*, 251 (4):60–71, 1984. URL http://www.jstor.org/stable/24969456.

J.D. Anderson, Tilman Spohn, and William Mckinnon. *Interior composition, structure and dynamics of the Galilean satellites*, pages 281–306. 01 2004. ISBN 0-521-81808-7.

Ove Andersson and Akira Inaba. Thermal conductivity of crystalline and amorphous ices and its implications on amorphization and glassy water. *Physical Chemistry Chemical Physics*, 7(7):1441–1449, 2005. ISSN 1463-9076. doi:10.1039/B500373C. URL http://dx.doi.org/10.1039/B500373C.

Sushil K Atreya, Elena Y Adams, Hasso B Niemann, Jaime E Demick-Montelara, Tobias C Owen, Marcello Fulchignoni, Francesca Ferri, and Eric H Wilson. Titan's methane cycle. *Planetary and Space Science*, 54(12):1177–1187, 10 2006. ISSN 00320633. doi:10.1016/j.pss.2006.05.028. URL https://linkinghub.elsevier.com/retrieve/pii/S0032063306001322.

Rose-Marie Baland, Gabriel Tobie, Axel Lefèvre, and Tim Van Hoolst. Titan's internal structure inferred from its gravity field, shape, and rotation state. *Icarus*, 237:29–41, 2014. ISSN 0019-1035. doi:https://doi.org/10.1016/j.icarus.2014.04.007. URL https://www.sciencedirect.com/science/article/pii/S0019103514001997.

W Bruce Banerdt, Suzanne E Smrekar, Don Banfield, Domenico Giardini, Matthew Golombek, Catherine L Johnson, Philippe Lognonné, Aymeric Spiga, Tilman Spohn, Clément Perrin, et al. Initial results from the insight mission on mars. *Nature Geoscience*, 13 (3):183–189, 2020.

Jason W. Barnes, Robert H. Brown, Laurence Soderblom, Bonnie J. Buratti, Christophe Sotin, Sebastien Rodriguez, Stephane Le Mouèlic, Kevin H. Baines, Roger Clark, and Phil Nicholson. Global-scale surface spectral variations on titan seen from cassini/vims. *Icarus*, 186(1):242–258, 2007. ISSN 0019-1035. doi:https://doi.org/10.1016/j.icarus.2006.08.021. URL https://www.sciencedirect.com/science/article/pii/S001910350600306X.

Jason W. Barnes, Elizabeth P. Turtle, Melissa G. Trainer, Ralph D. Lorenz, Shannon M. MacKenzie, William B. Brinckerhoff, Morgan L. Cable, Carolyn M. Ernst, Caroline Freissinet, Kevin P Hand, Alexander G Hayes, Sarah M Hörst, Jeffrey R Johnson, Erich Karkoschka, David J Lawrence, Alice Le Gall, Juan M Lora, Christopher P McKay, Richard S Miller, Scott L Murchie, Catherine D Neish, Claire E Newman, Jorge Núñez, Mark P Panning, Ann M Parsons, Patrick N Peplowski, Lynnae C Quick, Jani Radebaugh, Scot C R Rafkin, Hiroaki Shiraishi, Jason M Soderblom, Kristin S Sotzen, Angela M Stickle, Ellen R Stofan, Cyril Szopa, Tetsuya Tokano, Thomas Wagner, Colin Wilson, R Aileen Yingst, Kris Zacny, and Simon C Stähler. Science Goals and Objectives for the

Dragonfly Titan Rotorcraft Relocatable Lander. *The Planetary Science Journal*, 2(4):130, 8 2021a. ISSN 2632-3338. doi:10.3847/PSJ/abfdcf. URL http://dx.doi.org/10.3847/PSJ/abfdcfhttps://iopscience.iop.org/article/10.3847/PSJ/abfdcf.

Jason W Barnes, Elizabeth P Turtle, Melissa G Trainer, Ralph D Lorenz, Shannon M MacKenzie, William B Brinckerhoff, Morgan L Cable, Carolyn M Ernst, Caroline Freissinet, Kevin P Hand, et al. Science goals and objectives for the dragonfly titan rotorcraft relocatable lander. *The Planetary Science Journal*, 2(4):130, 2021b.

Christian Béghin, Orélien Randriamboarison, Michel Hamelin, Erich Karkoschka, Christophe Sotin, Robert C Whitten, Jean-Jacques Berthelier, Réjean Grard, and Fernando Simões. Analytic theory of titan's schumann resonance: Constraints on ionospheric conductivity and buried water ocean. *Icarus*, 218(2):1028–1042, 2012.

Moritz Beyreuther, Robert Barsch, Lion Krischer, Tobias Megies, Yannik Behr, and Joachim Wassermann. ObsPy: A python toolbox for seismology. *Seismological Research Letters*, 81(3):530–533, 2010.

Ondřej Čadek, Klára Kalousová, Jakub Kvorka, and Christophe Sotin. The density structure of Titan's outer ice shell. *Icarus*, 364:114466, 8 2021. ISSN 00191035. doi:10.1016/j.icarus.2021.114466. URL https://www.sciencedirect.com/science/article/pii/S0019103521001457https://linkinghub.elsevier.com/retrieve/pii/S0019103521001457.

F Cammarano, V Lekic, M Manga, Mark P. Panning, and B Romanowicz. Long-period seismology on Europa: 1. Physically consistent interior models. *Journal of Geophysical Research-Planets*, 111(E12), 2006. doi:Artn E12009 10.1029/2006je002710.

Evan Carnahan, Natalie S. Wolfenbarger, Jacob S. Jordan, and Marc A. Hesse. New insights into temperature-dependent ice properties and their effect on ice shell convection for icy ocean worlds. *Earth and Planetary Science Letters*, 563:116886, 2021. ISSN 0012821X. doi:10.1016/j.epsl.2021.116886. URL https://doi.org/10.1016/j.epsl.2021.116886.

Evan Carnahan, Steven D Vance, Marc A Hesse, Baptiste Journaux, and Christophe Sotin. Dynamics of Mixed Clathrate-Ice Shells on Ocean Worlds. *Geophysical Research Letters*, 49(8):e2021GL097602, 4 2022. ISSN 0094-8276. doi:10.1029/2021GL097602. URL https://doi.org/10.1029/2021GL097602.

Mathieu Choukroun and Christophe Sotin. Is Titan's shape caused by its meteorology and carbon cycle? *Geophysical Research Letters*, 39(4):n/a–n/a, 2 2012. ISSN 00948276. doi:10.1029/2011GL050747. URL http://doi.wiley.com/10.1029/2011GL050747.

Mathieu Choukroun, Olivier Grasset, Gabriel Tobie, and Christophe Sotin. Stability of methane clathrate hydrates under pressure: Influence on outgassing processes of methane on Titan. *Icarus*, 205(2):581–593, 2 2010. ISSN 00191035. doi:10.1016/j.icarus.2009.08.011. URL https://linkinghub.elsevier.com/retrieve/pii/S0019103509003509.

J A D Connolly. The geodynamic equation of state: what and how. *Geochemistry, Geophysics, Geosystems*, 10(Q10014), 2009. doi:10.1029/2009GC002540.

M. A. Cordiner, M. Y. Palmer, C. A. Nixon, P. G. J. Irwin, N. A. Teanby, S. B. Charnley, M. J. Mumma, Z. Kisiel, J. Serigano, Y.-J. Kuan, Y.-L. Chuang, and K.-S. Wang. Ethyl cyanide on titan: Spectroscopic detection and mapping using alma. *The Astrophysical Journal Letters*, 800(1):L14, feb 2015. doi:10.1088/2041-8205/800/1/L14. URL https://dx.doi.org/10.1088/2041-8205/800/1/L14.

M. A. Cordiner, C. A. Nixon, S. B. Charnley, N. A. Teanby, E. M. Molter, Z. Kisiel, and V. Vuitton. Interferometric imaging of titan's hc3n, h13cccn, and hccc15n. *The Astrophysical Journal Letters*, 859(1):L15, may 2018. doi:10.3847/2041-8213/aac38d. URL https://dx.doi.org/10.3847/2041-8213/aac38d.

H. P. Crotwell, T. J. Owens, and J. Ritsema. The TauP Toolkit: Flexible Seismic Travel-time and Ray-path Utilities. *Seismological Research Letters*, 70(2):154–160, 3 1999a. ISSN 0895-0695. doi:10.1785/gssrl.70.2.154. URL https://pubs.geoscienceworld.org/srl/article/70/2/154-160/142385.

H Philip Crotwell, Thomas J Owens, and Jeroen Ritsema. The taup toolkit: Flexible seismic travel-time and ray-path utilities. *Seismological Research Letters*, 70(2):154–160, 1999b.

Frédéric Deschamps, Olivier Mousis, Carmen Sanchez-Valle, and Jonathan I. Lunine. The role of methanol in the crystallization of titan's primordial ocean. *The Astrophysical Journal*, 724(2):887, nov 2010. doi:10.1088/0004-637X/724/2/887. URL https://dx.doi.org/10.1088/0004-637X/724/2/887.

Frédéric Deschamps and Christophe Sotin. Thermal convection in the outer shell of large icy satellites. *Journal of Geophysical Research E: Planets*, 106(E3):5107–5121, 2001. ISSN 01480227. doi:10.1029/2000JE001253.

James Dewey and Perry Byerly. The early history of seismometry (to 1900). *Bulletin of the Seismological Society of America*, 59(1):183–227, 02 1969. ISSN 0037-1106. doi:10.1785/BSSA0590010183. URL https://doi.org/10.1785/BSSA0590010183.

Jennifer Dooley. Mission concept for a europa lander. In *2018 IEEE Aerospace Conference*, pages 1–10. IEEE, 2018.

Daniele Durante, D.J. Hemingway, P. Racioppa, L. Iess, and D.J. Stevenson. Titan's gravity field and interior structure after cassini. *Icarus*, 326:123–132, 2019. ISSN 0019-1035. doi:https://doi.org/10.1016/j.icarus.2019.03.003. URL https://www.sciencedirect.com/science/article/pii/S0019103518307267.

Sydney N Dybing, Adam T Ringler, David C Wilson, and Robert E Anthony. Characteristics and spatial variability of wind noise on near-surface broadband seismometers. *Bulletin of the Seismological Society of America*, 109(3):1082–1098, 2019.

A. Dziewonski, S. Bloch, and M. Landisman. A technique for the analysis of transient seismic signals. *Bulletin of the Seismological Society of America*, 59(1):427–444, 02 1969. ISSN 0037-1106. doi:10.1785/BSSA0590010427. URL https://doi.org/10.1785/BSSA0590010427.

Adam M. Dziewonski and Don L. Anderson. Preliminary Reference Earth Model. *Physics of the Earth and Planetary Interiors*, 25(4):297–356, 1981. doi:10.1016/0031-9201(81)90046-7.

C Elachi, S Wall, M Allison, Y Anderson, R Boehmer, P Callahan, P Encrenaz, E Flamini, G Franceschetti, Y Gim, G Hamilton, S Hensley, M Janssen, W Johnson, K Kelleher, R Kirk, R Lopes, Ralph D. Lorenz, J Lunine, D Muhleman, S Ostro, F Paganelli, G Picardi, F Posa, L Roth, R Seu, S Shaffer, L Soderblom, B Stiles, E Stofan, S Vetrella, R West, C Wood, L Wye, and H Zebker. Cassini Radar Views the Surface of Titan. *Science*, 308(5724):970–974, 2005. doi:10.1126/science.1109919.

A.D. Fortes. Titan's internal structure and the evolutionary consequences. *Planetary and Space Science*, 60(1):10–17, 2012. ISSN 0032-0633. doi:https://doi.org/10.1016/j.pss.2011.04.010. URL https://www.sciencedirect.com/science/article/pii/S0032063311001401. Titan Through Time: A Workshop on Titan's Formation, Evolution and Fate.

Raphael F. Garcia, Amir Khan, Mélanie Drilleau, Ludovic Margerin, Taichi Kawamura, Daoyuan Sun, Mark A. M.A. Wieczorek, Attilio Rivoldini, Ceri Nunn, R.C. Renee C. Weber, Angela G. Marusiak, Philippe Lognonné, Yosio Nakamura, and Peimin Zhu. Lunar Seismology: An Update on Interior Structure Models. *Space Science Reviews*, 215(8):50, 11 2019. ISSN 1572-9672. doi:10.1007/s11214-019-0613-y. URL http://link.springer.com/10.1007/s11214-019-0613-yhttps://doi.org/10.1007/s11214-019-0613-y.

Domenico Giardini, Philippe Lognonné, William Bruce Banerdt, W T Pike, U Christensen, S Ceylan, J F Clinton, M van Driel, Simon C. Stähler, M Böse, Raphael F. Garcia, A Khan, Mark P. Panning, C Perrin, D Banfield, E Beucler, C Charalambous, F Euchner, A Horleston, A Jacob, T Kawamura, S Kedar, G Mainsant, J.-R. Scholz, S E Smrekar, A Spiga, C Agard, D Antonangeli, S Barkaoui, E Barrett, P Combes, V Conejero, I Daubar, M Drilleau, C Ferrier, T Gabsi, T Gudkova, K Hurst, F Karakostas, S King, M Knapmeyer, B Knapmeyer-Endrun, R Llorca-Cejudo, A Lucas, L Luno, L Margerin, J B McClean, D Mimoun, N Murdoch, F Nimmo, M Nonon, C Pardo, A Rivoldini, J A Rodriguez Manfredi, H Samuel, M Schimmel, A E Stott, E Stutzmann, N Teanby, T Warren, Renee C. Weber, M Wieczorek, and C Yana. The seismicity of Mars. *Nature Geoscience*, 13(3):205–212, 3 2020. ISSN 1752-0894. doi:10.1038/s41561-020-0539-8. URL https://doi.org/10.1038/s41561-020-0539-8http://www.nature.com/articles/s41561-020-0539-8.

Stephen P. Grand, Rob D. van der Hilst, and Sri Widiyantoro. Global Seismic Tomography: A Snapshot of Convection in the Earth. *GSA Today*, 7(4):1–7, 1997. ISSN 10525173. doi:10.1130/GSAT01707GW.1.

O Grasset, C Sotin, and F Deschamps. On the internal structure and dynamics of titan. *Planetary and Space Science*, 48(7-8):617–636, 2000.

Beno Gutenberg. Microseisms and weather forecasting. *Journal of Atmospheric Sciences*, 4 (1):21–28, 1947.

Kevin P Hand, Christopher F Chyba, Robert W Carlson, and John F Cooper. Clathrate Hydrates of Oxidants in the Ice Shell of Europa. *Astrobiology*, 6(3):463–482, 6 2006. ISSN 1531-1074. doi:10.1089/ast.2006.6.463. URL http://www.liebertpub.com/doi/10.1089/ast.2006.6.463.

Kevin P Hand, Cynthia B Phillips, A Murray, JB Garvin, EH Maize, RG Gibbs, G Reeves, AM San Martin, GH Tan-Wang, J Krajewski, et al. Science goals and mission architecture of the europa lander mission concept. *The Planetary Science Journal*, 3(1):22, 2022.

Alexander G Hayes. The lakes and seas of titan. *Annual Review of Earth and Planetary Sciences*, 44:57–83, 2016.

Alexander G Hayes, Ralph D Lorenz, and Jonathan I Lunine. A post-Cassini view of Titan's methane-based hydrologic cycle. *Nature Geoscience*, 11(5):306–313, 2018. ISSN 1752-0908. doi:10.1038/s41561-018-0103-y. URL https://doi.org/10.1038/s41561-018-0103-y.

Paul O. Hayne, Thomas B. McCord, and Christophe Sotin. Titan's surface composition and atmospheric transmission with solar occultation measurements by cassini vims. *Icarus*, 243: 158–172, 2014. ISSN 0019-1035. doi:https://doi.org/10.1016/j.icarus.2014.08.045. URL https://www.sciencedirect.com/science/article/pii/S001910351400462X.

M. B. Helgerud, W. F. Waite, S. H. Kirby, and A. Nur. Measured temperature and pressure dependence of Vp and Vs in compacted, polycrystalline sI methane and sII methane-ethane hydrate. *Canadian Journal of Physics*, 81(1-2):47–53, 2003. ISSN 00084204. doi:10.1139/p03-016.

M. B. Helgerud, W. F. Waite, S. H. Kirby, and A. Nur. Elastic wave speeds and moduli in polycrystalline ice Ih, sI methane hydrate, and sII methane-ethane hydrate. *Journal of Geophysical Research*, 114(B2):B02212, 2 2009. ISSN 0148-0227. doi:10.1029/2008JB006132. URL http://doi.wiley.com/10.1029/2008JB006132.

D Hemingway, F Nimmo, H Zebker, and L Iess. A rigid and weathered ice shell on Titan. *Nature*, 500(7464):550–552, 2013. ISSN 1476-4687. doi:10.1038/nature12400. URL https://doi.org/10.1038/nature12400.

S. M. Hörst. Titan's atmosphere and climate. *Journal of Geophysical Research: Planets*, 122(3):432–482, 2017. doi:https://doi.org/10.1002/2016JE005240. URL https://agupubs.onlinelibrary.wiley.com/doi/abs/10.1002/2016JE005240.

Terry A. Hurford, W.G. Henning, Ross Maguire, Vedran Lekic, Nicholas C. Schmerr, Mark P. Panning, V.J. Bray, M Manga, S.A. Kattenhorn, L.C. Quick, and A.R. Rhoden. Seismicity on tidally active solid-surface worlds. *Icarus*, 338:113466, 3 2020. ISSN 00191035. doi:10.1016/j.icarus.2019.113466. URL http://www.sciencedirect.com/science/article/pii/S0019103518307243https://linkinghub.elsevier.com/retrieve/pii/S0019103518307243.

Luciano Iess, Robert A. Jacobson, Marco Ducci, David J. Stevenson, Jonathan I. Lunine, John W. Armstrong, Sami W. Asmar, Paolo Racioppa, Nicole J. Rappaport, and Paolo Tortora. The tides of titan. *Science*, 337(6093):457–459, 2012. doi:10.1126/science.1219631. URL https://www.science.org/doi/abs/10.1126/science.1219631.

Luciano Iess, D J Stevenson, M Parisi, D Hemingway, R A Jacobson, J I Lunine, Francis Nimmo, J W Armstrong, S W Asmar, M Ducci, and P. Tortora. The Gravity Field and Interior Structure of Enceladus. *Science*, 344(6179):78–80, 4 2014. ISSN 0036-8075. doi:10.1126/science.1250551. URL https://www.sciencemag.org/lookup/doi/10.1126/science.1250551.

Heiner Igel. *Computational Seismology: A Practical Introduction*. Oxford University Press, 2017.

M.A. Janssen, R.D. Lorenz, R. West, F. Paganelli, R.M. Lopes, R.L. Kirk, C. Elachi, S.D. Wall, W.T.K. Johnson, Y. Anderson, R.A. Boehmer, P. Callahan, Y. Gim, G.A. Hamilton, K.D. Kelleher, L. Roth, B. Stiles, and A. Le Gall. Titan's surface at 2.2-cm wavelength imaged by the cassini radar radiometer: Calibration and first results. *Icarus*, 200(1): 222–239, 2009. ISSN 0019-1035. doi:https://doi.org/10.1016/j.icarus.2008.10.017. URL https://www.sciencedirect.com/science/article/pii/S0019103508003801.

M.A. Janssen, A. Le Gall, R.M. Lopes, R.D. Lorenz, M.J. Malaska, A.G. Hayes, C.D. Neish, A. Solomonidou, K.L. Mitchell, J. Radebaugh, S.J. Keihm, M. Choukroun, C. Leyrat, P.J. Encrenaz, and M. Mastrogiuseppe. Titan's surface at 2.18-cm wavelength imaged by the cassini radar radiometer: Results and interpretations through the first ten years of observation. *Icarus*, 270:443–459, 2016. ISSN 0019-1035. doi:https://doi.org/10.1016/j.icarus.2015.09.027. URL https://www.sciencedirect.com/science/article/pii/S0019103515004327. Titan's Surface and Atmosphere.

DE Jennings, V Cottini, CA Nixon, RK Achterberg, FM Flasar, VG Kunde, PN Romani, RE Samuelson, A Mamoutkine, NJP Gorius, et al. Surface temperatures on titan during northern winter and spring. *The Astrophysical Journal Letters*, 816(1):L17, 2016.

B Journaux, I Daniel, R Caracas, G Montagnac, and H Cardon. Influence of NaCl on ice VI and ice VII melting curves up to 6 GPa, implications for large icy moons. *Icarus*, 226(1): 355–363, 2013.

B Journaux, J M Brown, A Pakhomova, I E Collings, S Petitgirard, P Espinoza, T Boffa Ballaran, S D Vance, J Ott, F Cova, G Garbarino, and M Hanfland. Holistic Approach for Studying Planetary Hydrospheres: Gibbs Representation of Ices Thermodynamics, Elasticity, and the Water Phase Diagram to 2,300 MPa. *Journal of Geophysical Research: Planets*, 125(1):e2019JE006176, 1 2020a. ISSN 2169-9097. doi:10.1029/2019JE006176. URL https://doi.org/10.1029/2019JE006176https://onlinelibrary.wiley.com/doi/10.1029/2019JE006176.

Baptiste Journaux, J. Michael Brown, Olivier Bollengier, Evan Abramson, Gabriel Tobie, and Steven D. Vance. SeaFreeze : A modular thermodynamic framework for modeling all solar system planetary hydrospheres, including ice polymorphs and aqueous solutions at high-pressures. In *EPSC-DPS*, 2019. URL https://meetingorganizer.copernicus.org/EPSC-DPS2019/EPSC-DPS2019-797-1.pdf.

Baptiste Journaux, Klára Kalousová, Christophe Sotin, Gabriel Tobie, Steve Vance, Joachim Saur, Olivier Bollengier, Lena Noack, Tina Rückriemen-Bez, Tim Van Hoolst, Krista M. Soderlund, and J. Michael Brown. Large Ocean Worlds with High-Pressure Ices. *Space Science Reviews*, 216(1), 2020b. ISSN 15729672. doi:10.1007/s11214-019-0633-7. URL http://dx.doi.org/10.1007/s11214-019-0633-7.

Klára Kalousová and Christophe Sotin. Dynamics of Titan's high-pressure ice layer. *Earth and Planetary Science Letters*, 545, 9 2020a. ISSN 0012821X. doi:10.1016/j.epsl.2020.116416.

Klára Kalousová and Christophe Sotin. The Insulating Effect of Methane Clathrate Crust on Titan's Thermal Evolution. *Geophysical Research Letters*, 47(13):e2020GL087481, 7 2020b. ISSN 0094-8276. doi:10.1029/2020GL087481. URL https://doi.org/10.1029/2020GL087481https://onlinelibrary.wiley.com/doi/10.1029/2020GL087481.

Shunichi Kamata, Francis Nimmo, Yasuhito Sekine, Kiyoshi Kuramoto, Naoki Noguchi, Jun Kimura, and Atsushi Tani. Pluto's ocean is capped and insulated by gas hydrates. *Nature Geoscience*, 12(6):407–410, 2019. ISSN 1752-0908. doi:10.1038/s41561-019-0369-8. URL https://doi.org/10.1038/s41561-019-0369-8.

B L N Kennett and E R Engdahl. Traveltimes for Global Earthquake Location and Phase Identification. *Geophysical Journal International*, 105(2):429–465, 1991. doi:DOI 10.1111/j.1365-246X.1991.tb06724.x.

Amir Khan, Savas Ceylan, Martin van Driel, Domenico Giardini, Philippe Lognonné, Henri Samuel, Nicholas C. Schmerr, Simon C. Stähler, Andrea C. Duran, Quancheng Huang, Doyeon Kim, Adrien Broquet, Constantinos Charalambous, John F. Clinton, Paul M. Davis, Mélanie Drilleau, Foivos Karakostas, Vedran Lekic, Scott M. McLennan, Ross R. Maguire, Chloé Michaut, Mark P. Panning, William T. Pike, Baptiste Pinot, Matthieu Plasman, John-Robert Scholz, Rudolf Widmer-Schnidrig, Tilman Spohn, Suzanne E. Smrekar, and William B. Banerdt. Upper mantle structure of Mars from InSight seismic data.

Science, 373(6553):434–438, 7 2021. ISSN 0036-8075. doi:10.1126/science.abf2966. URL https://www.sciencemag.org/lookup/doi/10.1126/science.abf2966.

Brigitte Knapmeyer-Endrun, Mark P Panning, Felix Bissig, Rakshit Joshi, Amir Khan, Doyeon Kim, Vedran Lekić, Benoit Tauzin, Saikiran Tharimena, Matthieu Plasman, Nicolas Compaire, Raphael F. Garcia, Ludovic Margerin, Martin Schimmel, Éléonore Stutzmann, Nicholas Schmerr, Ebru Bozdağ, Ana-catalina Plesa, Mark A Wieczorek, Adrien Broquet, Daniele Antonangeli, Scott M. McLennan, Henri Samuel, Chloé Michaut, Lu Pan, Suzanne E Smrekar, Catherine L Johnson, Nienke Brinkman, Anna Mittelholz, Attilio Rivoldini, Paul M Davis, Philippe Lognonné, Baptiste Pinot, John-Robert Scholz, Simon Stähler, Martin Knapmeyer, Martin van Driel, Domenico Giardini, and W Bruce Banerdt. Thickness and structure of the martian crust from InSight seismic data. *Science*, 373(6553):438–443, 7 2021. ISSN 0036-8075. doi:10.1126/science.abf8966. URL https://www.sciencemag.org/lookup/doi/10.1126/science.abf8966.

Robert L. Kovach and Christopher F. Chyba. Seismic Detectability of a Subsurface Ocean on Europa. *Icarus*, 150(2):279–287, 4 2001. ISSN 00191035. doi:10.1006/icar.2000.6577. URL https://linkinghub.elsevier.com/retrieve/pii/S0019103500965771.

Siddharth Krishnamoorthy, Attila Komjathy, James A Cutts, Phlippe Lognonne, Raphael Garcia, Mark P Panning, Paul K Byrne, Robin S Matoza, Art D Jolly, Jonathan B Snively, et al. Seismology on venus with infrasound observations from balloon and orbit. In *Planetary Science and Astrobiology Decadal Survey 2023-2032 white paper e-id. 061; Bulletin of the American Astronomical Society*, volume 53, 2022.

J. C.-Y. Lai, M. A. Cordiner, C. A. Nixon, R. K. Achterberg, E. M. Molter, N. A. Teanby, M. Y. Palmer, S. B. Charnley, J. E. Lindberg, Z. Kisiel, M. J. Mumma, and P. G. J. Irwin. Mapping vinyl cyanide and other nitriles in titan's atmosphere using alma. *The Astronomical Journal*, 154(5):206, nov 2017. doi:10.3847/1538-3881/aa8eef. URL https://dx.doi.org/10.3847/1538-3881/aa8eef.

Stéphane Le Mouélic, Philippe Paillou, Michael A. Janssen, Jason W. Barnes, Sébastien Rodriguez, Christophe Sotin, Robert H. Brown, Kevin H. Baines, Bonnie J. Buratti, Roger N. Clark, Marc Crapeau, Pierre J. Encrenaz, Ralf Jaumann, Dirk Geudtner, Flora Paganelli, Laurence Soderblom, Gabriel Tobie, and Steve Wall. Mapping and interpretation of sinlap crater on titan using cassini vims and radar data. *Journal of Geophysical Research: Planets*, 113(E4), 2008. doi:https://doi.org/10.1029/2007JE002965. URL https://agupubs.onlinelibrary.wiley.com/doi/abs/10.1029/2007JE002965.

Jean Pierre Lebreton, Athena Coustenis, Jonathan Lunine, François Raulin, Tobias Owen, and Darrell Strobel. Results from the Huygens probe on Titan, 2009. ISSN 09354956.

Marika A Leitner and Jonathan I Lunine. Modeling early Titan's ocean composition. *Icarus*, 333:61–70, 2019.

P Lognonne and C L Johnson. Planetary seismology. In G Schubert and T Spohn, editors, *Treatise Geophysics*, volume 10, chapter 3. Elsevier, 2009. ISBN 9780444534651.

Philippe Lognonné, William Bruce Banerdt, D. Giardini, W T Pike, U Christensen, P. Laudet, S. de Raucourt, P. Zweifel, S. Calcutt, M. Bierwirth, K J Hurst, F Ijpelaan, J. W. Umland, R. Llorca-Cejudo, S. A. Larson, Raphael F. Garcia, Sharon Kedar, Brigitte Knapmeyer-Endrun, Da Mimoun, A. Mocquet, M. P. Panning, Re Weber, A. Sylvestre-Baron, G. Pont, N. Verdier, L. Kerjean, L. J. Facto, V. Gharakanian, J. E. Feldman, T. L. Hoffman, D. B. Klein, K. Klein, N. P. Onufer, J. Paredes-Garcia, M. P. Petkov, J. R. Willis, S. E. Smrekar, M. Drilleau, T. Gabsi, T. Nebut, O. Robert, S. Tillier, C. Moreau, M. Parise, G. Aveni, S. Ben Charef, Y. Bennour, T. Camus, P. A. Dandonneau, C. Desfoux, B. Lecomte, O. Pot, P. Revuz, D. Mance, J. TenPierick, N. E. Bowles, C. Charalambous, A. K. Delahunty, J. Hurley, R. Irshad, Huafeng Liu, A. G. Mukherjee, I. M. Standley, A. E. Stott, J. Temple, T. Warren, M. Eberhardt, A. Kramer, W. Kühne, E.-P. Miettinen, M. Monecke, C. Aicardi, M. André, J. Baroukh, A. Borrien, A. Bouisset, P. Boutte, K. Brethomé, C. Brysbaert, T. Carlier, M. Deleuze, J. M. Desmarres, D. Dilhan, C. Doucet, D. Faye, N. Faye-Refalo, R. Gonzalez, C. Imbert, C. Larigauderie, E. Locatelli, L. Luno, J.-R. Meyer, F. Mialhe, J. M. Mouret, M. Nonon, Y. Pahn, A. Paillet, P. Pasquier, G. Perez, R. Perez, L. Perrin, B. Pouilloux, A. Rosak, I. Savin de Larclause, J. Sicre, M. Sodki, N. Toulemont, B. Vella, C. Yana, F. Alibay, O. M. Avalos, M. A. Balzer, P. Bhandari, E. Blanco, B. D. Bone, J. C. Bousman, P. Bruneau, F. J. Calef, R. J. Calvet, S. A. D'Agostino, G. de los Santos, R. G. Deen, R. W. Denise, J. Ervin, N. W. Ferraro, H. E. Gengl, F. Grinblat, D. Hernandez, M. Hetzel, M. E. Johnson, L. Khachikyan, J. Y. Lin, S. M. Madzunkov, S. L. Marshall, I. G. Mikellides, E. A. Miller, W. Raff, J. E. Singer, C. M. Sunday, J. F. Villalvazo, M. C. Wallace, D. Banfield, J. A. Rodriguez-Manfredi, C. T. Russell, A. Trebi-Ollennu, J. N. Maki, E. Beucler, M. Böse, C. Bonjour, J. L. Berenguer, S. Ceylan, J. Clinton, V. Conejero, I. Daubar, V. Dehant, P. Delage, F. Euchner, I. Estève, L. Fayon, L. Ferraioli, C. L. Johnson, J. Gagnepain-Beyneix, M. Golombek, Amir Khan, T. Kawamura, B. Kenda, P. Labrot, N. Murdoch, C. Pardo, C. Perrin, L. Pou, A. Sauron, D. Savoie, S. Stähler, E. Stutzmann, N. A. Teanby, J. Tromp, M. van Driel, M. Wieczorek, R. Widmer-Schnidrig, and J. Wookey. SEIS: Insight's Seismic Experiment for Internal Structure of Mars. *Space Science Reviews*, 215(1):12, 2 2019. ISSN 0038-6308. doi:10.1007/s11214-018-0574-6. URL `http://link.springer.com/10.1007/s11214-018-0574-6`.

R. M. C. Lopes, S. D. Wall, C. Elachi, S. P. D. Birch, P. Corlies, A. Coustenis, A. G. Hayes, J. D. Hofgartner, M. A. Janssen, R. L. Kirk, A. LeGall, R. D. Lorenz, J. I. Lunine, M. J. Malaska, M. Mastroguiseppe, G. Mitri, C. D. Neish, C. Notarnicola, F. Paganelli, P. Paillou, V. Poggiali, J. Radebaugh, S. Rodriguez, A. Schoenfeld, J. M. Soderblom, A. Solomonidou, E. R. Stofan, B. W. Stiles, F. Tosi, E. P. Turtle, R. D. West, C. A. Wood, H. A. Zebker, J. W. Barnes, D. Casarano, P. Encrenaz, T. Farr, C. Grima, D. Hemingway, O. Karatekin, A. Lucas, K. L. Mitchell, G. Ori, R. Orosei, P. Ries, D. Riccio, L. A. Soderblom, and Z. Zhang. Titan as revealed by the cassini radar. *Space Science Reviews*, 215(4):33, 2019. doi:10.1007/s11214-019-0598-6. URL `https://doi.org/10.1007/s11214-019-0598-6`.

Rosaly MC Lopes, Karl L Mitchell, Stephen D Wall, Giuseppe Mitri, Michael Janssen, Steven

Ostro, Randolph L Kirk, Alexander G Hayes, Ellen R Stofan, Jonathan I Lunine, et al. The lakes and seas of titan. *EOS, Transactions American Geophysical Union*, 88(51): 569–570, 2007.

Ralph D Lorenz and Alice Le Gall. Schumann resonance on titan: A critical re-assessment. *Icarus*, 351:113942, 2020.

Ralph D Lorenz, Elizabeth P Turtle, Jason W Barnes, Melissa G Trainer, Douglas S Adams, Kenneth E Hibbard, Colin Z Sheldon, Kris Zacny, Patrick N Peplowski, David J Lawrence, et al. Dragonfly: A rotorcraft lander concept for scientific exploration at titan. *Johns Hopkins APL Technical Digest*, 34(3):14, 2018.

Ralph D. Lorenz, Mark P. Panning, Simon Stähler, H Shiraishi, R Yamada, E P Turtle, Simon Stähler, H Shiraishi, R Yamada, and Elizabeth P. Turtle. Titan Seismology with Dragonfly: Probing the Internal Structure of the Most Accessible Ocean World. *50th Lunar and Planetary Science Conference*, 57(763):Abstract #2173, 2019. URL `http://www.lpi.usra.edu/meetings/lpsc2019/pdf/2173.pdf`.

Ralph D. Lorenz, Shannon M. MacKenzie, Catherine D. Neish, Alice Le Gall, Elizabeth P. Turtle, Jason W. Barnes, Melissa G. Trainer, Alyssa Werynski, Joshua Hedgepeth, and Erich Karkoschka. Selection and characteristics of the dragonfly landing site near Selk crater, Titan. *Planetary Science Journal*, 2(1):24, 2021a. ISSN 26323338. doi:10.3847/PSJ/abd08f. URL `http://dx.doi.org/10.3847/PSJ/abd08f`.

Ralph D. Lorenz, Hiroaki Shiraishi, Mark Panning, and Kristin Sotzen. Wind and surface roughness considerations for seismic instrumentation on a relocatable lander for Titan. *Planetary and Space Science*, 206:105320, 7 2021b. ISSN 0032-0633. doi:10.1016/j.pss.2021.105320. URL `https://www.sciencedirect.com/science/article/pii/S0032063321001598https://doi.org/10.1016/j.pss.2021.105320https://linkinghub.elsevier.com/retrieve/pii/S0032063321001598`.

Jonathan I Lunine and David J Stevenson. Thermodynamics of clathrate hydrate at low and high pressures with application to the outer solar system. *Astrophysical Journal Supplement Series*, 58(3):493–531, 1985. ISSN 0067-0049.

Jonathan I Lunine and David J Stevenson. Clathrate and ammonia hydrates at high pressure: Application to the origin of methane on Titan. *Icarus*, 70(1):61–77, 1987. ISSN 0019-1035.

Shannon M MacKenzie, Samuel PD Birch, Sarah Hörst, Christophe Sotin, Erika Barth, Juan M Lora, Melissa G Trainer, Paul Corlies, Michael J Malaska, Ella Sciamma-O'Brien, et al. Titan: Earth-like on the outside, ocean world on the inside. *The Planetary Science Journal*, 2(3):112, 2021.

Shannon M Mackenzie, Marc Neveu, Alfonso F Davila, Jonathan I Lunine, Kathleen L Craft, Morgan L Cable, Charity M Phillips-lander, Jason D Hofgartner, Jennifer L Eigenbrode, J Hunter Waite, Christopher R Glein, Robert Gold, Peter J Greenauer, Karen Kirby,

Christopher Bradburne, Samuel P Kounaves, Michael J Malaska, Frank Postberg, G Wesley Patterson, Carolyn Porco, Jorge I Núñez, Chris German, Julie A Huber, Christopher P Mckay, Jean-pierre De Vera, John Robert Brucato, and Linda J Spilker. The Enceladus Orbilander Mission Concept : Balancing Return and Resources in the Search for Life. *The Planetary Science Journal*, 2(2):77, 2021. ISSN 2632-3338. doi:10.3847/PSJ/abe4da. URL http://dx.doi.org/10.3847/PSJ/abe4da.

Shannon M MacKenzie, Marc Neveu, Alfonso F Davila, Jonathan I Lunine, Morgan L Cable, Charity M Phillips-Lander, Jennifer L Eigenbrode, J Hunter Waite, Kate L Craft, Jason D Hofgartner, et al. Science objectives for flagship-class mission concepts for the search for evidence of life at enceladus. *Astrobiology*, 22(6):685–712, 2022.

Ross R Maguire, Nicholas C Schmerr, Vedran Lekić, Terry A Hurford, Lenore Dai, and Alyssa R Rhoden. Constraining Europa's ice shell thickness with fundamental mode surface wave dispersion. *Icarus*, 369:114617, 2021. ISSN 0019-1035. doi:10.1016/j.icarus.2021.114617. URL https://www.sciencedirect.com/science/article/pii/S0019103521002815.

Angela G Marusiak, Steven D. Vance, Mark P Panning, Marie Běhounková, Paul K Byrne, Gaël Choblet, Mohit Melwani Daswani, Kynan Hughson, Baptiste Journaux, Ana H Lobo, Britney E Schmidt, Kateřina Pleiner Sládková, Krista M Soderlund, WenZhan Song, Ondřej Souček, Gregor Steinbrügge, Andrew F. Thompson, and Sili Wang. Exploration of Icy Ocean Worlds Using Geophysical Approaches. *The Planetary Science Journal*, 2(4):150, 8 2021. ISSN 2632-3338. doi:10.3847/PSJ/ac1272. URL https://iopscience.iop.org/article/10.3847/PSJ/ac1272.

Angela G. Marusiak, Steven Vance, Mark P. Panning, Andrea S. Bryant, Marc A. Hesse, Evan Carnahan, and Baptiste Journaux. The Effects of Methane Clathrates on the Thermal and Seismic Profile of Titan's Icy Lithosphere. *The Planetary Science Journal*, 3(7): 167, 7 2022. ISSN 2632-3338. doi:10.3847/PSJ/ac787e. URL https://iopscience.iop.org/article/10.3847/PSJ/ac787e.

Angela G. Marusiak, Saikiran Tharimena, Mark P. Panning, Steven D. Vance, Christian Boehm, Simon Stähler, and Martin Van Driel. Estimating the 3d structure of the enceladus ice shell from flexural and crary waves using seismic simulations. *Earth and Planetary Science Letters*, 603:117984, 2023. ISSN 0012-821X. doi:https://doi.org/10.1016/j.epsl.2022.117984. URL https://www.sciencedirect.com/science/article/pii/S0012821X22006203.

G Masters, John H. Woodhouses, and G. Freeman. Mineos, 2011.

Giuseppe Mitri and Adam P. Showman. Thermal convection in ice-i shells of titan and enceladus. *Icarus*, 193(2):387–396, 2008. ISSN 0019-1035. doi:https://doi.org/10.1016/j.icarus.2007.07.016. URL https://www.sciencedirect.com/science/article/pii/S0019103507003429. Saturn's Icy Satellites from Cassini.

Giuseppe Mitri, Rachele Meriggiola, Alex Hayes, Axel Lefevre, Gabriel Tobie, Antonio Genova, Jonathan I Lunine, and Howard Zebker. Shape, topography, gravity anomalies and tidal deformation of Titan. *Icarus*, 236:169–177, 7 2014. ISSN 00191035. doi:10.1016/j.icarus.2014.03.018. URL http://www.sciencedirect.com/science/article/pii/S0019103514001444https://linkinghub.elsevier.com/retrieve/pii/S0019103514001444.

Olivier Mousis, Jonathan I Lunine, Sylvain Picaud, Daniel Cordier, J. Hunter Waite, Jr., and Kathleen E Mandt. Removal of Titan's Atmospheric Noble Gases by Their Sequestration in Surface Clathrates. *The Astrophysical Journal*, 740(1):L9, 10 2011. ISSN 2041-8205. doi:10.1088/2041-8205/740/1/L9. URL https://iopscience.iop.org/article/10.1088/2041-8205/740/1/L9.

Olivier Mousis, Eric Chassefiere, Nils G Holm, Alexis Bouquet, Jack Hunter Waite, Wolf Dietrich Geppert, Sylvain Picaud, Yuri Aikawa, Mohamad Ali-Dib, Jean-Luc Charlou, et al. Methane clathrates in the solar system. *Astrobiology*, 15(4):308–326, 2015.

Y. Nakamura, G. V. Latham, and H. J. Dorman. Apollo Lunar Seismic Experiment—Final summary. *Lunar and Planetary Science Conference Proceedings*, 87:117–A123, January 1982. doi:10.1029/JB087iS01p0A117.

Yosio Nakamura. Rebirth of extraterrestrial seismology. *Nature Geoscience*, 13(3):178–179, 2020.

Engineering National Academies of Sciences, Medicine, et al. Origins, worlds, and life: a decadal strategy for planetary science and astrobiology 2023-2032. 2022.

C. D. Neish, J. W. Barnes, C. Sotin, S. MacKenzie, J. M. Soderblom, S. Le Mouélic, R. L. Kirk, B. W. Stiles, M. J. Malaska, A. Le Gall, R. H. Brown, K. H. Baines, B. Buratti, R. N. Clark, and P. D. Nicholson. Spectral properties of titan's impact craters imply chemical weathering of its surface. *Geophysical Research Letters*, 42(10):3746–3754, 2015. doi:https://doi.org/10.1002/2015GL063824. URL https://agupubs.onlinelibrary.wiley.com/doi/abs/10.1002/2015GL063824.

Adrien Néri, François Guyot, Bruno Reynard, and Christophe Sotin. A carbonaceous chondrite and cometary origin for icy moons of Jupiter and Saturn. *Earth and Planetary Science Letters*, 530:115920, 1 2020. ISSN 0012821X. doi:10.1016/j.epsl.2019.115920. URL https://www.sciencedirect.com/science/article/pii/S0012821X19306120https://linkinghub.elsevier.com/retrieve/pii/S0012821X19306120.

H B Niemann, S K Atreya, S J Bauer, G R Carignan, J E Demick, R L Frost, D Gautier, J A Haberman, D N Harpold, D M Hunten, G. Israel, J. I. Lunine, W. T. Kasprzak, T. C. Owen, M. Paulkovich, F. Raulin, E. Raaen, and S. H. Way. The abundances of constituents of Titan's atmosphere from the GCMS instrument on the Huygens probe. *Nature*, 438(7069):779–784, 12 2005. ISSN 0028-0836. doi:10.1038/nature04122. URL http://www.nature.com/articles/nature04122.

F. Nimmo and B.G. Bills. Shell thickness variations and the long-wavelength topography of titan. *Icarus*, 208(2):896–904, 2010. ISSN 0019-1035. doi:https://doi.org/10.1016/j.icarus.2010.02.020. URL https://www.sciencedirect.com/science/article/pii/S0019103510000941.

T Nissen-Meyer, Martin van Driel, S C Stähler, K Hosseini, S Hempel, L Auer, A Colombi, and A Fournier. AxiSEM: broadband 3-D seismic wavefields in axisymmetric media. *Solid Earth*, 5(1):425–445, 2014. doi:10.5194/se-5-425-2014. URL http://www.solid-earth.net/5/425/2014/.

Conor A. Nixon, Alexander E. Thelen, Martin A. Cordiner, Zbigniew Kisiel, Steven B. Charnley, Edward M. Molter, Joseph Serigano, Patrick G. J. Irwin, Nicholas A. Teanby, and Yi-Jehng Kuan. Detection of cyclopropenylidene on titan with alma. *The Astronomical Journal*, 160(5):205, oct 2020. doi:10.3847/1538-3881/abb679. URL https://dx.doi.org/10.3847/1538-3881/abb679.

Ceri Nunn, Raphael F. Garcia, Yosio Nakamura, Angela G. Marusiak, Taichi Kawamura, Daoyuan Sun, Ludovic Margerin, Renee Weber, Mélanie Drilleau, Mark A. Wieczorek, Amir Khan, Attilio Rivoldini, Philippe Lognonné, and Peimin Zhu. Lunar seismology: A data and instrumentation review. *Space Science Reviews*, 216(5):89, 2020. doi:10.1007/s11214-020-00709-3.

Ceri Nunn, Yosio Nakamura, Sharon Kedar, and Mark P Panning. A new archive of apollo's lunar seismic data. *The Planetary Science Journal*, 3(9):219, 2022.

Mark P. Panning, Ved Lekic, M Manga, F Cammarano, and B Romanowicz. Long-period seismology on Europa: 2. Predicted seismic response. *Journal of Geophysical Research: Planets*, 111(E12):n/a–n/a, 12 2006. ISSN 01480227. doi:10.1029/2006JE002712. URL http://doi.wiley.com/10.1029/2006JE002712.

Mark P. Panning, Simon C Stähler, Steven D. Vance, Sharon Kedar, Victor C. Tsai, William T Pike, Ralph D. Lorenz, Hsin-Hua Huang, Steven D Vance, Sharon Kedar, Victor C Tsai, William T Pike, and Ralph D. Lorenz. Expected seismicity and the seismic noise environment of Europa. *Journal of Geophysical Research: Planets*, 123(1):163–179, 1 2018. ISSN 21699097. doi:10.1002/2017JE005332. URL http://onlinelibrary.wiley.com/doi/10.1002/2017JE005332/abstract.

Mark P Panning, Ralph Lorenz, Hiroaki Shiraishi, Ryuhei Yamada, Simon Stähler, Elizabeth P Turtle, Terry Hurford, Naomi Murdoch, and Steven Vance. Seismology on titan: A seismic signal and noise budget in preparation for dragonfly. In *SEG International Exposition and Annual Meeting*, page D041S079R005. SEG, 2020.

Robert T. Pappalardo, Steven D. Vance, F Bagenal, B G Bills, D L Blaney, D D Blankenship, W B Brinckerhoff, J E Connerney, K P Hand, T M Hoehler, J S Leisner, W S Kurth, M A McGrath, M T Mellon, J M Moore, G W Patterson, L M Prockter, D A Senske, B E Schmidt, E L Shock, D E Smith, and K M Soderlund. Science potential from a

Europa lander. *Astrobiology*, 13(8):740–773, 2013. doi:10.1089/ast.2013.1003. URL http://www.ncbi.nlm.nih.gov/pubmed/23924246.

C C Porco, Paul Helfenstein, P C Thomas, A P Ingersoll, J Wisdom, Robert West, Gerhard Neukum, Tilmann Denk, Roland Wagner, and Thomas Roatsch. Cassini observes the active south pole of Enceladus. *Science*, 311(5766):1393–1401, 2006. doi:10.1126/science.1123013.

L Pou, MP Panning, MJ Styczinski, M Melwani Daswani, SD Vance, and C Nunn. Tidal seismicity in the moon and implications for the silicate interior of europa. *LPI Contributions*, 3040:1816, 2024.

AT Ringler and CR Hutt. Self-noise models of seismic instruments. *Seismological research letters*, 81(6):972–983, 2010.

Peter W Rodgers. Self-noise spectra for 34 common electromagnetic seismometer/preamplifier pairs. *Bulletin of the Seismological society of America*, 84(1):222–228, 1994.

S. Rodriguez, S. Le Mouélic, C. Sotin, H. Clénet, R.N. Clark, B. Buratti, R.H. Brown, T.B. McCord, P.D. Nicholson, and K.H. Baines. Cassini/vims hyperspectral observations of the huygens landing site on titan. *Planetary and Space Science*, 54(15):1510–1523, 2006. ISSN 0032-0633. doi:https://doi.org/10.1016/j.pss.2006.06.016. URL https://www.sciencedirect.com/science/article/pii/S0032063306001437. First Results on Titan from VIMS Observations Onboard the Cassini/huygens Mission/Astrobiology: The Detection of Life in the Solar System.

Lauren R Schurmeier and Andrew J Dombard. Crater relaxation on Titan aided by low thermal conductivity sand infill. *Icarus*, 305:314–323, 5 2018. ISSN 00191035. doi:10.1016/j.icarus.2017.10.034. URL https://www.sciencedirect.com/science/article/pii/S0019103517303998https://linkinghub.elsevier.com/retrieve/pii/S0019103517303998.

Lauren R. Schurmeier, Andrew J. Dombard, Michael J. Malaska, Sarah A. Fagents, Jani Radebaugh, and Daniel E. Lalich. An intrusive cryomagmatic origin for northern radial labyrinth terrains on titan and implications for the presence of crustal clathrates. *Icarus*, 404:115664, 2023. ISSN 0019-1035. doi:https://doi.org/10.1016/j.icarus.2023.115664. URL https://www.sciencedirect.com/science/article/pii/S0019103523002415.

Peter M Shearer. *Introduction to Seismology*. Cambridge University Press, 2019.

Jason M Soderblom, Robert H Brown, Laurence A Soderblom, Jason W Barnes, Ralf Jaumann, Stéphane Le Mouélic, Christophe Sotin, Katrin Stephan, Kevin H Baines, Bonnie J Buratti, et al. Geology of the selk crater region on titan from cassini vims observations. *Icarus*, 208(2):905–912, 2010.

Laurence A. Soderblom, Randolph L. Kirk, Jonathan I. Lunine, Jeffrey A. Anderson, Kevin H. Baines, Jason W. Barnes, Janet M. Barrett, Robert H. Brown, Bonnie J. Buratti, Roger N. Clark, Dale P. Cruikshank, Charles Elachi, Michael A. Janssen, Ralf Jaumann, Erich Karkoschka, Stéphane Le Mouélic, Rosaly M. Lopes, Ralph D. Lorenz, Thomas B. McCord, Philip D. Nicholson, Jani Radebaugh, Bashar Rizk, Christophe Sotin, Ellen R. Stofan, Tracie L. Sucharski, Martin G. Tomasko, and Stephen D. Wall. Correlations between cassini vims spectra and radar sar images: Implications for titan's surface composition and the character of the huygens probe landing site. *Planetary and Space Science*, 55(13):2025–2036, 2007. ISSN 0032-0633. doi:https://doi.org/10.1016/j.pss.2007.04.014. URL `https://www.sciencedirect.com/science/article/pii/S0032063307001304`. Titan as seen from Huygens.

F Sohl, H Hussmann, B Schwentker, T Spohn, and Ralph D. Lorenz. Interior structure models and tidal Love numbers of Titan. *Journal of Geophysical Research: Planets*, 108 (E12), 12 2003. ISSN 01480227. doi:10.1029/2003JE002044. URL `http://doi.wiley.com/10.1029/2003JE002044`.

F. Sohl, A. Solomonidou, F. W. Wagner, A. Coustenis, H. Hussmann, and D. Schulze-Makuch. Structural and tidal models of titan and inferences on cryovolcanism. *Journal of Geophysical Research: Planets*, 119(5):1013–1036, 2014. doi:https://doi.org/10.1002/2013JE004512. URL `https://agupubs.onlinelibrary.wiley.com/doi/abs/10.1002/2013JE004512`.

Christophe Sotin, Klára Kalousová, and Gabriel Tobie. Titan's Interior Structure and Dynamics After the Cassini-Huygens Mission. *Annual Review of Earth and Planetary Sciences*, 49(1):579–607, 5 2021. ISSN 0084-6597. doi:10.1146/annurev-earth-072920-052847. URL `https://doi.org/10.1146/annurev-earth-072920-052847`.

Simon C. Stähler, Mark P. Panning, Steven D. Vance, Ralph D. Lorenz, Martin van Driel, Tarje Nissen-Meyer, Sharon Kedar, Martin van Driel, Tarje Nissen-Meyer, and Sharon Kedar. Seismic Wave Propagation in Icy Ocean Worlds. *Journal of Geophysical Research: Planets*, 123(1):206–232, 2017. ISSN 2169-9097. doi:10.1002/2017JE005338. URL `http://onlinelibrary.wiley.com/doi/10.1002/2017JE005338/abstract`.

Simon C. Stähler, Mark P. Panning, Céline Hadziioannou, Ralph D. Lorenz, Steve Vance, Knut Klingbeil, and Sharon Kedar. Seismic signal from waves on Titan's seas. *Earth and Planetary Science Letters*, 520:250–259, 8 2019. ISSN 0012821X. doi:10.1016/j.epsl.2019.05.043. URL `https://linkinghub.elsevier.com/retrieve/pii/S0012821X19303255`.

Simon C Stähler, Amir Khan, W Bruce Banerdt, Philippe Lognonné, Domenico Giardini, Savas Ceylan, Mélanie Drilleau, A Cecilia Duran, Raphaël F. Garcia, Quancheng Huang, Doyeon Kim, Vedran Lekic, Henri Samuel, Martin Schimmel, Nicholas Schmerr, David Sollberger, Éléonore Stutzmann, Zongbo Xu, Daniele Antonangeli, Constantinos Charalambous, Paul M. Davis, Jessica C. E. Irving, Taichi Kawamura, Martin Knapmeyer,

Ross Maguire, Angela G Marusiak, Mark P Panning, Clément Perrin, Ana-Catalina Plesa, Attilio Rivoldini, Cédric Schmelzbach, Géraldine Zenhäusern, Éric Beucler, John Clinton, Nikolaj Dahmen, Martin van Driel, Tamara Gudkova, Anna Horleston, W. Thomas Pike, Matthieu Plasman, and Suzanne E. Smrekar. Seismic detection of the martian core. *Science*, 373(6553):443–448, 7 2021. ISSN 0036-8075. doi:10.1126/science.abi7730. URL https://www.sciencemag.org/lookup/doi/10.1126/science.abi7730.

Ellen R Stofan, C Elachi, Jonathan I. Lunine, Ralph D. Lorenz, B Stiles, K L Mitchell, S Ostro, L Soderblom, C Wood, H Zebker, S. Wall, M. Janssen, R. Kirk, R. Lopes, F. Paganelli, J. Radebaugh, L. Wye, Y. Anderson, M. Allison, R. Boehmer, P. Callahan, P. Encrenaz, E. Flamini, G. Francescetti, Y. Gim, G. Hamilton, S. Hensley, W. T. K. Johnson, K. Kelleher, D. Muhleman, P. Paillou, G. Picardi, F. Posa, L. Roth, R. Seu, S. Shaffer, S. Vetrella, and R. West. The lakes of Titan. *Nature*, 445(7123):61–64, 1 2007. ISSN 0028-0836. doi:10.1038/nature05438. URL http://www.nature.com/articles/nature05438.

M. J. Styczinski, S. D. Vance, and M. Melwani Daswani. *PlanetProfile:* self-consistent interior structure modeling for terrestrial bodies in python. *Earth and Space Science*, 10 (8):e2022EA002748, 2023a. doi:10.1029/2022EA002748.

Marshall J. Styczinski, Steven D. Vance, Mara Niesyt, Artyom Lisitsyn, Mohit Melwani Daswani, A G Marusiak, Kathy Vega, and Andrea S. Bryant. vancesteven/PlanetProfile: Core thermal profile fix, 2023b.

Marshall J. Styczinski, Steven D. Vance, Mara Niesyt, Artyom Lisitsyn, Mohit Melwani Daswani, Angela G Marusiak, Kathy Vega, and Andrea S. Bryant. vancesteven/PlanetProfile, 2024. URL https://doi.org/10.5281/zenodo.844130.

Yixin Sun, Jiutong Zhao, Chuanpeng Hou, and Weixin Jiao. Highlight advances in planetary physics in the solar system: In situ detection over the past 20 years. *Space: Science & Technology*, 3:0007, 2023. doi:10.34133/space.0007. URL https://spj.science.org/doi/abs/10.34133/space.0007.

Alexander E. Thelen, C.A. Nixon, N.J. Chanover, M.A. Cordiner, E.M. Molter, N.A. Teanby, P.G.J. Irwin, J. Serigano, and S.B. Charnley. Abundance measurements of titan's stratospheric hcn, hc3n, c3h4, and ch3cn from alma observations. *Icarus*, 319: 417–432, 2019. ISSN 0019-1035. doi:https://doi.org/10.1016/j.icarus.2018.09.023. URL https://www.sciencedirect.com/science/article/pii/S0019103518304184.

Alexander E. Thelen, Martin A. Cordiner, Conor A. Nixon, Véronique Vuitton, Zbigniew Kisiel, Steven B. Charnley, Maureen Y. Palmer, Nicholas A. Teanby, and Patrick G. J. Irwin. Detection of ch3c3n in titan's atmosphere. *The Astrophysical Journal Letters*, 903 (1):L22, nov 2020. doi:10.3847/2041-8213/abc1e1. URL https://dx.doi.org/10.3847/2041-8213/abc1e1.

Gabriel Tobie, Olivier Grasset, Jonathan I Lunine, Antoine Mocquet, and Christophe Sotin. Titan's internal structure inferred from a coupled thermal-orbital model. *Icarus*, 175(2): 496–502, 2005. doi:https://doi.org/10.1016/j.icarus.2004.12.007. URL http://www.sciencedirect.com/science/article/pii/S0019103504004269.

Gabriel Tobie, Jonathan I Lunine, and Christophe Sotin. Episodic outgassing as the origin of atmospheric methane on titan. *Nature*, 440(7080):61–64, Mar 2006. ISSN 1476-4687 (Electronic); 0028-0836 (Linking). doi:10.1038/nature04497.

Gabriel Tobie, Mathieu Choukroun, Olivier Grasset, Stephane Le Mouélic, J I Lunine, Christophe Sotin, Olivier Bourgeois, Daniel Gautier, Mathieu Hirtzig, and Sébastien Lebonnois. Evolution of Titan and implications for its hydrocarbon cycle. *Philosophical Transactions of the Royal Society A: Mathematical, Physical and Engineering Sciences*, 367(1889):617–631, 2009. ISSN 1364-503X. doi:10.1098/rsta.2008.0246.

EP Turtle and RD Lorenz. The dragonfly mission to titan: technological development and science converge to enable new exploration. *The Bridge*, 51(3):59–66, 2021.

M. van Driel, L. Krischer, S. C. Stähler, K. Hosseini, and T. Nissen-Meyer. Instaseis: instant global seismograms based on a broadband waveform database. *Solid Earth*, 6(2):701–717, 6 2015. ISSN 1869-9529. doi:10.5194/se-6-701-2015. URL http://www.solid-earth.net/6/701/2015/.

Steven D. Vance, Sharon Kedar, Mark P. Panning, Simon C. Stähler, Bruce G Bills, Ralph D Lorenz, Hsin-Hua Huang, W.T. Pike, Julie C. Castillo, Philippe Lognonné, Victor C Tsai, and Alyssa Rose Rhoden. Vital Signs: Seismology of Icy Ocean Worlds. *Astrobiology*, 18 (1):37–53, 1 2018a. ISSN 1531-1074. doi:10.1089/ast.2016.1612. URL http://online.liebertpub.com/doi/abs/10.1089/ast.2016.1612http://www.liebertpub.com/doi/10.1089/ast.2016.1612.

Steven D. Vance, Mark P. Panning, Simon Stähler, Fabio Cammarano, Bruce G. Bills, Gabriel Tobie, Shunichi Kamata, Sharon Kedar, Christophe Sotin, William T. Pike, Ralph D. Lorenz, Hsin-Hua Hua Huang, Jennifer M. Jackson, and Bruce Banerdt. Geophysical Investigations of Habitability in Ice-Covered Ocean Worlds. *Journal of Geophysical Research: Planets*, 123(1):180–205, 11 2018b. ISSN 2169-9097. doi:10.1002/2017JE005341. URL http://doi.wiley.com/10.1002/2017JE005341https://doi.org/10.1002/2017JE005341.

Steven Douglas Vance, Angela G. Marusiak, Mohit Melwani Daswani, M J Styczinski, Artyom Lisitsyn, Kathy Vega, and Andrea Bryant. PlanetProfile: Supplementary Data: Effects of Methane Clathrate Lids on Titan's Ice Shell and added TauP functionality, 2022.

T. H. Vu, M. Choukroun, C. Sotin, V. Muñoz-Iglesias, and H. E. Maynard-Casely. Rapid Formation of Clathrate Hydrate From Liquid Ethane and Water Ice on Titan. *Geophysical Research Letters*, 47(4):1–8, 2020. ISSN 19448007. doi:10.1029/2019GL086265.

W F Waite, L A Stern, S H Kirby, W J Winters, and D H Mason. Simultaneous determination of thermal conductivity, thermal diffusivity and specific heat in sI methane hydrate. *Geophysical Journal International*, 169(2):767–774, 5 2007. ISSN 0956-540X. doi:10.1111/j.1365-246X.2007.03382.x. URL `https://doi.org/10.1111/j.1365-246X.2007.03382.x`.

J. H. Woodhouse. The calculation of eigenfrequencies and eigenfunctions of the free oscillations of the earth and the sun. *Seismological Algorithms*, pages pp. 321– 370, 1988.

Ryuhei Yamada, Tanguy Nébut, Hiroaki Shiraishi, Philippe Lognonné, Naoki Kobayashi, and Satoshi Tanaka. Frequency band enlargement of the penetrator seismometer and its application to moonquake observation. *Advances in Space Research*, 56(2):341–354, 2015.